Investigation into the Anisotropy of the Ocean Continent Transition zone of the Nova Scotia margin

by

Maria C. Whitehead

Submitted in partial fulfilment of the requirements for the
degree of Combined Honours Bachelor of Science in Earth Science and Oceanography

at

Dalhousie University
Halifax, Nova Scotia
April, 2011

Distribution License

DalSpace requires agreement to this non-exclusive distribution license before your item can appear on DalSpace.

NON-EXCLUSIVE DISTRIBUTION LICENSE

You (the author(s) or copyright owner) grant to Dalhousie University the non-exclusive right to reproduce and distribute your submission worldwide in any medium.

You agree that Dalhousie University may, without changing the content, reformat the submission for the purpose of preservation.

You also agree that Dalhousie University may keep more than one copy of this submission for purposes of security, back-up and preservation.

You agree that the submission is your original work, and that you have the right to grant the rights contained in this license. You also agree that your submission does not, to the best of your knowledge, infringe upon anyone's copyright.

If the submission contains material for which you do not hold copyright, you agree that you have obtained the unrestricted permission of the copyright owner to grant Dalhousie University the rights required by this license, and that such third-party owned material is clearly identified and acknowledged within the text or content of the submission.

If the submission is based upon work that has been sponsored or supported by an agency or organization other than Dalhousie University, you assert that you have fulfilled any right of review or other obligations required by such contract or agreement.

Dalhousie University will clearly identify your name(s) as the author(s) or owner(s) of the submission, and will not make any alteration to the content of the files that you have submitted.

If you have questions regarding this license please contact the repository manager at dalspace@dal.ca.

Grant the distribution license by signing and dating below.

_____ _____

Name of signatory Date

TABLE OF CONTENTS

TABLE OF FIGURES

TABLE OF TABLES

ABSTRACT

The eastern North American continental margin features a shift from volcanic style rifting off the eastern USA, to nonvolcanic style off Newfoundland; the Nova Scotia margin has been suggested to be a transitional style margin between the two. The composition of a layer in the lower crust (the High Velocity Lower Crust or HVLC) in the Ocean Continent Transition has been debated. The composition of this layer has a large impact on the classification of the margin, as it has been proposed to be either gabbro (suggesting volcanic style rifting) or serpentinized mantle (suggesting nonvolcanic). These show similar seismic velocities; however, gabbro is isotropic and serpentinite is anisotropic. Previously created P-wave velocity model of margin-perpendicular, wide-angle seismic line SMART1 shows a layer of partially serpentinized mantle above the mantle. Using forward modeling of the refracted arrivals of one OBS to create a 1D model, the newly collected margin-parallel, wide-angle seismic line OCTOPUS also shows this layer, however, with slower velocities than those observed in the SMART1 model (6.8 to 6.9 km/s as compared to 7.2 to 7.6 km/s). These differing velocities suggest anisotropy, therefore suggesting the HVLC is composed of serpentinized mantle. The degree of anisotropy observed was 6 – 9 %; this is within a similar range to values observed along the west Iberia margin and also along the Mid Ocean Ridge where the fast direction is parallel to the direction of spreading, (given that olivine crystals are likely to align their fast axis with the direction of stress (rifting)). This gives further evidence towards the conclusion that the HVLC is composed of serpentinized olivine-rich mantle rather than volcanics. Along strike marginal variations in the HLVC were also observed along the OCTOPUS line; these variations are consistent with the variations observed in previous work showing the HVLC thinning towards the southwest.

TABLE OF ABBREVIATIONS

COB	Continent Ocean Boundary
DF	Detachment Faults
ECMA	East Coast Magnetic Anomaly
FB	Faulted Blocks
HSM	Highly Serpentinized Mantle
HVLC	High Velocity Lower Crust
MCS	Multi-Channel Seismic
MOR	Mid Ocean Ridge
NF	Normal Faults
OBS	Ocean Bottom Seismometer
OCT	Ocean Continent Transition
OCTOPUS	Ocean Continent TransitiOn Profile Using Seismic
PSI	Pound per Square Inch
PSM	Partially Serpentinized Mantle
SDP	Slope Diapiric Province
SDR	Seaward Dipping Reflectors
SMART	Scotia MARgin Transects

ACKNOWLEDGEMENTS

I would like to extend my deepest gratitude my supervisor, Keith Louden, for providing me with an interesting topic, the opportunity to be a part of a wide-angle seismic cruise, and all the assistance and support I needed to complete this thesis. I would also like to thank to Helen Lau for all her software expertise and patience. Without these two people this thesis would not have been possible. I would also like to extend my gratitude to Mladen Nedimovic for his support while at sea and for providing me with a workspace in his lab at Dalhousie. And to Louise Watremez for her willingness to help at any point in time. I would also like to thank the crew of the R.V. Strait Explorer for not making me feel like a landlubber in the stormy November North Atlantic seas. And finally, to my friends and family for their continuous support.

CHAPTER 1: INTRODUCTION

The separation of continents leads to the creation of ocean basins and is caused by continental rifting. Continental rifting begins as the extension and thinning of continental crust. As the rifting process continues, eventually the very thin continental crust becomes brittle and breaks apart, creating ocean basins and rifted continental margins (Perez-Gussinye and Reston, 2001).

Volcanism during this rifting process can occur; this volcanism can change the margin. Margins are classified as volcanic or nonvolcanic based on the amount of volcanism that took place during rifting. Margins do not have to be either volcanic or nonvolcanic; margins also can be formed during an in-between stage with some volcanism, but not enough to dominate. Figure 1.0 shows the world-wide distribution of volcanic, nonvolcanic and mixed margins.

At a certain point during the rifting process, there is a major transition between rifting causing the thinning and extension of continental crust, and seafloor spreading forming new oceanic crust. This shift is known because it has been observed in crustal units (Keen and Potter, 1995b). This transition, which is represented along the rifted continental margins, has been of significant interest both scientifically and commercially because it is potentially a site of great sediment deposition and therefore has high resource potential. With newer technologies in the oil and gas industry and diminishing supplies in shallower deposits there is an urge to look deeper into these transitional margins.

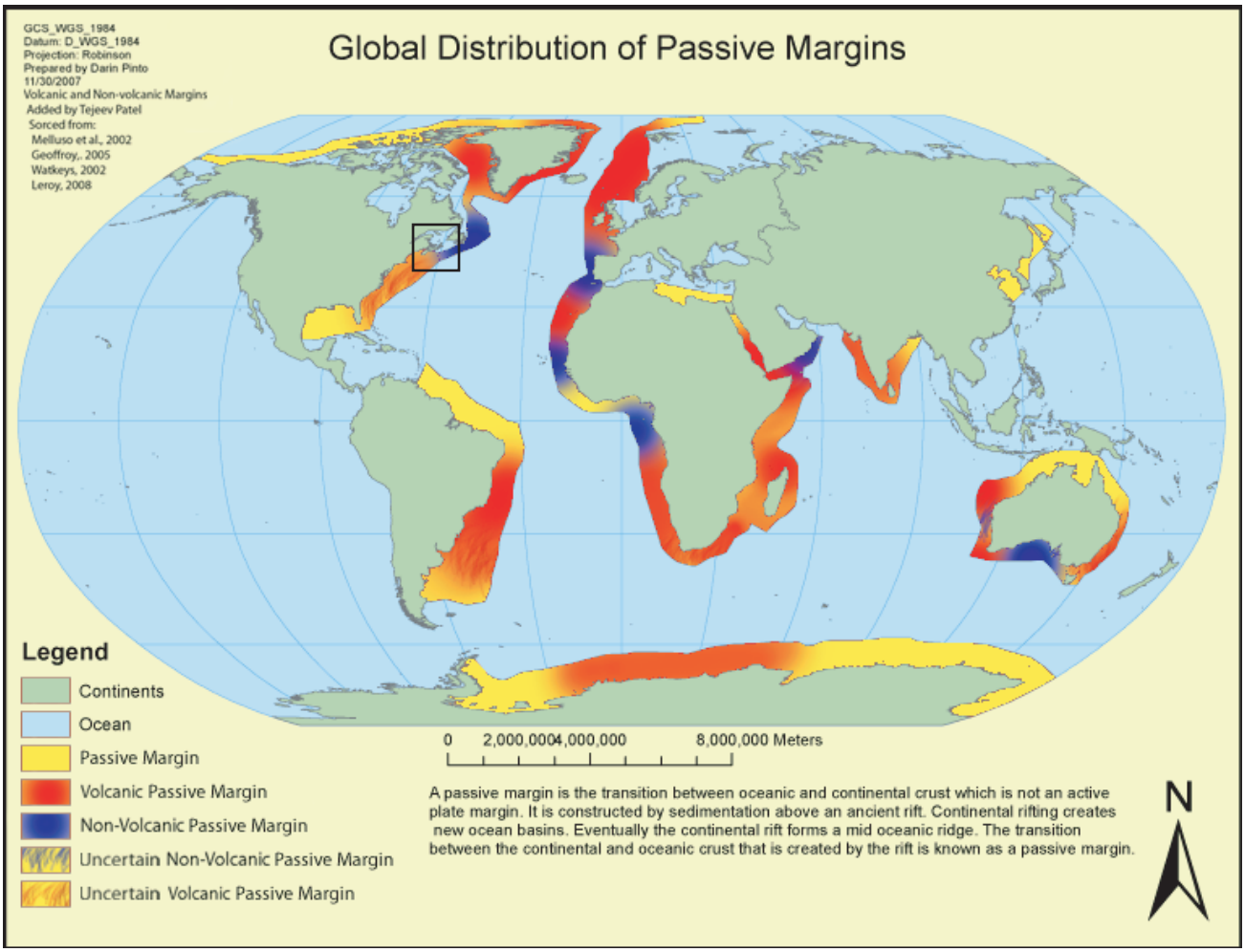

Figure 1.0 Global distribution of margin types: volcanic, nonvolcanic and mixed margins. Black rectangle shows the Nova Scotia margin, and the volcanic natured margin to the south, and the nonvolcanic natured margin to the north. (Modified from http://www.thefullwiki.org/Mid-ocean_ridge).

1.1 Ocean Continent Transition

This major transition between continental rifting and seafloor spreading is represented by the Ocean Continent Transition (OCT). The OCT is the zone along a margin between the extended continental crust and the start of oceanic crust. It is characterized by a distinct velocity anomaly in crustal layers between the thinning of pre-existing continental crust and the accretion of new oceanic crust. This transition zone varies with the amount of active volcanism present during the rifting process.

Previously the transition between extended continental crust and oceanic crust was thought to be a sharp boundary called the Continent Ocean Boundary (COB), and it may still be in many places, particularly on volcanic margins. Figure 1.1.1 illustrates the basic crustal features of both nonvolcanic (magma-poor) and volcanic (magma-dominated) rifted margins, as well as the observed trend in the width of the boundary. The width of the boundary generally depends on the presence of volcanism. Volcanic margins tend to be much narrower than non-volcanic margins. Non-volcanic rifted continental margins tend to be more complex as they are rifted to the extreme before producing melt (and new oceanic crust).

1.2 Study Location

The study area is located along the Nova Scotia continental margin, southeast of Sable Island in the Scotian Basin. Figure 1.2.1 is a map of the study area showing regional seismic lines that have been shot in the area, including the new OCTOPUS

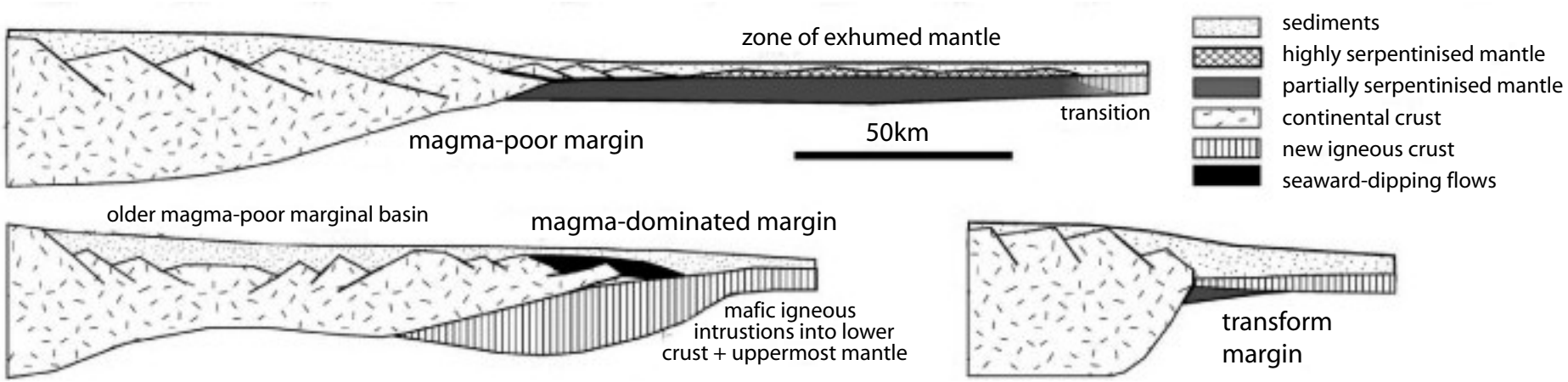

Figure 1.1.1 Basic crustal features of nonvolcanic (magma-poor) and volcanic (magma dominated) margins. The width of the zone of tranistion between the two crust types is large in the nonvolcanic margin as compared to the volcanic margins (after Reston 2009).

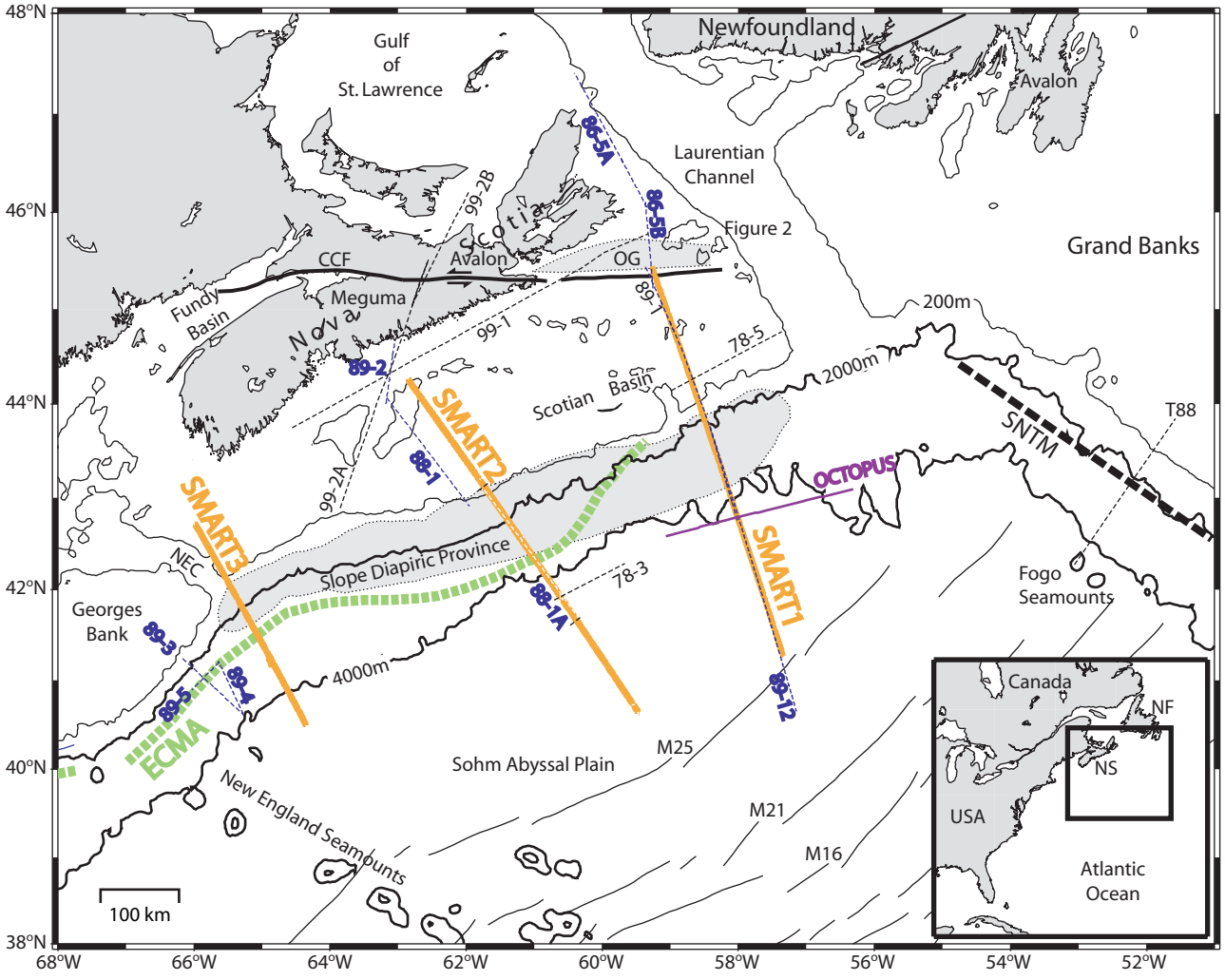

Figure 1.2.1 Regional map of the Nova Scotia margin showing regional seismics lines. Most important to this study are coloured. Newly collected OCTOPUS line is shown in purple.The East Coast Magnetic Anomaly (ECMA) is roughly denoted in green. (After Funck et al. 2004).

(Ocean Continent TransitiOn Profile Using Seismic) line and the SMART1 (Scotia MARgin Transects) line from Funck et al. (2004).

The North Atlantic passive margin features a shift from volcanic to non-volcanic rifting styles towards the north. This transition of rifting styles is thought to be related to the weakening and disappearance of the East Coast Magnetic Anomaly (ECMA) (Keen and Potter, 1995a). Figure 1.2.2 is a magnetic anomaly map of the North Atlantic showing this gradual weakening and disappearance of the ECMA towards the northeast. From this map it is clear that our study location is located after the ECMA has disappeared. There are differing hypotheses about where the ECMA terminates; some hypothesize that the ECMA terminates in the south, while others believe that it carries on through the central and north part of the margin and it just much weaker in these areas. This debate sparks the question as to where the northern part of the margin is truly nonvolcanic; thus there are differing interpretations of the OCT high velocity body.

In the central and northern area, the non-volcanic portion of the margin, the transition from continental crust to oceanic crust is marked by a wide transition zone between the thinning continental crust and the oceanic crust, the OCT.

The area has previously been studied using wide-angle seismic surveys; most specific to this project is the work done by Funck et al. (2004) along the SMART1 seismic line which crosses the margin as seen in Figure 1.2.1.

1.3 Thesis Objectives

The overall objective of this honour's thesis is to conduct a preliminary study into the composition of the OCT in the Nova Scotia non-volcanic margin. There are two

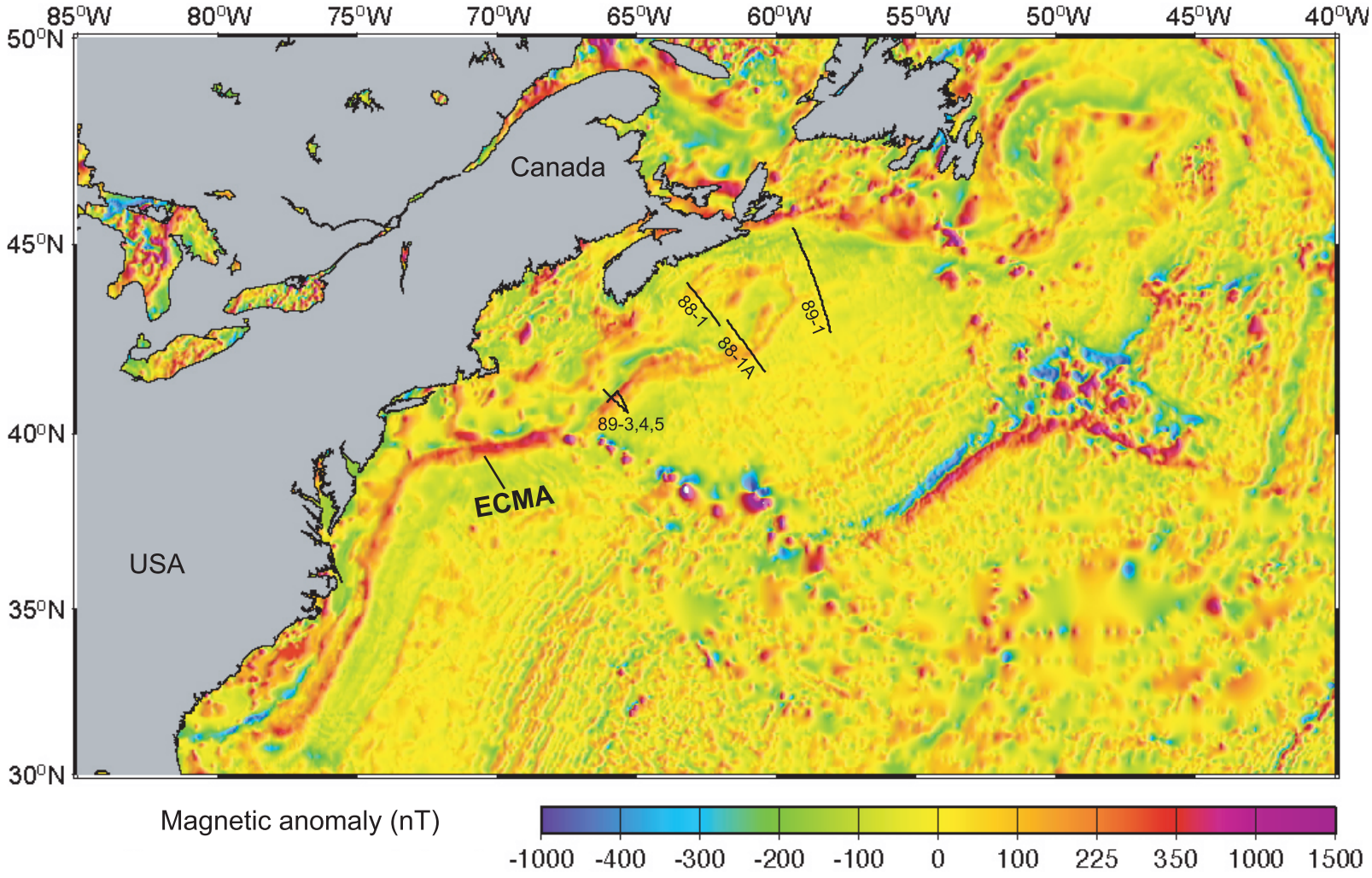

Figure 1.2.2 Magnetic anomaly map of the northeastern North American margin showing the strong East Coast Magnetic Anomaly (ECMA) along eastern USA diminishing to a weak or nonexistent ECMA along the Nova Scotia margin. (After Wu, 2007).

differing ideas about the composition of the OCT in this area (Minshull, 2008): either it is formed by an underplated mantle melt body composed of gabbro, or it is serpentinized mantle composed of serpentinite. Underplating occurs as the result of partial melting of the mantle. The melt rises up through the mantle and "ponds" at the base of the crust as it is denser than the crust itself. Serpentinization is a low-temperature metamorphic process involving hydrothermal fluids which causes the alteration of the mineral olivine to the mineral serpentine. Both potential OCT compositions can have similarly high velocities, but the gabbro is isotropic (meaning its velocity does not change with direction) and the serpentinized mantle is anisotropic (meaning that its velocity does change with direction).

The west Iberia margin is a conjugate margin to the Newfoundland margin; and as such previous results in the Iberia margin give an idea of the velocity variation to be expected. Cole et al. (2002) conducted a study on the P-wave azimuthal seismic anisotropy of the margin in order to relate the direction of anisotropy to a direction of extension in the area. This study is useful to us because it provides insight into the velocity variations to be expected, and also the variation in the degree of anisotropy. Cole et al. (2002) found that between depths of 3 to 7 km, the degree of anisotropy ranged from 5 to 8 percent.

We plan to use two intersecting perpendicular wide angle seismic lines, one across the margin, which has been previously modeled by Funck et al. (2004), and a new profile along the margin which was collected in November 2010 (as shown in Figure 1.2.1). Results from these profiles will be analyzed to investigate the degree of anisotropy of the OCT which will give further evidence for its composition.

CHAPTER 2: GEOLOGIC BACKGROUND AND PREVIOUS WORKS

2.1 Formation of the Scotia Margin

The continental crust of eastern Canada was formed during the Appalachian Orogen (Keen et al., 1990). Figure 2.1.1 is a geologic map of eastern Canada showing the two main terranes of Nova Scotia, the Meguma and the Avalon. As seen in Figure 2.1.1 the Meguma Terrane makes up the southern part of the province. It is composed of fine-grained siliciclastic turbidites and based on its dispersal pattern is likely Gondwanan (Schenck, 1970). The Meguma terrane is intruded by granitiod plutons (William, 1979; Keppie, 1989; Clarke and Chatterjee, 1992). The largest of these plutons is the South Mountain Batholith, the largest of the Appalachian Orogen (Benn et al., 1997); Keppie and Dallmeyer (1995) suggested that these basement rocks are Precambrian, and that Palaeozoic intrusions occurred from 380-370 Ma. The South Mountain Batholith is the largest of these intrusions (Benn et al., 1997). The Meguma terrane is separated from the Avalon terrane to the north by the Cobequid-Chedabucto fault zone (Withjack et al., 1995). This fault is steeply dipping until about 6km depth (Webster et al., 1998). Together the Meguma and Avalon terranes make up the basement rocks of Nova Scotia The basement rocks of eastern Canada have recorded the history of late-Precambrian rifting, as well as the development of Palaeozoic basement rocks. These rocks formed during the opening of the Iapetus Ocean, which was a Palaeozoic ocean equivalent to the modern Atlantic Ocean. The closing of the Iapetus Ocean during the Ordovician created the Appalachian Orogen.

Rifting during the Mesozoic and the later sea-floor spreading formed the modern day North Atlantic and its passive margin system. Figure 2.1.2 shows plate

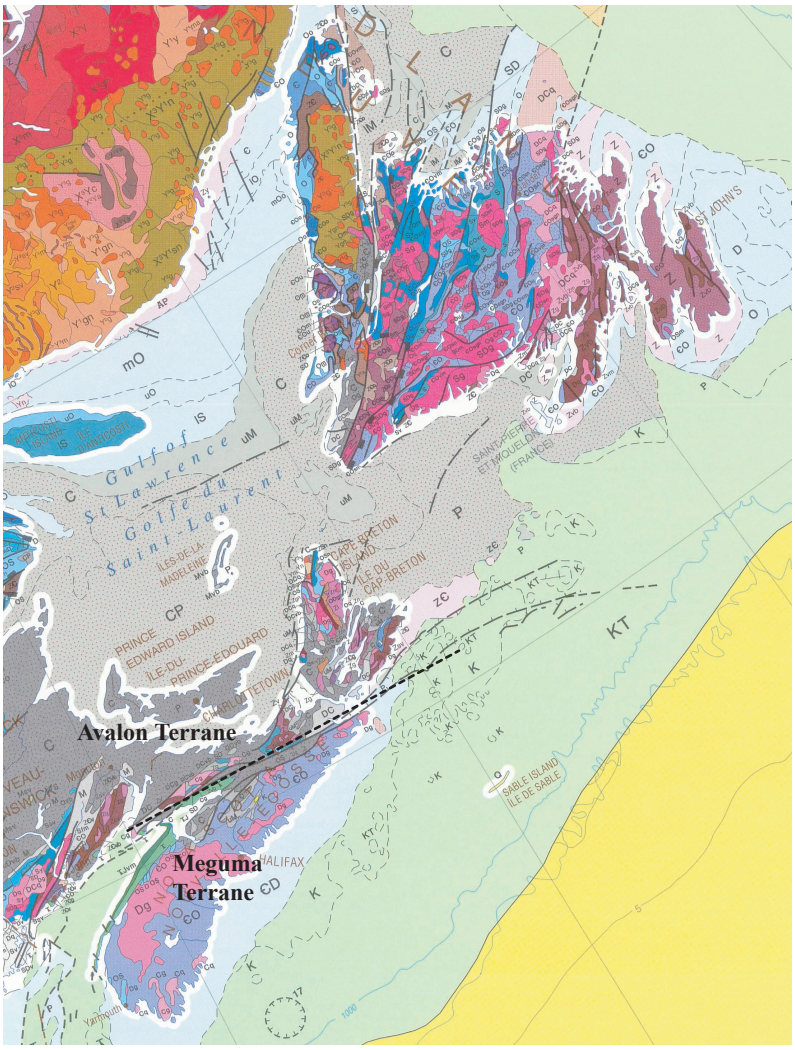

Figure 2.1.1 Geologic map of eastern Canada showing Meguma and Avalon Terranes. Black dashed line show the approximate location of the Cobequid-Chedabucto fault zone (Modfified from Wheeler et al. 1997, GSC map 1860a).

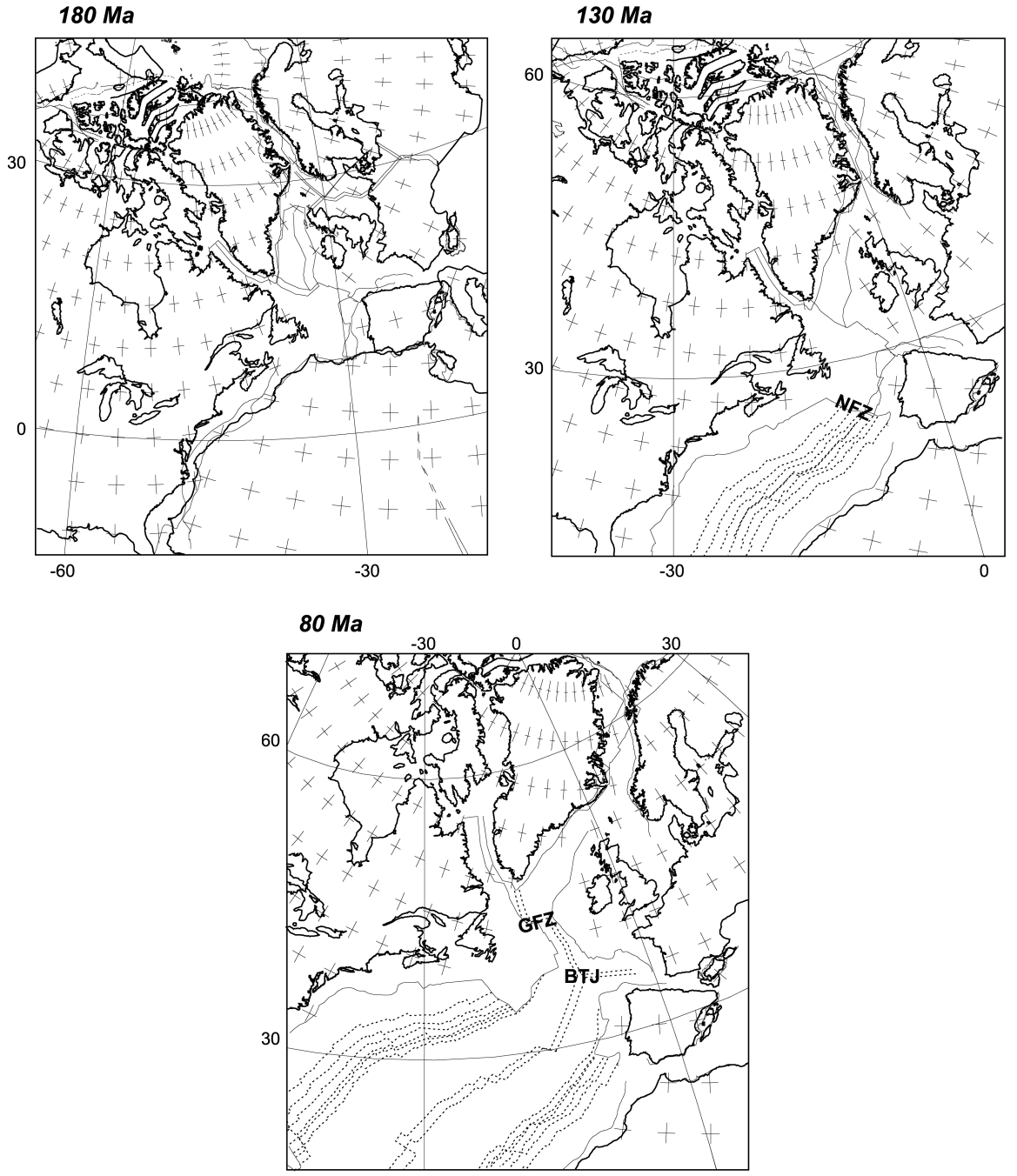

Figure 2.1.2 Plate reconstructions of the North Atlantic during the formation of the Atlantic Ocean. Panels are at 180Ma, 130Ma and 80Ma respectively. Dashed lines denote the magnetic anomalies of the ocean crust, NFZ – Newfoundland Fracture Zone, GFZ- Charlie-Gibbs Fracture Zone, BTJ- Biscay Triple Junction. (Reconstructions from Coffin et al. (1992), After Louden and Chian 1999)

reconstructions of the North Atlantic during the Mesozoic separation. The Nova Scotia margin was formed during the mid Triassic to early Jurassic (230-175Ma) when Africa and North America separated during the break-up of the supercontinent Pangea (Welsink et al., 1989). This was followed by Newfoundland margin to the north (~80Ma) (Hiscott et al., 1990; Watt, 1969; Moullade et al., 1988; Louden and Chian, 1999).

2.2 Volcanism during Rifting

There have been two periods of magmatism associated with continental rifting of eastern Canada. The first period of syn-rift magmatism occurred by intrusion during the earliest stages of rifting during the Mesozoic (214-239Ma (Pe-Piper and Jansa, 1986)). This period is represented in the rock record by alkaline dikes in the Northumberland Straight F-25 well as well as in southwest Nova Scotia (Wu, 2007). The second and more extensive period of syn-rift magmatism occurred during the main phase of Mesozoic rifting. This period of volcanism is represented by dykes and extensive lava flows; the precise dates of these dikes tend to cluster into two age groups, one roughly 191Ma and one 201Ma (Pe-Piper et al., 1992). Examples of these dikes are the Shelburne dike and the Caraquet dike. The basaltic lava flows from this period of volcanism are also featured along the shores of the Bay of Fundy. The North Mountain Basalt is one of these second stage Mesozoic flows. It has been dated using K/Ar dating to determine an age range of 195 ± 4 Ma (Armstrong and Besancon, 1970) to 200 ± 10 Ma (Carmichael and Palmer, 1968).

During the Cretaceous, volcanism was present along the Nova Scotia margin. However, this volcanism was associated with the production of new oceanic crust along the Mid Ocean Ridge (MOR).

Although the Scotia margin does display some volcanism during rifting, compared to margins classified as volcanic the magnitude of this volcanism is very minor. These periods of volcanism during rifting are different than the volcanism associated with seafloor spreading following the rifting process.

2.3 Previous Seismic Studies

The Nova Scotia margin has been extensively studied for both academic and commercial purposes; however, there are few regional lines. Figure 2.3.1 is a map showing the seismic lines of the Nova Scotia margin. The margin was first imaged using seismic reflection lines. Keen and Potter (1995a) used three multichannel profiles (89-3, 89-4 and 89-5) to investigate the volcanic portion of the rifted margin off the coast of eastern Canada. Figure 2.3.1 shows that line 89-3 runs across the ECMA and line 89-5 runs along the trend of the ECMA. The ECMA has been shown to be associated with a Jurassic volcanic wedge which is characterized by seaward dipping reflectors (SDR) found just below the basement (White et al., 1987). The SDR are similar to volcanic reflectors found worldwide along volcanic rifted margins. These have been drilled, for example in the North Atlantic, and found to be subaerially extruded basalts that were extruded at the start or just prior to the start of seafloor spreading (Eldholm et al., 1989). Along the US margin, this volcanic wedge is underlain by a high velocity layer thought to be the addition of new igneous material during and just after rifting (Austin et al, 1990;

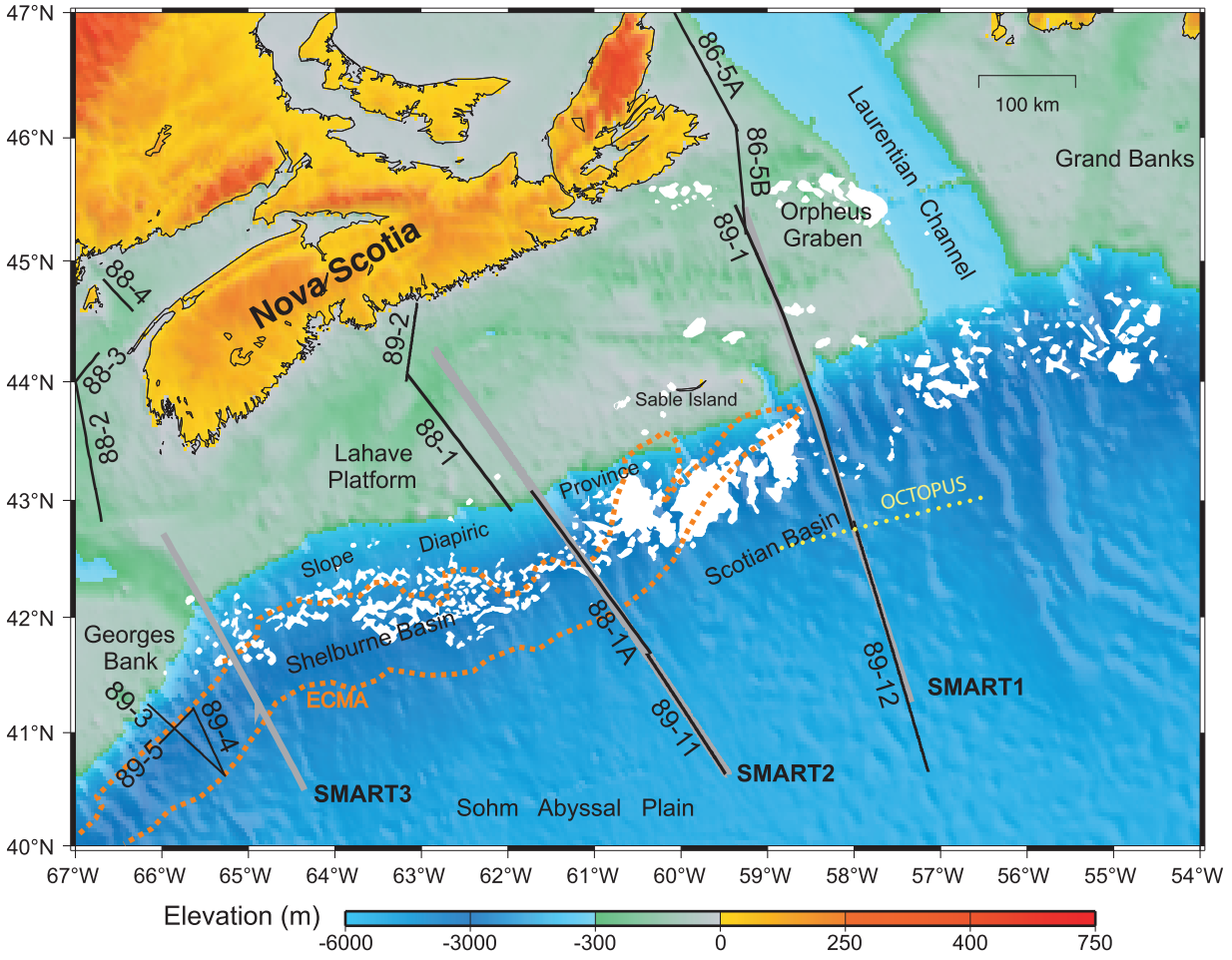

Figure 2.3.1 Map of the Scotian margin showing previous seismic reflection profiles. Previous seismic reflection profiles include 88-1, 1A (Keen et al. 1991b), 88-2 (Keen et al 1991a), 89-1 (Keen and Potter 1995a), 89-3, 4, 5 (Keen and Potter 1995b), BGR lines 89-11 and 89-12 (unpublished, data courtesy the German Federal Agency of Geosciences and Nature Resources). Grey lines show the position of the wide angle refraction/reflection SMART lines 1, 2, and 3. Yellow dotted line shows position of the OCTOPUS line.The orange dotted region shows the ECMA; and the white area denotes the salt distribution along the slope diapiric province (After Wade and MacLean 1990).

Sheridan et al., 1993). Keen and Potter (1995a) examined lines 89-3, 89-4, 89-5 (shown in Figure 2.3.1) and observed SDR at depths of 2.5 to 5km, and a total width of about 65km. Figure 2.3.2 is a line drawing of line 89-3 showing the SDR identified by Keen and Potter (1995a). Keen and Potter (1995a) determined that properties of the SDR along these lines could be explained by the continuous accretion of igneous and sedimentary material in a subsiding and widening rift zone. They also determined that the SDR package was comparable to the observed SDR on other rifted margins such as the eastern US margin, which is known to be volcanic, thus showing that this southern part of the margin is volcanic in nature. They did identify that the main difference was the thickness of these SDR; however, they also indicated that this thickness is limited by the depth of the first water-borne multiple reflection in their data. Keen and Potter (1995a) also attempted to construct a model for the ECMA including their observations. From these models they came to the conclusion that a wide range of structures could be responsible for the ECMA; and that a strongly magnetized SDR zone with the observed dimensions is most likely the largest contributor.

Keen and Potter (1995a) also discussed the transition between volcanic and nonvolcanic margin types within their study area. To the north of their study area the ECMA weakens and disappears (Fig. 2.3.3). The wedge of SDR also disappears in this area. They concluded that as the presence of SDR disappears northeast of B (shown in Figure 2.3.3) a major along-strike change must occur in the margin, from a volcanic margin in the south to a nonvolcanic margin in the north. Keen and Potter (1995a) also argue that the weakened ECMA starting at point B in Figure 2.3.**3** could also arise from an edge effect between the continental and oceanic crust. At point B, the change in the

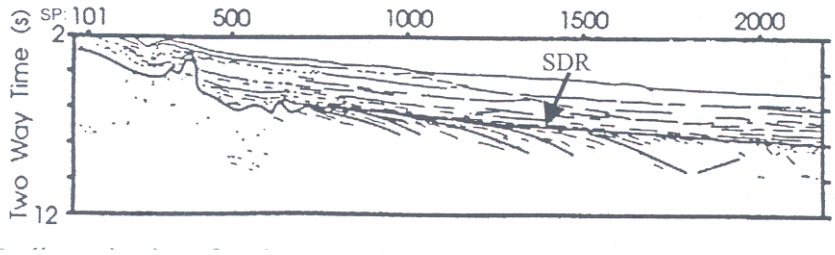

Figure 2.3.2 Line drawing on MCS line 89-3 showing SDR idenitified by Keen and Potter (1995a) at depths of 2.5-5km. See Figure 2.3.1 for line location (After Keen and Potter (1995a) and Wu (2006).

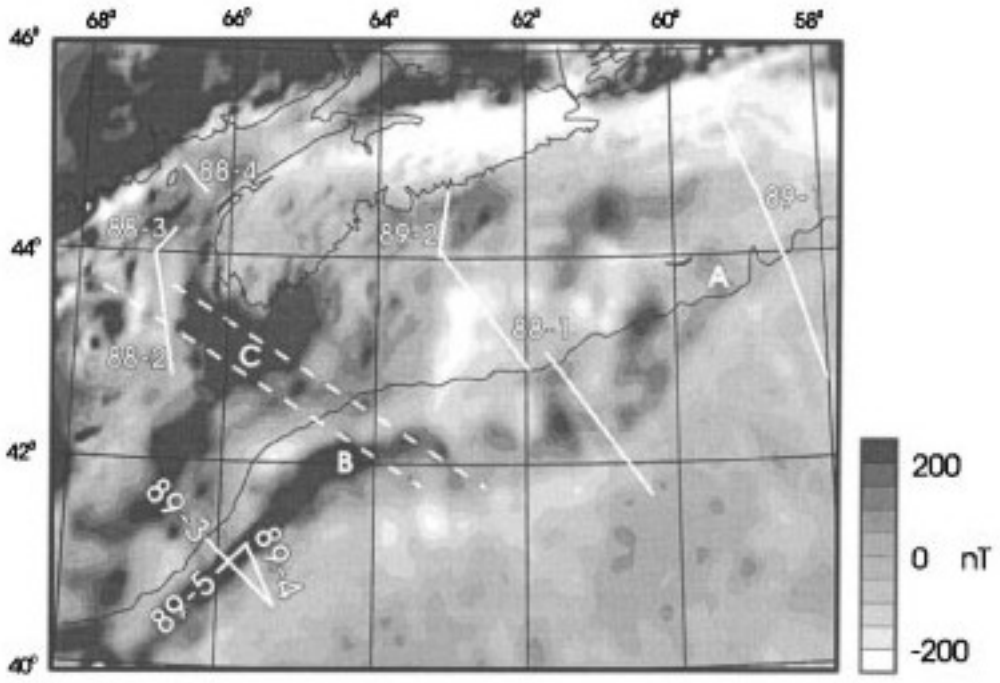

Figure 2.3.3 Magnetic anomaly map of Nova Scotia margin with locations of AGC seismic reflection lines. The 500-m bathymetric contour (black line) indicates the shelf break. Showing locations of lines 89-3, 89-4, 89-5 studied by Keen and Potter 1995a, and the weakening of the ECMA after point B (After Keen and Potter 1995a).

ECMA could be associated with the landward migration of the Jurassic marginal carbonate reef which occurs around the same locale. The presence of Triassic aged salt diapirs also increases northeast of point B. Both of these points Keen and Potter (1995a) thought may indicate greater subsidence in this northeast area, indicating perhaps that subsidence was more important than volcanism during rifting.

Keen and Potter (1995a) also examined the width of the transition zone and its relation to the presence of volcanism during rifting. They determined that to the south of their study area, along the US margin where the ECMA and SDR are still pronounced, the transition from thick continental crust to thin oceanic crust occurs rapidly; the transition zone is only tens of kilometres. Contrasting this is the transition along the Nova Scotia margin where the continental crust thins more gradually causing the transition zone to be over 100 km wide.

Moving towards the northern portion of the region away from where the SDR package has been identified, Keen and Potter (1995b) also examined the formation and evolution of the Nova Scotia rifted margin using deep seismic reflection line 89-1 (location shown in Figure 2.3.1). As is visible in this figure, Line 89-1 runs across the margin, crossing the deepest part of the Scotian Basin as well as extending into the oceanic regions of the crust, thus allowing the OCT to be imaged. They determined that a 100-km wide zone of thin crust lies below the continental slope and rise along line 89-1; this crustal layer is overlain by syn-rift sediments. Keen and Potter (1995b) thought this crustal layer to be a syn-rift feature, not a product of seafloor spreading. They also determined from line 89-1 that the continent-ocean crustal boundary lies at the seaward (eastern) end of this wide thinned crustal layer. Figure 2.3.4 is a line drawing and

interpreted line drawing of line 89-1 showing the different layers identified by Keen and Potter (1995b) including the OCT.

More recently, Funck et al. (2004) created a P-wave velocity model from the data collected from a wide-angle seismic survey along the SMART1 line, which runs across the Nova Scotia continental margin through the Scotian Basin. The SMART1 line is coincident with line 89-1 discussed earlier by Keen and Potter (1995b). Line SMART1 is shown in Figure 2.3.5.

Funck et al. (2004) observed a 150-km-wide transition zone between thinned continental crust and oceanic crust (the OCT) in this area. The 5-km thick lower layer of this wide transition zone was observed to have velocities from 7.2 to 7.6km/s and they interpreted it as partially serpentinized mantle (PSM). The P-wave velocity model created by Funck et al. (2004) is shown in Figure 2.3.6.

Towards mainland Nova Scotia, the 5-km thick lower layer is partially overlain by highly altered continental crust displaying velocities of 5.4km/s. Farther towards the east (seaward) of this OCT zone, Funck et al. (2004) observed the upper layer with 5.1km/s P-wave velocities, interpreted as exhumed and highly serpentinized mantle (HSM). The lower layer here is separated from the upper layer by the presence of subhorizontal reflectivity.

Figure 2.3.6 displays the P-wave velocity models of both SMART1 (Funck et al., 2004) and SMART2 (Wu et al., 2006) lines and therefore displays the along strike variations of the Nova Scotia margin. Wu et al. (2006) discussed the SMART2 line and its comparison to the SMART1 model of Funck et al.(2004). Wu et al. (2006) determined that both models display nonvolcanic characteristics for the northeastern part

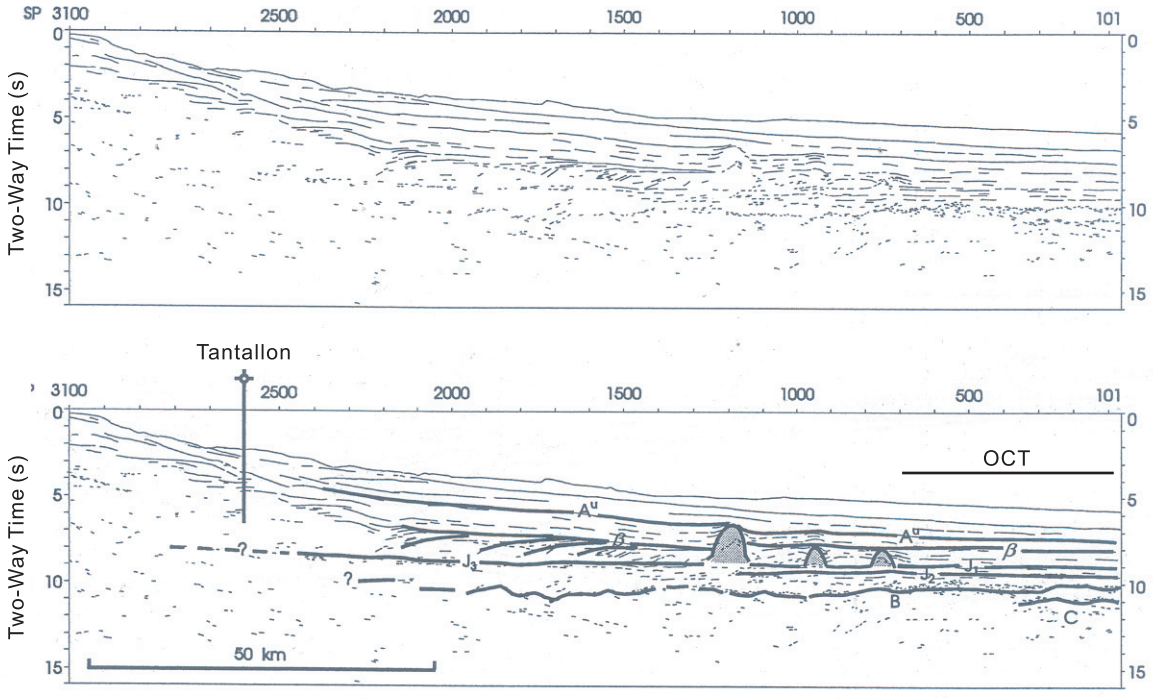

Figure 2.3.4 Line drawing (upper) and interpreted line drawing (lower) of MCS line 89-1. Heavy lines and lettering in lower drawing are interpretations. OCT is labled in lower drawing. (After Keen and Potter 1995b).

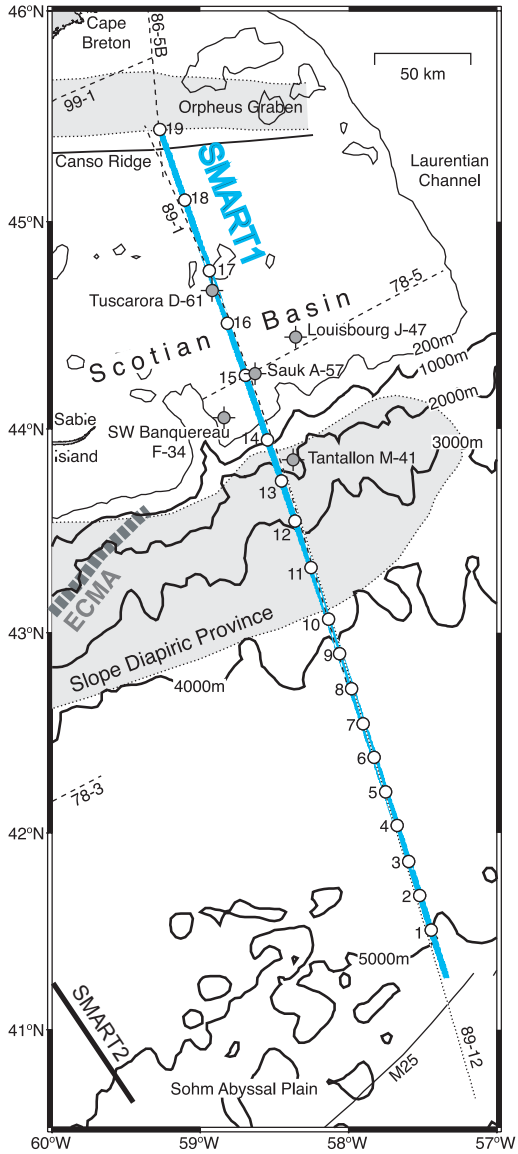

Figure 2.3.5 Detailed location map of SMART line 1 (in blue) with OBS postitions marked and numbered. (After Funck et al., 2004).

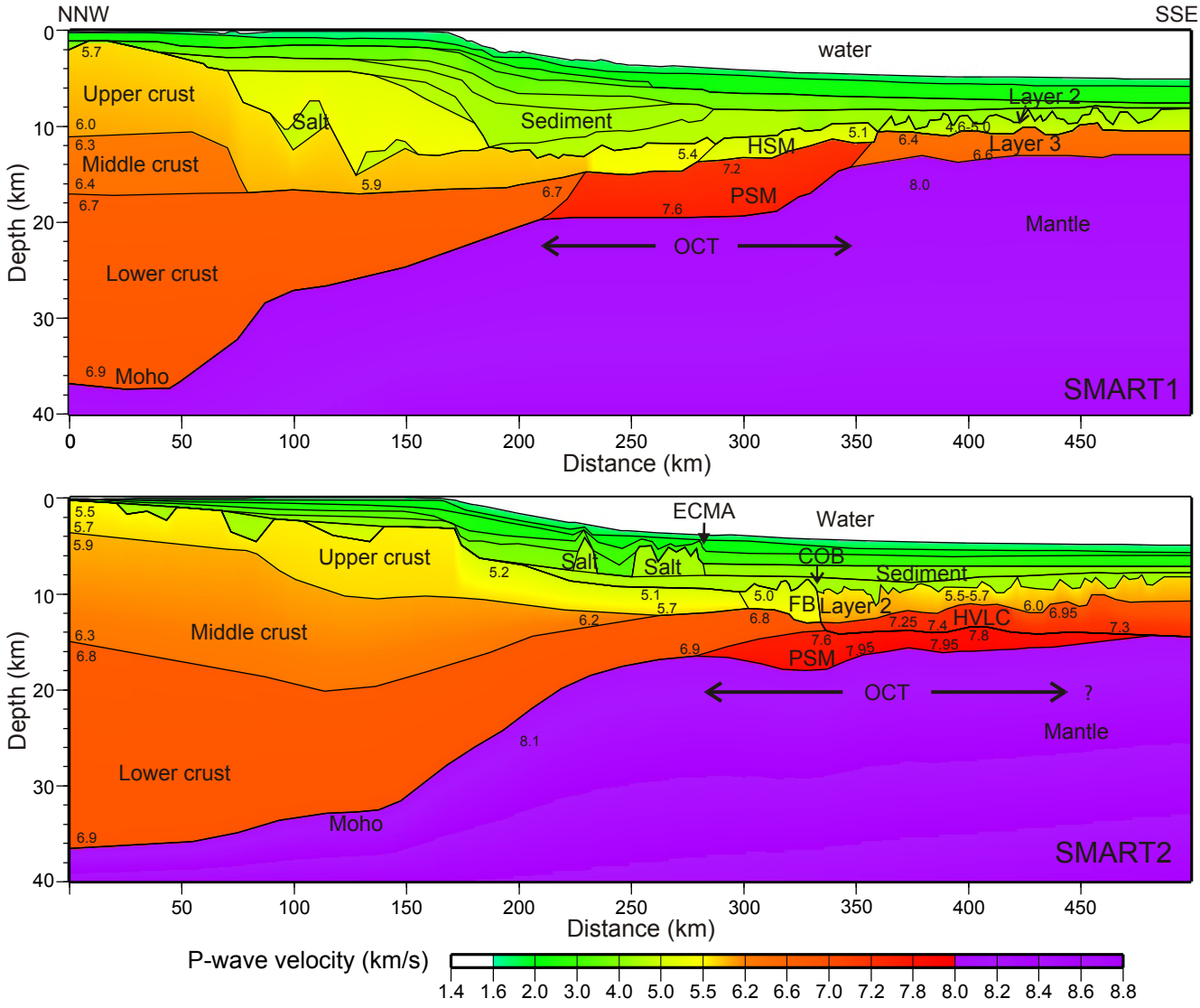

Figure 2.3.6 P-wave velocity models of SMART lines 1 (upper) and 2 (lower) as modeled by Funck et al. (2004) and Wu (2006), showing along strike margin variations in the OCT. Abbreviations HSM: highly sperpentinized mantle; PSM: partially sperentinized mantle; HVLC: high velocity lower crust; ECMA: east coast magnetic anomaly; FB: faulted blocks; COB: continent-ocean boundary. See Figure 2.3.1 for line locations (After Wu, 2006).

of the Scotian margin; however, they display significant differences due to differences occurring during the continental extension and the transition to seafloor spreading. There are two different time phases in the margin formation that these differences fall into as discussed by Wu et al. (2006); rift-to-drift and syn-rift transitions. In the rift-to-drift phase it is apparent from the P-wave velocity models that both SMART1 and SMART2 show an OCT zone (as seen in Figure 2.3.6). The OCT zone along the SMART2 line consists of a PSM overlain by a highly faulted continental crust to the northwest and oceanic crust to the southeast (Wu et al., 2006) and thin oceanic crust forms immediately seaward of continental break-up. SMART1 has a 70-km wide upper layer of exhumed and HSM with an overlying PSM layer (Wu et al., 2006). Wu et al. (2006) suggest that this indicates that at the time of break-up there was only limited magma generation across the central margin while no melt was created across the north segment of the Scotian margin. Wu et al. (2006) also compared the velocities of the OCT layer in SMART1 and 2; along SMART1 the OCT is ~ 6km thick with velocities from 7.2 – 7.6 km/s. Along SMART2 in the corresponding layer is roughly 4km thick and has higher P-wave velocities of 7.6 –7.9 km/s; suggesting that there is a relatively low degree of mantle serpentinisation along SMART2 and a higher degree of mantle serpentinisation along SMART1 (Wu et al., 2006).

Wu et al. (2006) also discusses the thickness of the oceanic crust along SMART1 and 2 and how this relates to the amount of magmatism after the initiation of seafloor spreading. Along SMART1 the oceanic crust is only ~4km thick as compared with normal oceanic crustal thicknesses of 7.1±0.8km (White et al., 1992). Wu et al. (2006) suggests that this indicates that the margin was magma starved after the initiation of

seafloor spreading. SMART2 displays a more normal oceanic crustal thickness of 5–7km (2–3km thicker than along SMART1) which is thicker than expected as it has mantle material incorporated into the high velocity lower crust (HVLC) layer, suggesting that it could have oceanic crustal thickness of around 4km. Wu et al. (2006) interpreted this crustal thickness variation to imply that an increase of magma supply occurred in the central margin as compared to the northern margin.

In the syn-rift phase of crustal thinning Wu et al. (2006) discusses the differences in the thinning of continental crust as calculated from the velocity models of SMART1 and 2. SMART2 shows that the continental crust underwent approximately 5km of gradual thinning over the outer continental shelf, with rapid thinning across the continental slope into the ocean basin (Wu et al., 2006). Contrasting this, SMART1 shows a dramatic thinning of continental crust right from the onset of rifting. This dramatic thinning was followed by a gradual thinning to the ocean basin (Wu et al., 2006). This dramatic thinning along SMART1 (in the northern segment of the margin) has given rise to rapid subsidence and the formation of the deep Sable Basin seawards of the hinge line. Wu et al. (2006) also discusses that these results are basically in agreement with the thermal-mechanical modeling results for the margin (Keen and Beaumont, 1990).

Wu et al. (2006) also discusses these results in relation to the ECMA. Figure 2.3.7 shows how the magnetic anomaly changes in width and sharpness along the eastern seaboard of North America. Wu et al. (2006) discusses how the magnetic anomaly becomes narrower and sharper as it approaches the southwest Scotian margin, thus suggesting a narrower zone of volcanism in this area (panels i-e in Figure 2.3.7).

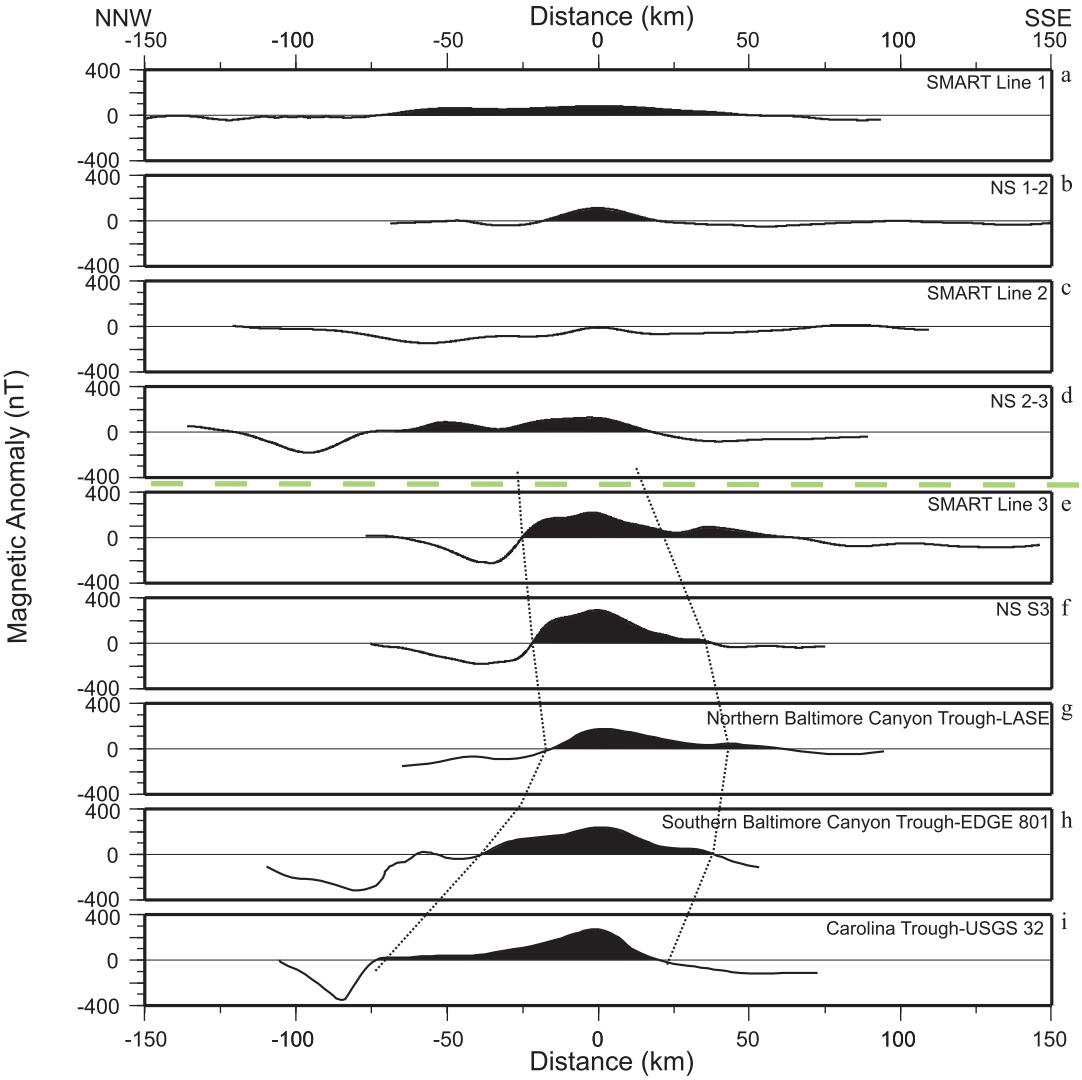

Figure 2.3.7 Changes in magnetic anomaly along the northeastern rifted margin of North Ameria, showing the distincitve change in width and amplitudue of magnetic anomlay between the SMART3 l and NS 2-3 lines. The ECMA is outlined with dotted lines, the green dashed line shows the location of this change. (After Wu, 2006).

Continuing on northward the magnetic anomaly becomes weaker (reduced amplitude) and broader (panels d-a in Figure 2.3.7), thus suggesting that the source of the anomaly changes in character between lines SMART3 and SMART 2**.** Wu et al. (2006) suggests that the weaker magnetic anomaly indicates that igneous material was not emplaced in this area. This conclusion is consistent with the P-wave velocity models of SMART1 and 2 in which no underplated material was identified in the OCT.

Keen et al. (1991) were interested in determining the variations in deep crustal structure across the COB and the Scotia Basin (a rifted sedimentary basin which occupies the outer continental shelf and slope). They used two deep seismic reflection line (88-1 and 88-1A) which together span the rifted margin from continental crust unaltered by rifting to the ocean basin. Figure 2.3.1 shows the locations of the lines; the break between the two lines occurs because fishing activity near the shelf break obstructed the program (Keen et al., 1991). Figure 2.3.8 is a line drawing of the composite profile of 88-1 and 88-1A. This figure shows some of the features identified by Keen et al. (1991) along the composite line. One of the most interesting features that this figure highlights is the detachment faults (DF) around the depth of the Moho (M) overlain by normal faults (NF). This normal faulting Keen et al. (1991) determine is associated with extension during rifting and the formation of basins. However, the lower faults (DF) suggest that during rifting extension in the lower crust is localized along a single large fault zone (Keen et al., 1991). Keen et al. (1991) identify that this double shear model is attractive as it explains how extension in the lower crust occurs below basin-bounding faults. It also partially explains why this extension has not produced a layered lower crust. However, a weakness in this model lies in that the upper shear zone is not seen in the reflection data.

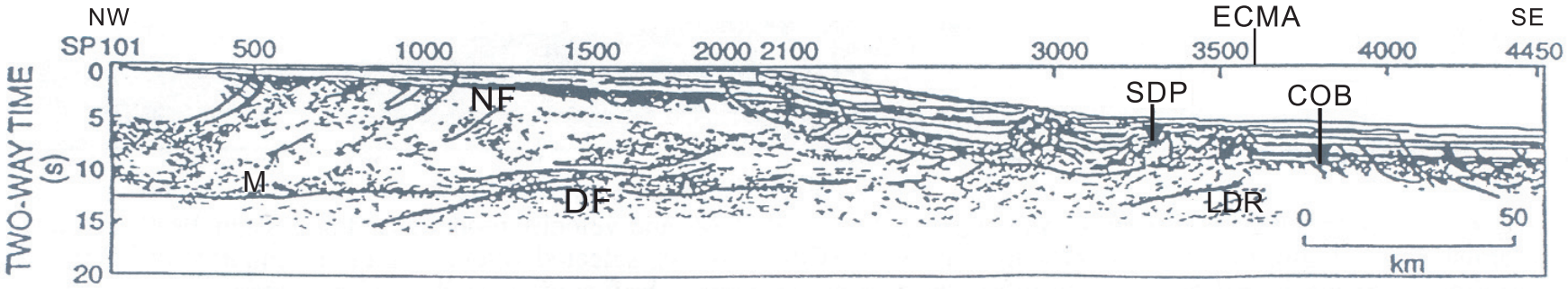

Figure 2.3.8 Line drawing of composite profile of seismic reflection lines 88-1 and 88-1A. Abbreviations SDP: slope diapiric province; COB: continent-ocean boundary; M: Moho; NF: normal faults; DF: detachment faults; LDR:landward dipping reflection; ECMA: east coast magnetic anomaly. See Figure 2.3.1 for line location (After Keen et al., 1991 and Wu, 2006).

Keen et al. (1991) do suggest that as there is no well established relationship between shearing and reflectivity this is an area for further investigation.

Keen et al. (1991) examine the COB along the composite line. They explain that the Slope Diapiric Province (SDP) masks the lower crustal structures below it; but on either side of the SDP the crustal structures are well defined in this line. Relying on earlier seismic and magnetic studies (such as Keen et al., 1975 and Jansa and Wade, 1975) they place the COB just seaward of the SDP. Keen et al. (1991) deduce that although the crustal structure below the COB is unclear, due to the presence of salt and water-bottom multiples, the landward dipping reflections below the SDR may represent magmatic underplating of thinned continental crust during rifting. The landward dipping reflection is labeled as LDR in Figure 2.3.8**.**

In the southern segment of the Nova Scotia margin lie the refraction lines SMART2 and 3. Funck et al. (2004) also briefly discussed along strike variations of the margin, by equating previous studies to what may be seen on SMART 2 and 3. SMART3 is located just 60km north of multichannel seismic (MCS) lines 89-3 and 89-4 (Fig 1.2.2). The ECMA changes nature and direction just north of SMART3, as shown in Figure 1.2.2, and runs SW-NE up to SMART2. SMART line 2 runs parallel to MCS line 88-1A, along which no SDR were identified (Keen et al., 1991); however, the salt structures of the SDP could be hiding the SDR. If this is not the case, then Funck et al. (2004) suggests that the volcanic extrusives making up the SDR may die out between SMART line 3 and line 2.

The combination of these previously studied seismic lines leads to the general conclusion that there is a reduction in the amount of volcanism during rifting towards the

north of the Scotian margin. However, with this reduction in volcanism and the disappearance of the SDR package, comes a high velocity layer (of unknown origin). There have been two very different interpretation of the composition of this layer: (a) it is a serpentinized body beneath a thinned crust, or (b) it is a volcanic body formed by underplating. The rock produced by both of these interpretations have very similar seismic velocities, making it difficult to determine the correct interpretation from seismic imaging. Thus raising the question of, which rock type is it?

CHAPTER 3: DATA AND METHODS

3.1 Data Collection

The data used to investigate the anisotropy of the high velocity layer was collected along the OCTOPUS line collected in November (7^{th}-17^{th}) 2010 on board the R.V. Strait Explorer. Along the OCTOPUS line 20 identical ocean bottom seismometers (OBS), built and owned by Dalhousie University Department of Oceanography and Geologic Survey of Canada were deployed. The station numbers, positions, water depth and OBS instrument identification can be seen in Table 3.1.1. The instruments were deployed at 10km intervals, making the OCTOPUS line 200km plus a 20 km lead-in on each end, thus creating a total line length of 240km. It is necessary for shots to be fired on the line before approaching the first OBS station (a lead-in) so that there are many shot fired over each OBS. This allows for the structures below the first and last OBS to be imaged properly.

This line is shown in Figure 3.1.1. This detailed map also shows some of the other seismic lines in the area, most notable to this study is the line SMART1 which is roughly perpendicular to the OCTOPUS line. (For a more detailed regional map refer back to Figure 2.3.1.) Figure 3.1.1 also shows the deployment positions of the 20 OBS. For this study, as we were interested in the area where SMART1 and OCTOPUS lines cross, we focused on only three OBS stations: 11, 13, and 14. Station 12 was omitted even though it was in the target area because during initial processing it was found to be very noisy. For the purposes of this study I will be referring to, for example, OBS 13, indicating the data from the instrument associated with OBS station 13 (as correlated in Table 3.1.1).

Station Number	Deployment Position			Deployment
	Latitude	Longitude	OBS instrument	Water depth (m)
1	43.033	56.547	GSC-A	3847
2	43.012	56.671	GSC-B	3868
3	42.991	56.791	GSC-E	3970
4	42.969	56.913	GCS-H	4104
5	42.947	57.034	GSC-J	4160
6	42.926	57.156	GSC-K	4292
7	42.904	57.278	GSC-L	4144
8	42.882	57.4	GSC-M	4230
9	42.86	57.521	GSC-S	4286
10	42.838	57.643	GSC-Z	4497
11	42.815	57.764	DAL-A	4379
12	42.792	57.885	DAL-B	4271
13	42.77	58.007	DAL-C	4227
14	42.747	58.131	DAL-D	4212
15	42.725	58.249	DAL-E	4092
16	42.702	58.369	DAL-G	4150
17	42.678	58.49	DAL-I	4210
18	42.655	58.611	DAL-J	4332
19	42.632	58.732	DAL-K	4285
20	42.608	58.852	DAL-N	4245

Table 3.1.1 Summary of the OCTOPUS line stations, OBS deployment positions, OBS instrument at each station, and water depths.

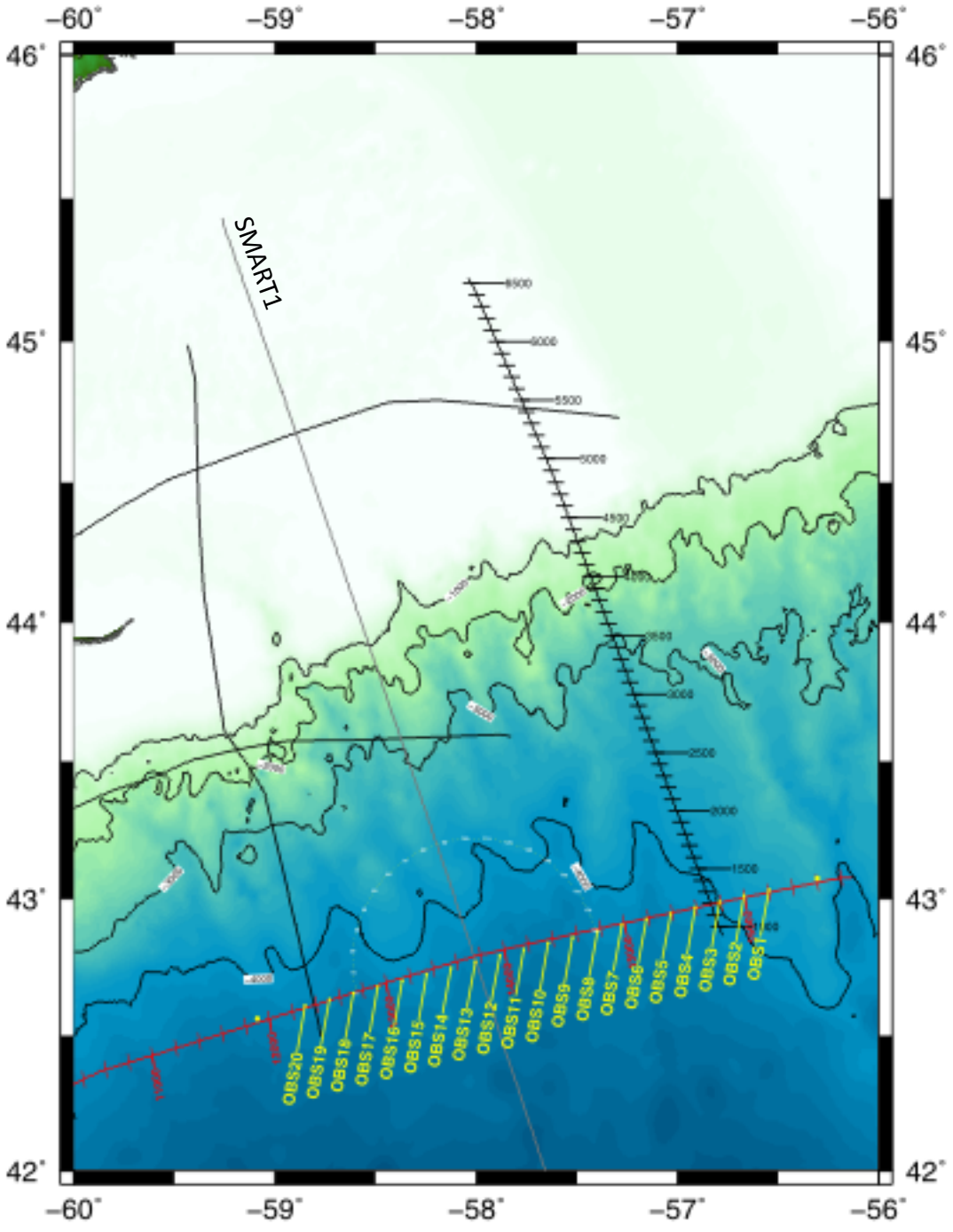

Figure 3.1.1 Bathymetric map of the OCTOPUS line (red). OBS drop locations are labeled in yellow, begining and end of line are unlabeled yellow dots.Light grey line is the SMART1 line. The numbered black line is the GeoPro line. Bathymetirc contours are labeled black lines.

Also visible in Figure 3.1.1 is the location of the GeoPro line to the west of the SMART1 line; these data are also available to be used, but lie outside the target area of this honour's thesis.

The energy source for this survey was an eight airgun array. The airguns were arranged in two clusters of four guns, towed at a depth of 7m. Each gun was 0.852L, with all eight guns producing a total volume of 6.82L of compressed air. During shooting, one gun in each of the two clusters broke; however, the pressure of the other guns was increased from 2700 PSI to 3000 PSI in order to compensate. Throughout the shooting, the guns were fired at 60 second intervals. Figure 3.1.2 is a picture of the two airgun clusters before they were deployed (a) and after recovery **(**b).

OBS and shot locations were determined by the Global Positioning System (GPS). Water depths along the profile were recorded using the ship's echosounder; however, this was not working properly during the majority of the cruise. As a result of this problem, water depths were found from heat-flow measurement data collected along the same line where very accurate water depths were present at specific locations. From this a correction was applied to the other depths to make them more accurate.

The 20 OBS were deployed for a period of six to seven days. Figure 3.1.3 is a photograph of an OBS before it was deployed. All the instruments are identical with a height of 1.1 m, length of 1.2 m and are 0.6 m wide. Each OBS has a weight of 82 Kg plus the 55kg attached anchor. Each OBS has a hydrophone and 3-component 4.5 Hz geophone and a 12.5 kHz pinger. After the shooting part of the experiment was concluded, the OBS were "pinged" (signaled) to release from their anchor and then the

Figure 3.1.2 (a) One airgun cluster (4 guns) prior to deployment with floats attached. **(b)** One airgun closter (4 guns) after gun recovery, support frame is partially broken. In both cases airguns and frame are secured to the shitp deck. Parts of the airgun system are as indicated in figure. (Photographs taken by (a) Maria Whitehead (b) Louise Watremez).

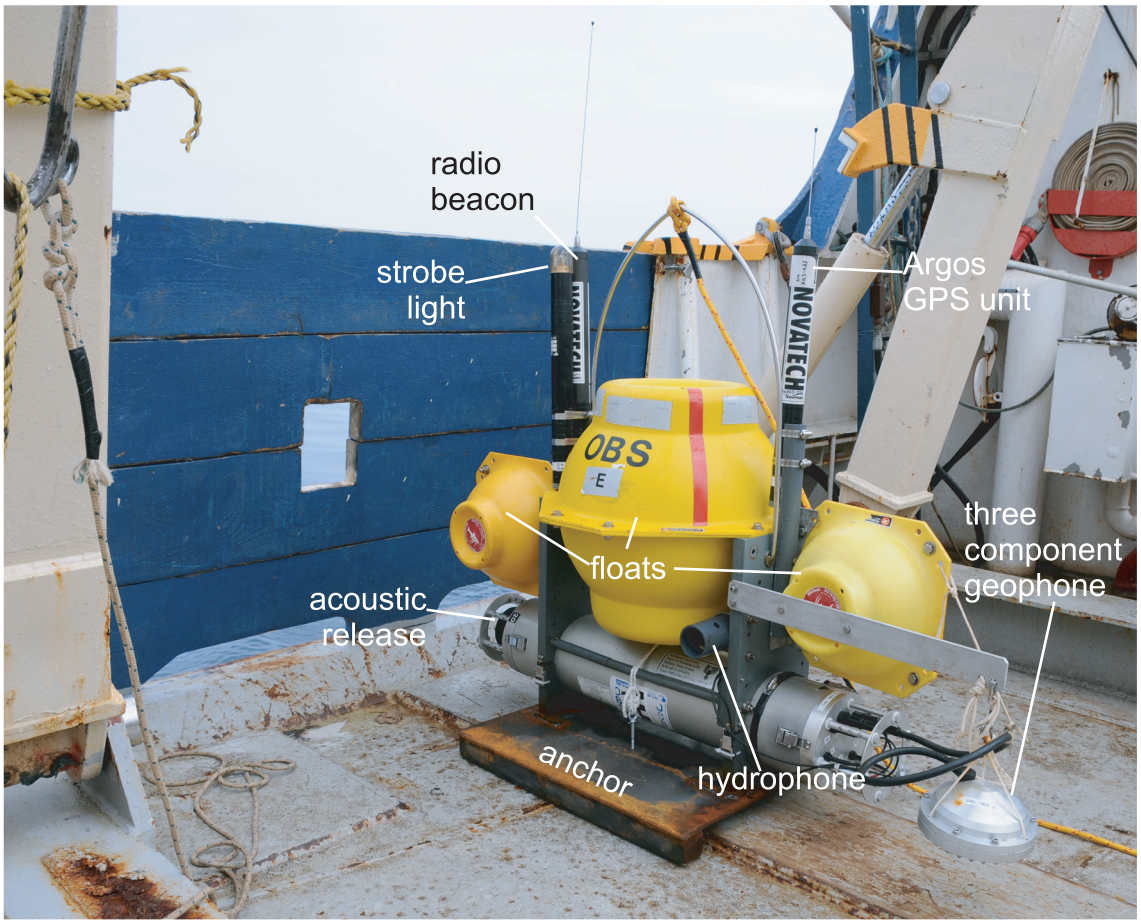

Figure 3.1.3 An OBS prior to deployment. Features are indicated in figure include: the radio beacon, the strobe light, the Argos GPS unit, the acoustic release, the floats, the hydrophone, the anchor and the three component geophone. (Photograph taken by Mladen Nedimovic).

floats provide each instrument with enough buoyancy to surface. The OBS rise to the surface at a rate of approximately 1 m/s. Each OBS is also set up with a secondary (or backup) release. That is, they are all programmed to release from their anchor at a certain date and time even if they have not been pinged. Each OBS is also equipped with a strobe light, a radio beacon, and an Argos GPS unit. Each OBS has a different Argos serial number; the pinger codes and radio channels are not unique to each OBS, but are spaced accordingly so that no two neighbouring OBS have the same ones (allowing for relative certainty that they will not interfere with one another). The Argos GPS system (ARGOS) works in connection with an Argos website, which will display the position of each OBS once they are observed by the satellites equipped with the Argos technology (transmitter). This system is used in the event that they cannot be found in their predicted recovery position. On this cruise two OBS (stations 6 and 7) did not respond to their pinging, popped up on their secondary release and were located using the Argos system. The radio beacons on each OBS are used to aid in recovery by using radio direction finders. The strobe lights make night OBS recovery very easy, as once surfaced the OBS can be seen from great distances. On this cruise all 20 OBS were successfully recovered.

3.2 Data Processing and Methodology

The processing and methodology used for this project followed a five step progression. Initially, the three OBS being examined were repositioned. Data files were then created in SEGY format for these three OBS with the new positions and offsets. SEGY format standard was developed by the Society of Exploration Geophysicists (SEG) for storing seismic data (traces) and header information (Barry et al., 1975).

Filtering was then applied to reduce noise, remove any bias; deconvolution was also applied. Deconvolution is step in seismic processing that improves the resolution of the seismic data by compressing the basic wavelet; it can also have the effect of removing a significant part of the multiple energy (Yilmaz, 1987). Finally, using Funck et al. (2004) SMART1velocity model as a base, a 1D model was created for one OBS.

Initially raw OBS data was downloaded from each OBS. Corrections for gun offset, gun delay and OBS clock drift were then applied. A correction for gun offset needs to be applied to correct for the offset of the guns from the GPS antenna on the ship, which is used to identify the position of each shot. Without applying this correction, the recorded locations of the shots would not be correct. Correcting for gun delay corrects for the mechanical lag time between the computer instructing the guns to fire and the firing of the guns. The clocks within an OBS will drift (they run either faster than standard time or slower) over the period of time when they are in the water. Correcting for this clock drift must be done in order to get results which are consistent with the ship's time.

3.2.1 OBS repositioning

OBS repositioning is required because the deployment position is not necessarily the same as the OBS position on the seafloor. As the OBS sinks, it will drift away from this initial position to the actual position where it collects data. To relocate the three OBS being examined here, first I picked the direct wave arrival using the GLOBE Claratis software. The actual relocation of each OBS is done using a Matlab based software routine (obsloc). For the purpose of OBS relocation a Conductivity-Temperature-Depth (CTD) cast was conducted while at sea at the start of the line at 42°33.88'N and

59°05.78’W; this was used to make a water column velocity profile. This profile is shown in Figure 3.2.0. Obsloc uses the water velocity data collected by the CTD cast, the shot tables and the direct wave arrivals to calculate the most likely position of each OBS. (Details of the obsloc program can be found in Appendix A.) This process must be done individually for each OBS. The relocation of OBS station 13, instrument DAL-C (OBS 13) is shown in Figure 3.2.1.1 (OBS stations 11 and 14 are shown in Appendix A). The errors of these relocated positions are from 0.0098 to 0.0129. From these new locations, new SEGY files must be created with the new positions and offsets of the OBS.

3.2.2 Noise reduction and filtering

The first step in noise reduction and filtering is to perform a data debias on all channels (1, 2, 3, and 4) of all three OBS. I did this using the program Seiswide. Seiswide is a program designed for displaying, processing, and ray tracing seismic data. The data can be wide-angle refraction (like the OCTOPUS data) as well as MCS or sonobuoy data in SEGY file format. A data debias must be performed on the initial data to shift the data so it is centered on zero amplitude. The debiased data of OBS 13 channel 2 is shown in Figure 3.2.2.1, OBS 13 channel 1, 3 and 4 and OBS 11, 14 all channels are shown in Appendix A. All raw data is also shown in Appendix A. After the data has been debiased it was then filtered to remove unwanted noise. In this case, I used a bandpass frequency filter removing all frequencies below 2-3 Hz and above 20 Hz. A filter of these frequencies was used because the signal we assume is between 2 to 9 Hz and all other amplitudes are noise. The filtered data of OBS 13 channel 2 is shown in Figure 3.2.2.2, OBS 11 and 14 (channel 2) can be found in Appendix A.

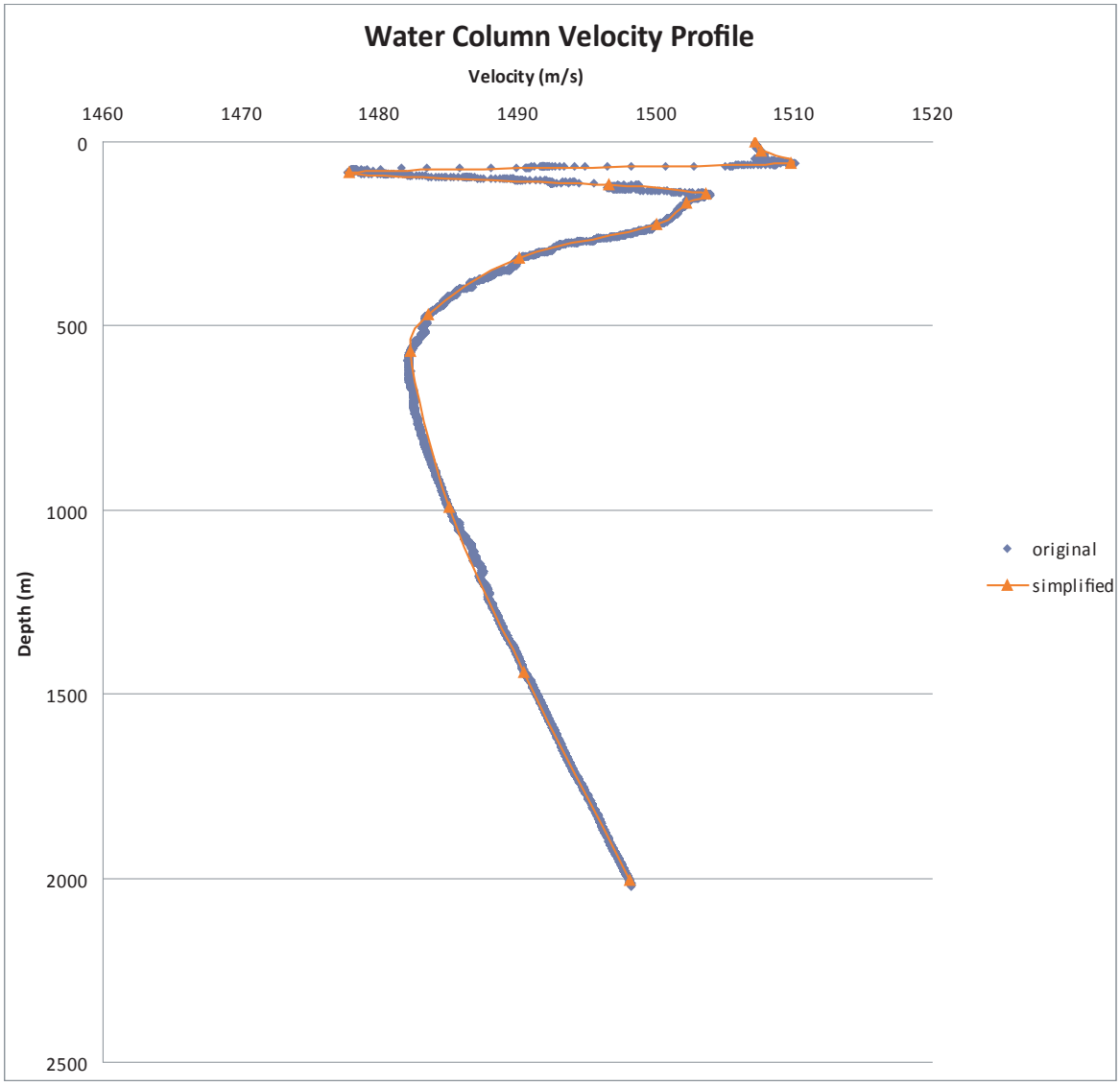

Figure 3.2.0 Water column velocity profile computed from Conductivity-Temperature-Depth (CTD) cast.

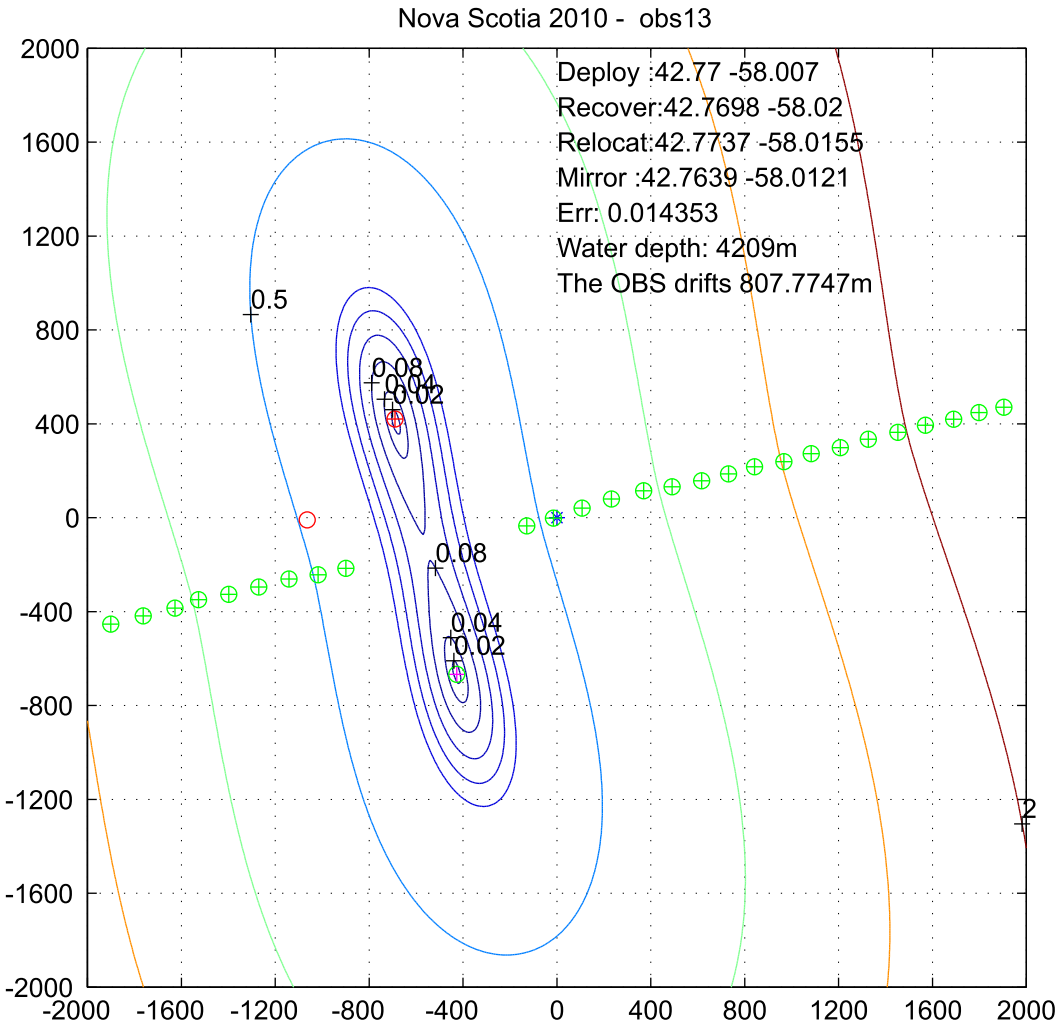

Figure 3.2.1.1 Relocation of OBS 13 in Matlab. Blue star indicates deployed position, open red circule indicates recovery position, green cricles with crosses are shot points along the OCTOPUS line, and the red cricle with cross is the relocated position. Deployment postition, recovery postion and relocated position are shown in latitude and longitude in the upper right corner as well as the calculated error, and water depth. The drift of the OBS from its deployment position to its relocated position is also shown.

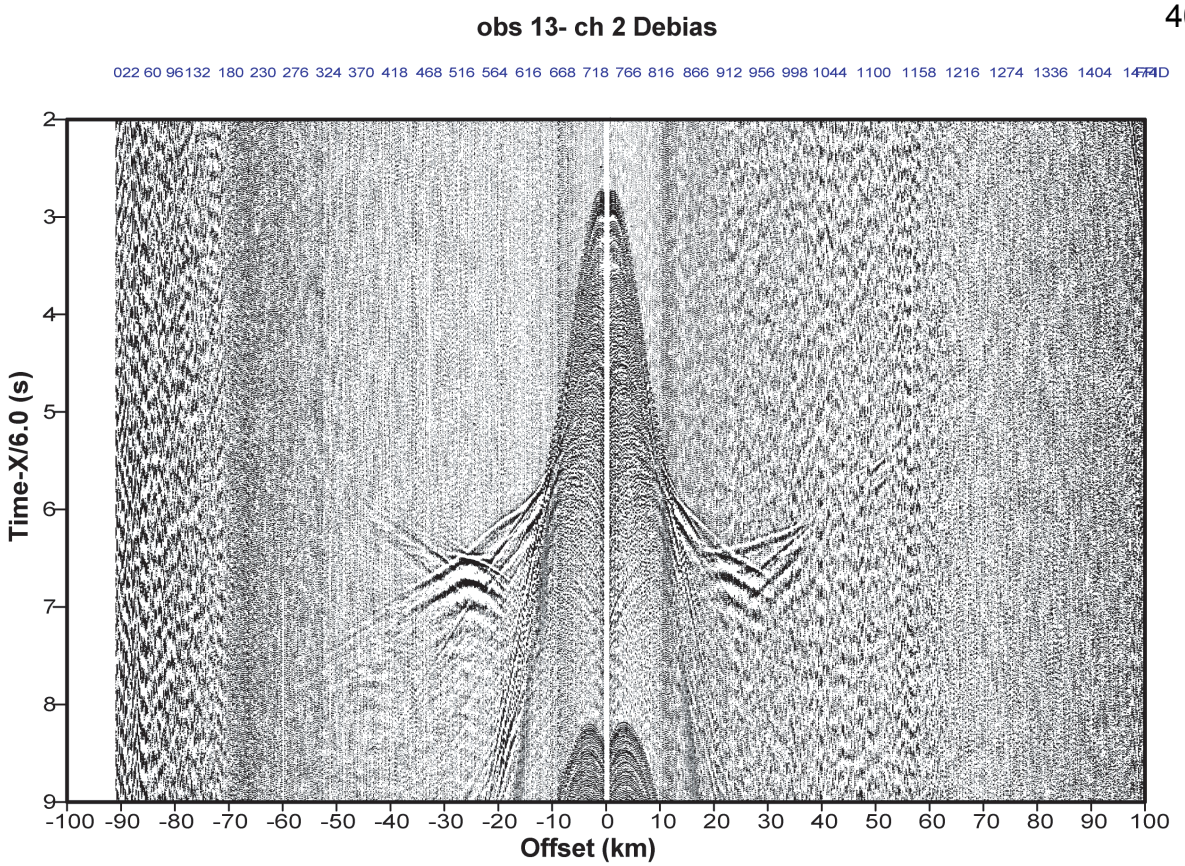

Figure 3.2.2.1 Plot of OBS station 13 channel 2 data with debias process applied

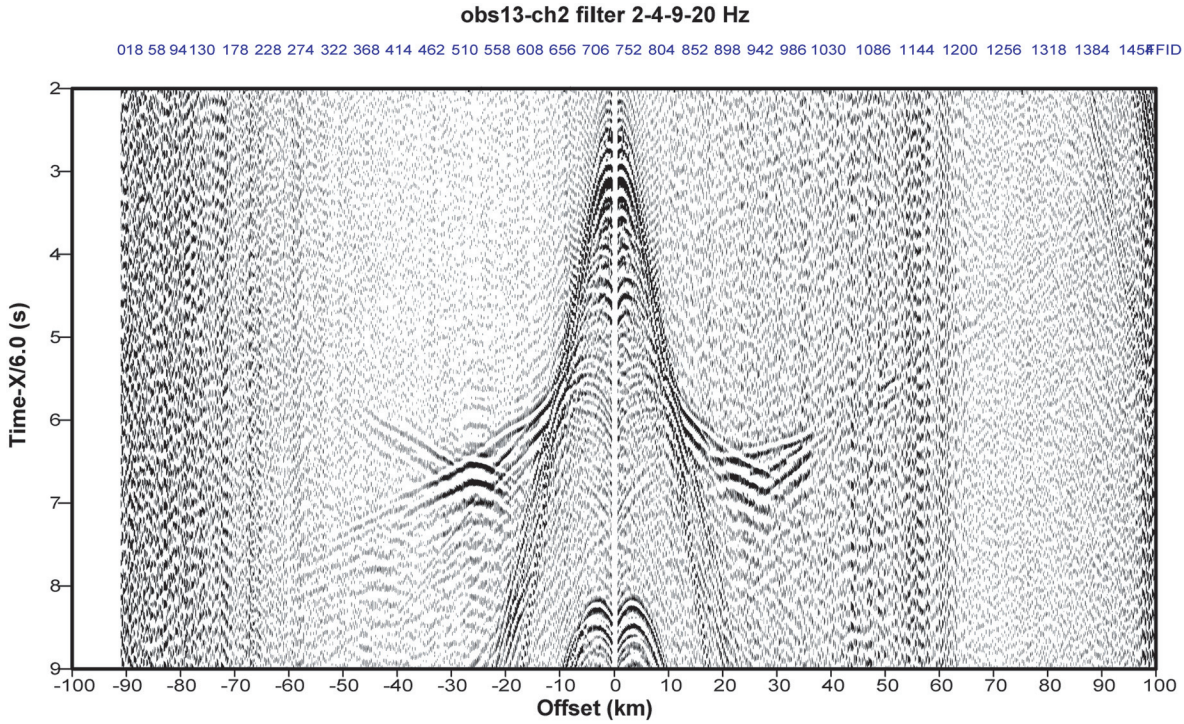

Figure 3.2.2.2 Plot of OBS station 13 data channel 2 with 2-4-9-20 Hz bandpass filter applied.

3.2.3 Velocity Modeling

Refraction waves are created when an incident wave hits a boundary and energy is transferred through the medium. Refraction waves are useful seismic studies as they do not simply reflect off each boundary (change in density in the subsurface), they travel through these layers, therefore giving a useful tool for determining velocities of the subsurface.

To create a 1D velocity model of the crustal layers, I used the P-wave velocity model of Funck et al. (2004) along the SMART1 seismic line (shown in Figure 2.3.6) as a base. In Seiswide, I created a new 1D model using the crustal properties (depth and top and bottom velocities) of Funck et al. (2004) below at approximately 320 km model distance (at approximately SMART1 OBS station 8), as this is approximately where the OCTOPUS line crosses the SMART1 line. This base model can be seen in Figure 4.1.1 with detailed parameters in Appendix C.

I chose to use OBS 13 channel 2 of the OCTOPUS line as the data for my 1D model, because it seemed to show the best deep refractions, and had the least noise disrupting these arrivals. The filtered data of OBS 13 channel 2 is shown in Figure 3.2.2.2. As is visible in this figure the two sides of the data are not the same; this is most likely due to lateral discontinuity in crustal structure along the line. As it seems that the right-hand side (towards the east of the OBS position) shows the high velocity layer the best, I focused my model on fitting this side.

To create a 1D model to fit the eastern side of OBS 13, I modified both the depths and top and bottom velocities of each of the eight layers in the 1D model created by

Funck et al. (2004), focusing on the deeper layers rather than the sediments. I used SeisWide to perform ray tracing on my model to visually examine the fit of my model to the data. Ray tracing is essentially a process in which a theoretic shot is fired over a model and using the model's properties, the program produces calculated travel times defined by the depths and velocities of the model's layers. The initial model is then modified (in both depth and velocity) until the computed and actual travel times agree. Ray tracing can take into account horizontal and vertical velocity gradients, irregularities, and discontinuities (Jones, 1999.

The subroutine I used in SeisWide (myrayinvr.exe) is a slight modification of RAYINVR. The RAYINVR program assumes a 2D (x, z) isotropic medium. The velocity model is composed of a sequence of layers which are separated by boundaries that must cross the model from left to right. The velocity within each layer is defined by top and bottom velocities, and a gradient exists through the layer between these two velocities. For ray tracing the model is automatically broken up into an irregular network of trapezoids. These trapezoids each have dipping upper and lower boundaries and vertical left and right sides. The velocities at the four corners of each trapezoid are used to interpolate the velocity within the trapezoid. This technique allows both horizontal and vertical velocity gradients to exist, as the velocity varies linearly along all four sides. The ray tracing itself is done by numerically solving the ray tracing equations for 2D media. These equations are first order ordinary differential equations and are solved using the Runge Kutta method (Zelt, 1993). This method is an implicit or explicit repetitive method for approximating the solutions of ordinary differential equations. The travel times

calculated by this program are produced by numerically integrating along ray paths using the trapezoid rule.

RAYINVR requires two main input files to run: r.in and v.in. The r.in file contains the program input parameters in five parts. (1) PLTPAR is a name list which contains the plotting parameters, (2) AXEPAR is a name list which contains the axes parameters, (3) TRAPAR is a name list which contains the parameters related to ray tracing, (4) INVPAR is a name list containing parameters related to inversion, and (5) AMPPAR is a name list containing amplitude parameters. To create my 1D model I used the r.in file of Funck et al. (2004) SMART1 model as a base and simplified it to only contain eight layers and one OBS. This file can be found is Appendix B. The v.in file contains the velocity model. It contains three separate lines for each layer: (1) top boundary of each layer location (in x and z), (2) top velocity of each layer (x and v), and (3) bottom velocity of each layer (x and v). The three lines for each layer cover all the parameters of the velocity model. I created a new model and specified eight layers. From this I interactively changed the depths and velocities (top and bottom) of each layer to closely match the arrivals of the layers in Funck et al. (2004) SMART1 v.in file for the layers below OBS 8. Thus reducing the total layers in the model from 16 (as in the SMART1 model) to 8. This velocity model is then output to a SeisWide .bin file. The myrayinvr.exe uses the SeisWide .bin file to perform the ray tracing, as opposed to a v.in file as for the original RAYINVR program. The v.in file of SMART1 created by Funck et al. (2004) as well as my final .bin file (in text form) can be seen in Appendix B.

After creating a 1D model to closely match the SMART1 model of below SMART1 OBS station 8, I then interactively changed the depths and top and bottom

velocities of each layer to make the theoretical data produced by ray tracing (myrayinv.exe) to match the eastern side of OBS 13. As I did not perform any picking of arrivals which correspond to layers, I did not get a numerical misfit, only a visual fit giving my results a purely qualitative value.

3.2.4 Calculation of anisotropy

To calculate the degree of anisotropy in the HVLC layer in question (layer 7) I extracted a velocity-depth profile for both models from SeisWide (these files are shown in Appendix C). I then plotted these two profiles together to examine the differences between the two models in terms of model properties. This plot is shown in Figure 4.3.1. To calculate the degree of anisotropy for layer 7, I looked at the change between the top and bottom velocities of this layer in both the SMART1 model and the OCTOPUS model.

I calculated the change in both the top and bottom velocities; then divided this change by the velocities of the SMART1 model to determine the degree of anisotropy in the OCTOPUS model. The formulas I used are shown below.

$\Delta V_t = V_t^S - V_t^O$

$\Delta V_b = V_b^S - V_b^O$

$\Delta V_t / V_t^S$ = anisotropy of top

$\Delta V_b / V_b^S$ = anisotropy of bottom

Where:

t represents top of the layer

b represents bottom of the layer

S represents velocities in the SMART1 model by Funck et al. (2004)

O represents OCTOPUS model velocity values

The calculations anisotropy using the top and bottom layer velocity differences between the two different models, allowed me to calculate a range of anisotropy for layer 7 in the OCTOPUS model.

CHAPTER 4: RESULTS AND DISCUSSION

4.1 Velocity Model

My adaptation of the SMART1 model into a 1D model below SMART1 OBS 8 is shown in Figure 4.1.1. The parameters of this model are shown in Appendix C. Using myrayinvr.exe in SeisWide to run ray tracing through this model the resulting theoretical data plotted against OCTOPUS OBS 13 is shown in Figure 4.1.2. This figure shows how the adaptation of Funck et al. (2004) SMART1 model does not fit the OBS 13 data in the lower layers (layers 6 though 8). The upper layers of sediment are very similar and the calculated arrival times are similar to the actual arrivals.

The 1D P-wave velocity model created to fit OCTOPUS OBS 13 is shown in Figure 4.1.3. Sediments compose layers 2 to 5; velocities of the sediments range from 1.8 to 4.7 km/s. The sediment cover has a thickness of 6.5 km. Below the sediment layers are layers 6 to 8; layer 6 has velocities ranging from 4.7 to 5 km/s and a thickness of 1.5 km. Layer 7, the HVLC, has velocities ranging from 6.8 to 6.9 km/s and a thickness of 4.2 km. Layer 8 is the mantle and shows velocities of 8 to 8.6 km/s. The detailed depths and velocities of each layer are summarized in Table 4.1.1 below.

Layer Number	Top Depth	Bottom Depth	Top Velocity	Bottom Velocity
1	0.0	4.2	1.5	1.5
2	4.2	4.9	1.8	1.9
3	4.9	6.6	2.2	2.3
4	6.6	8.2	3.7	3.8
5	8.2	10.7	4.6	4.7
6	10.7	12.2	5.0	5.2
7	12.2	16.4	6.8	6.9
8	16.4	40.0	8.0	8.6

Table 4.1.1 Summary of resulting OCTOPUS model. Layer numbers correspond to those in Figure 4.1.3, depths are in kilometers, and velocities are in km/s.

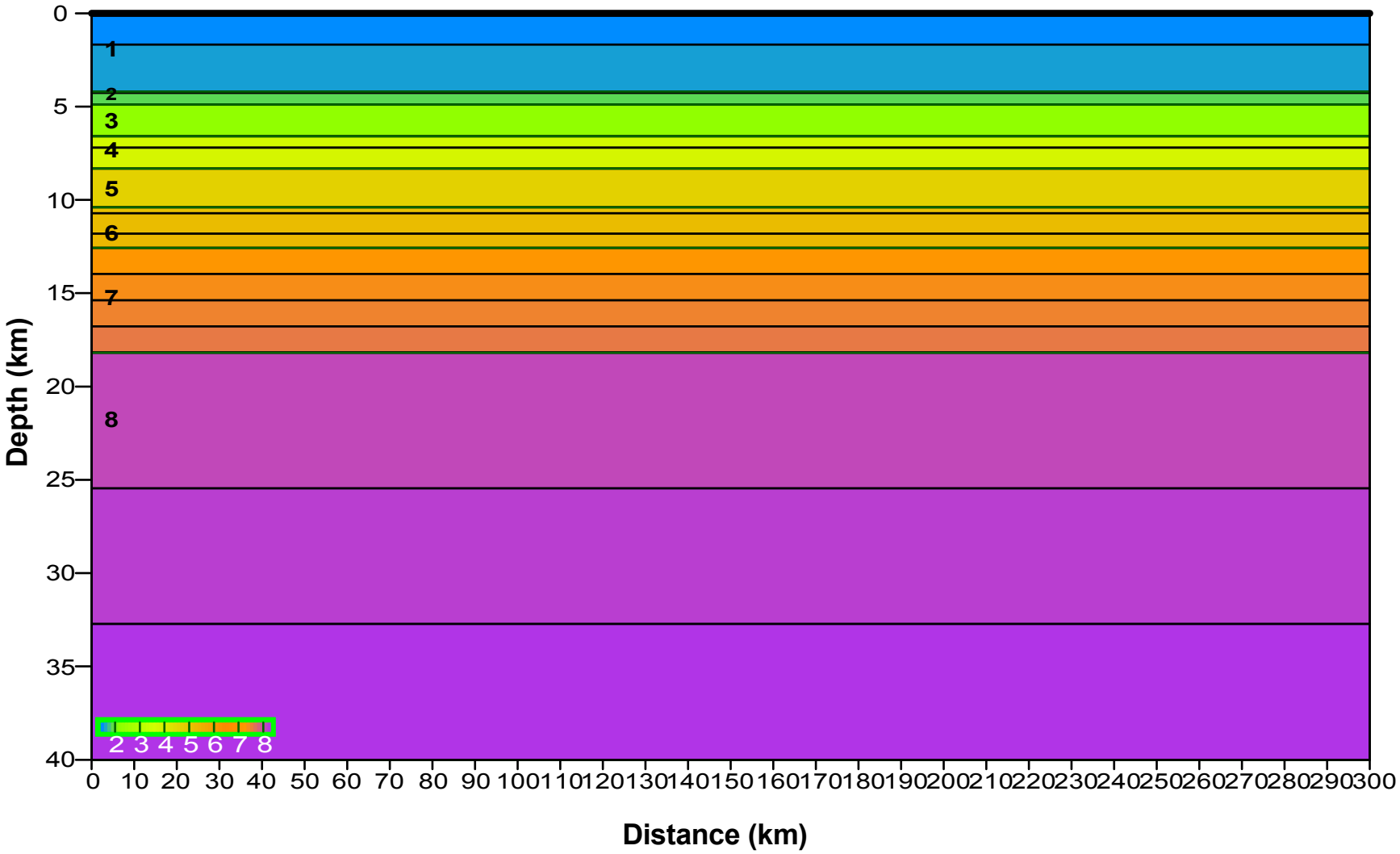

Figure 4.1.1 P- wave velocity model adapation of SMART1 model below OBS 8 (at approximately 320 km model distance). Layer numbers are as indicated, with layer 1 being the water, layer 2 - 5 are sediments, layer 6 is PSM, layer 7 is HVLC and layer 8 is mantle.

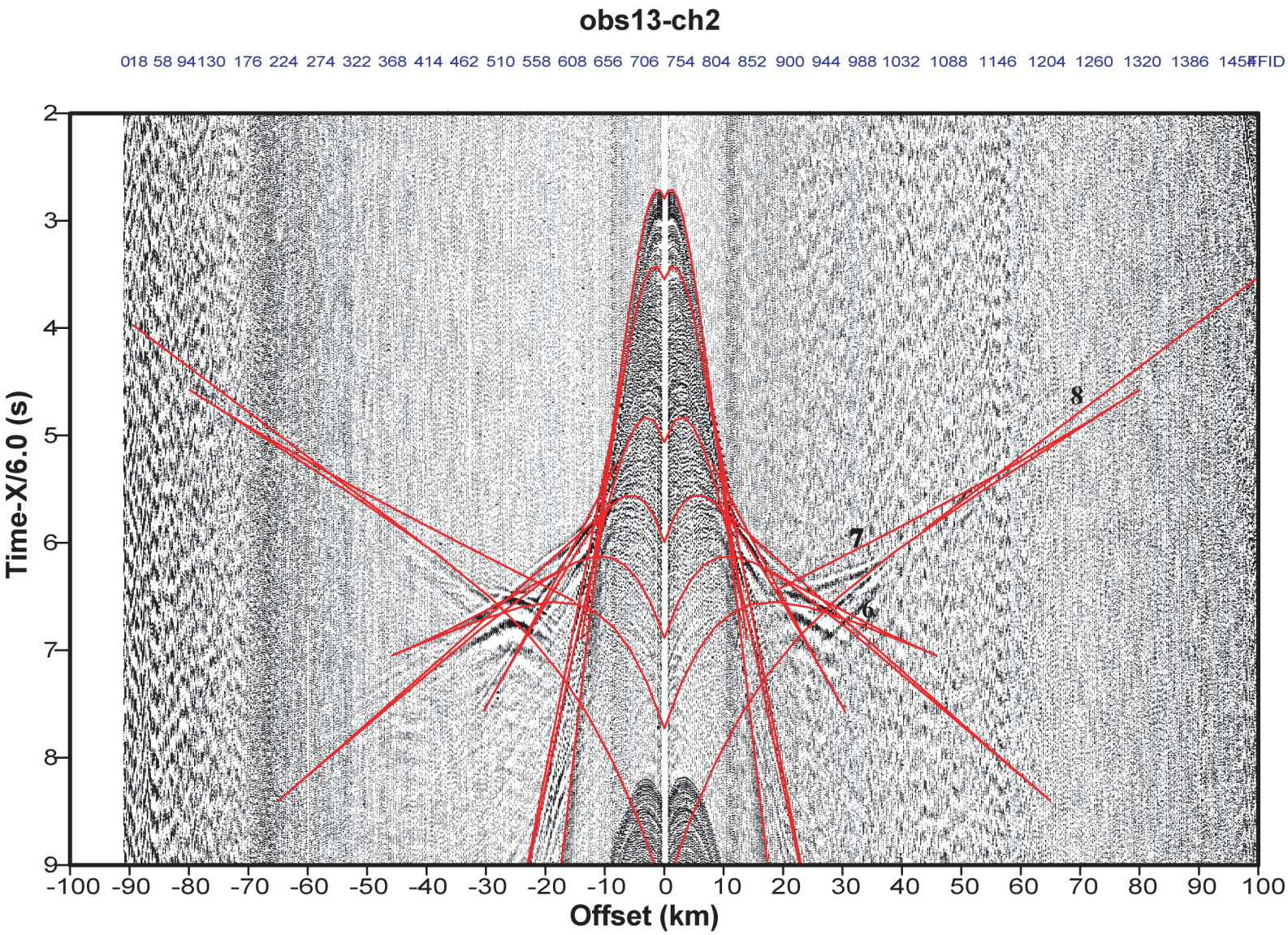

Figure 4.1.2 OBS station 13 channel 2 arrivals with computed rays from adaptation of SMART1 model. Sediment layer arrivals (computed and acutal) fit relatively well, lower crustal layers do not. Computed refraction lines for layers 6, 7, and 8 are labeled.

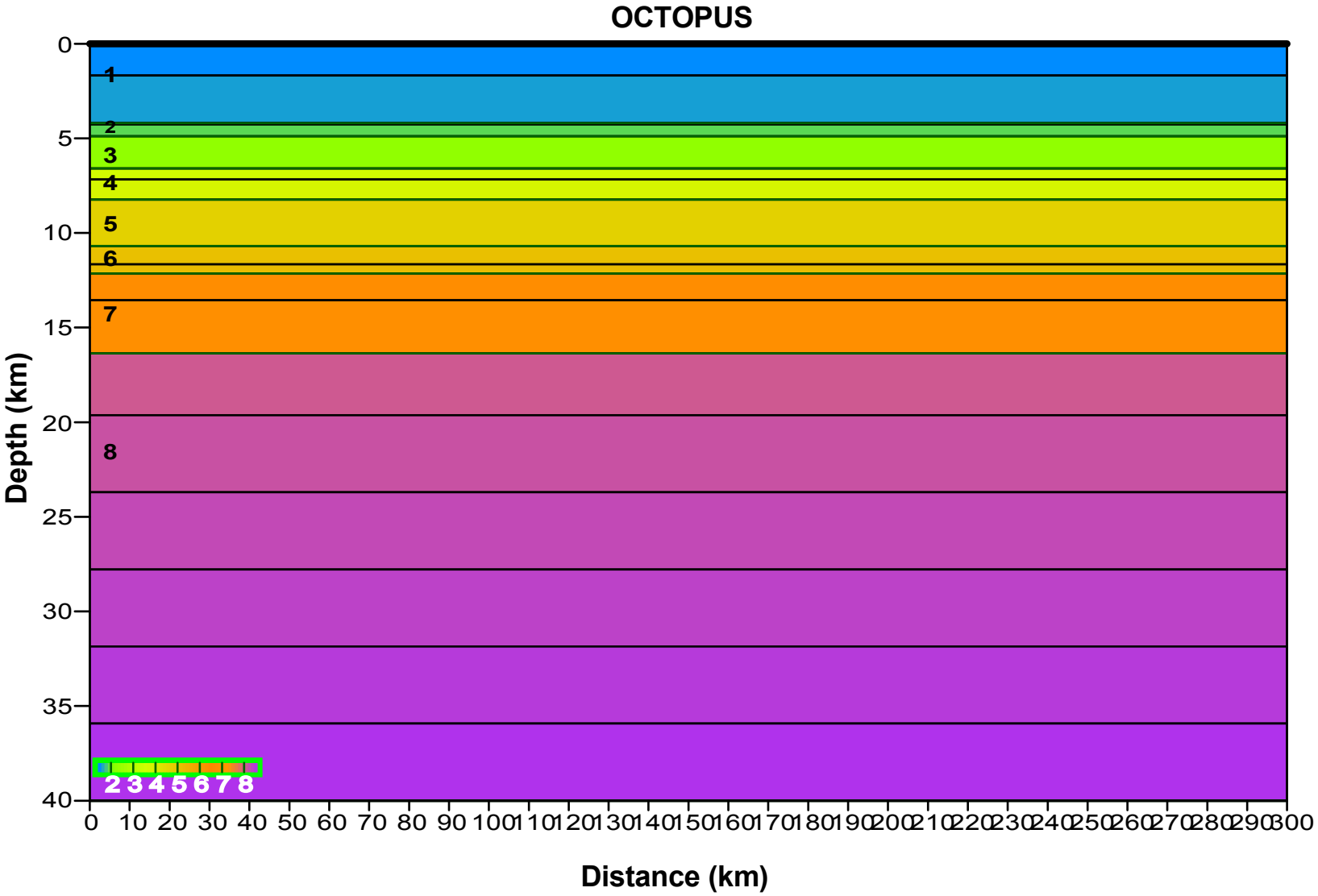

Figure 4.1.3 P-wave velocity model of OBS station 13 along the OCTOPUS line, layers are as numbered.

Figure 4.1.4 shows the OCTOPUS model with computed rays and the fit of these rays on OBS 13 channel 2. The corresponding layers in these data are labeled with respect to the layer numbers in Figure 4.1.3. As previously mentioned, the northeastern and southwestern sides of these data are not the same, and so the modeling was focused on the northeastern side. However, these data towards the southwest clearly show the same trends, simply without a layer 7. Although the arrival times of the computer rays are off on this southwestern side, this figure makes it clear that the overall slopes of the rays are correct.

4.2 Calculations of Anisotropy

Using the methodology previously outlined, I calculated that the difference in top velocity of layer 7 with roughly 90° direction change (between SMART1 and OCTOPUS) as 0.5km/s. The difference between the bottom velocities of layer 7 is 0.7 km/s. The data used to calculate these results is shown in Table 4.2.1.
From these results, I calculated 6% anisotropy from the top velocities and 9 % anisotropy from the bottom layers, producing a range in anisotropy from 6 to 9%.

Input data		**Calculated results**	
VtO	6.8	ΔVt	0.5
VbO	6.9	ΔVb	0.7
VtS	7.2	ΔVt/ VtS	6.3
VbS	7.6	ΔVb/ VbS	8.9

Table 4.2.1 Data used to calculate degree of anisotropy between SMART1 and OCOTPUS lines in layer 7. Velocities extracted from the velocity-depth profile shown in Figure 4.3.1. t denotes top, b denotes bottom, S denotes SMART1 model of Funck et al. (2004) and O denotes OCTOPUS model.

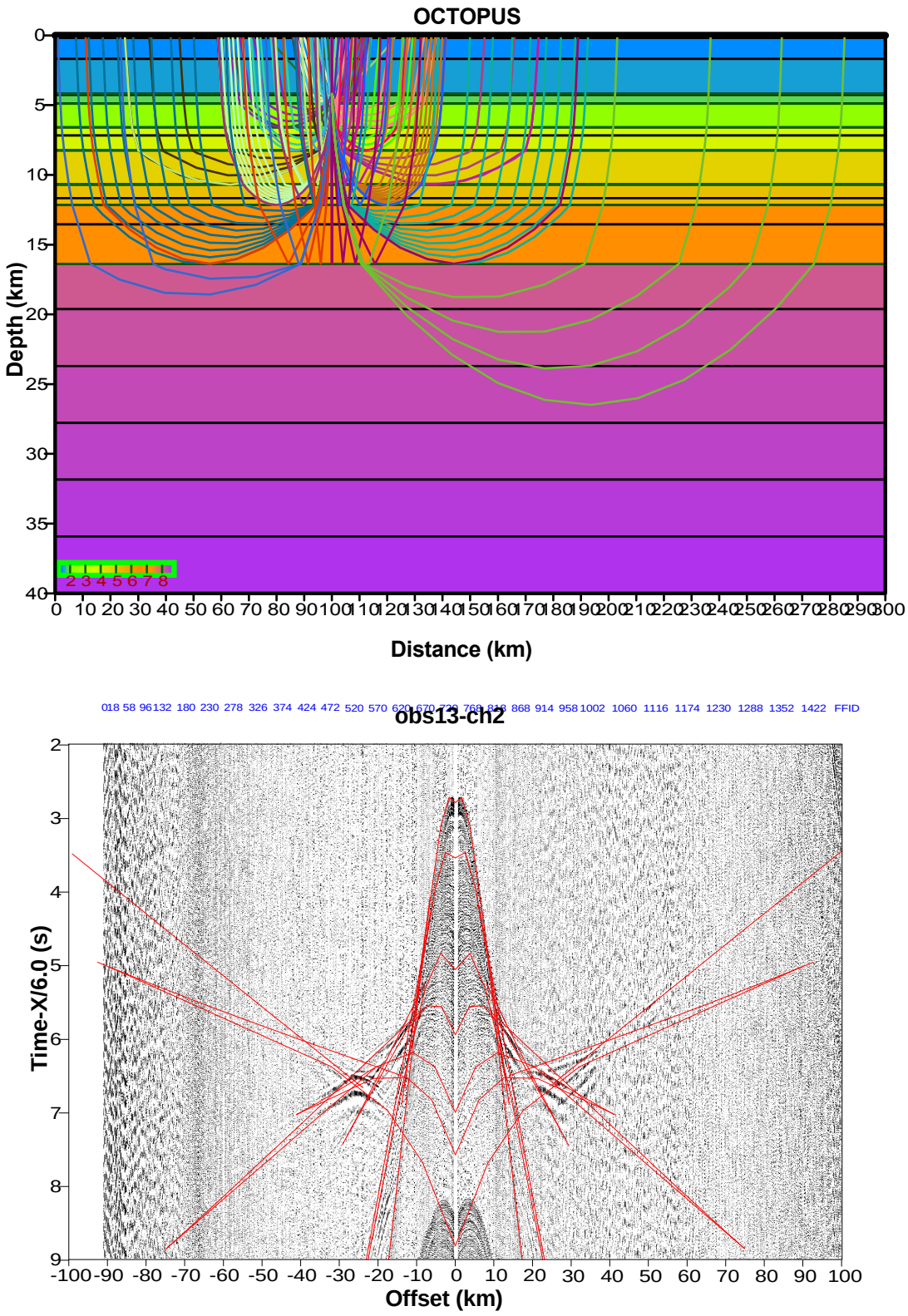

Figure 4.1.4 OCTOPUS model with computed rays (a), fit of computed rays on OBS station 13 channel 2 data (b)

4.3 Comparison with SMART1

Comparison of velocities and thicknesses of layers of the OCTOPUS model with the SMART1 model is summarized in the velocity-depth profile shown in Figure 4.3.1**.** This figure shows the variations of velocity with depth of the two models. The OCTOPUS model is shown in blue and the SMART1 model is shown in red. Layer numbers are indicated in this figure, and show that layers 1 through 5 are very similar with slight variations occurring in layer 6. It is in layer 7 however, that there is a large difference. Layer 7 was identified by Funck et al. (2004) to be PSM with velocities of 7.2 to 7.6 km/s; in the OCTOPUS model layer 7 shows slower velocities of 6.8 to 6.9 km/s. This change in velocity of layer 7 is clearly visible in Figure 4.3.1 as the two lines do not overlap. This figure also shows the change in thickness of layer 7 between the two models. In the SMART1 model (at approximately 320km where the OCTOPUS line crosses) layer 7 is approximately 5.6 km thick; in the OCTOPUS model layer 7 is much thinner, with a thickness of 4.2 km. That is a difference of 1.4 km in thickness. This change in velocity and thickness can also been seen in the comparison of my adaptation of the SMART1 model at OBS8 to the OCTOPUS model as seen in Figure 4.3.2. Both models have the same colour scale, and thus make it easy to visually ascertain the difference in thickness and velocities of each layer. The most significant difference visible in this figure is the difference in thickness and velocities of layers 7 and 8. The OCTOPUS model displays a greater mantle velocity gradient than the SMART1 model; this change can also been seen nicely in Figure 4.3.1.

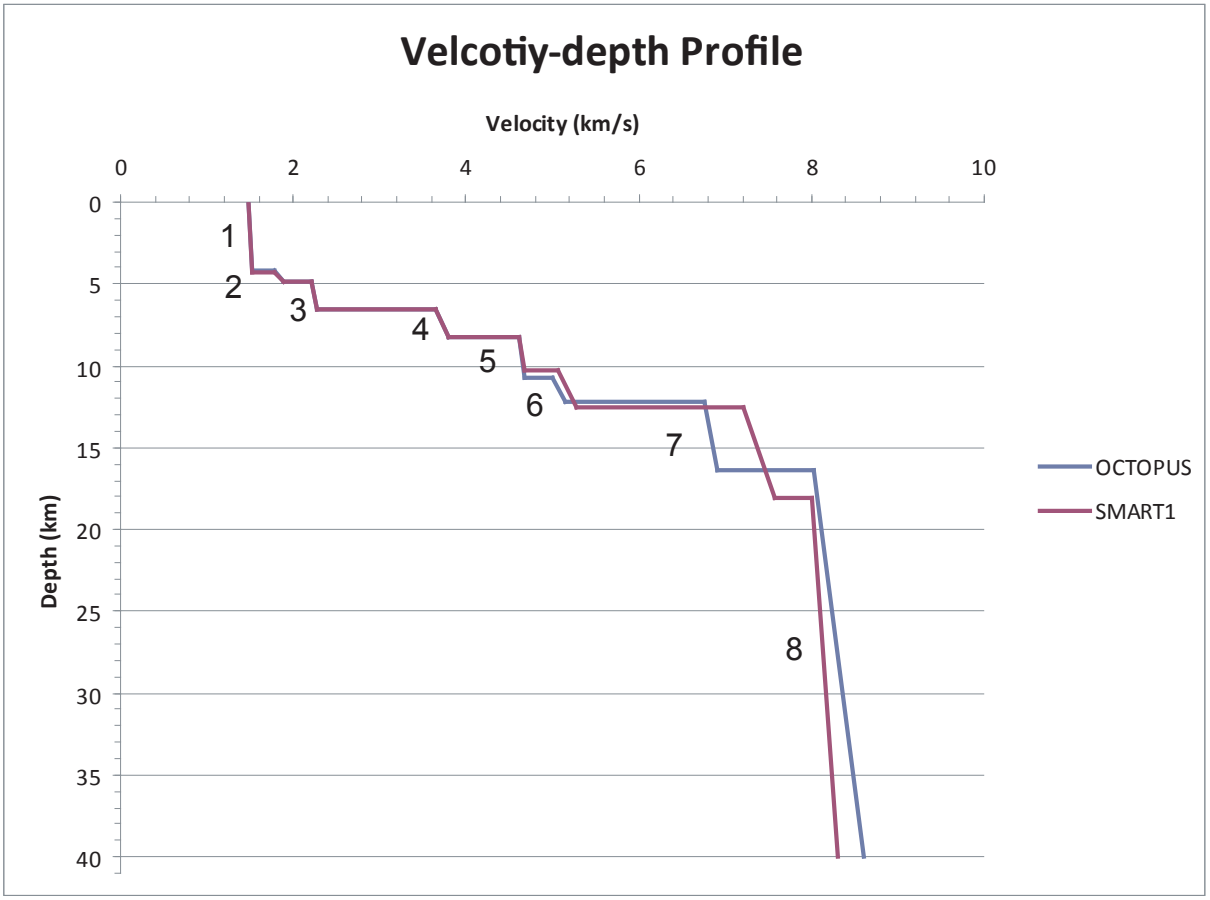

Figure 4.3.1 Velocity-depth profile of SMART1 model below OBS 8 (red) and OCTOPUS model below OBS 13 (blue) showing the change in velocity and thickness of the HVLC (layer 7). Layer numbers (from OCTOPUS model) are as indicated in figure.

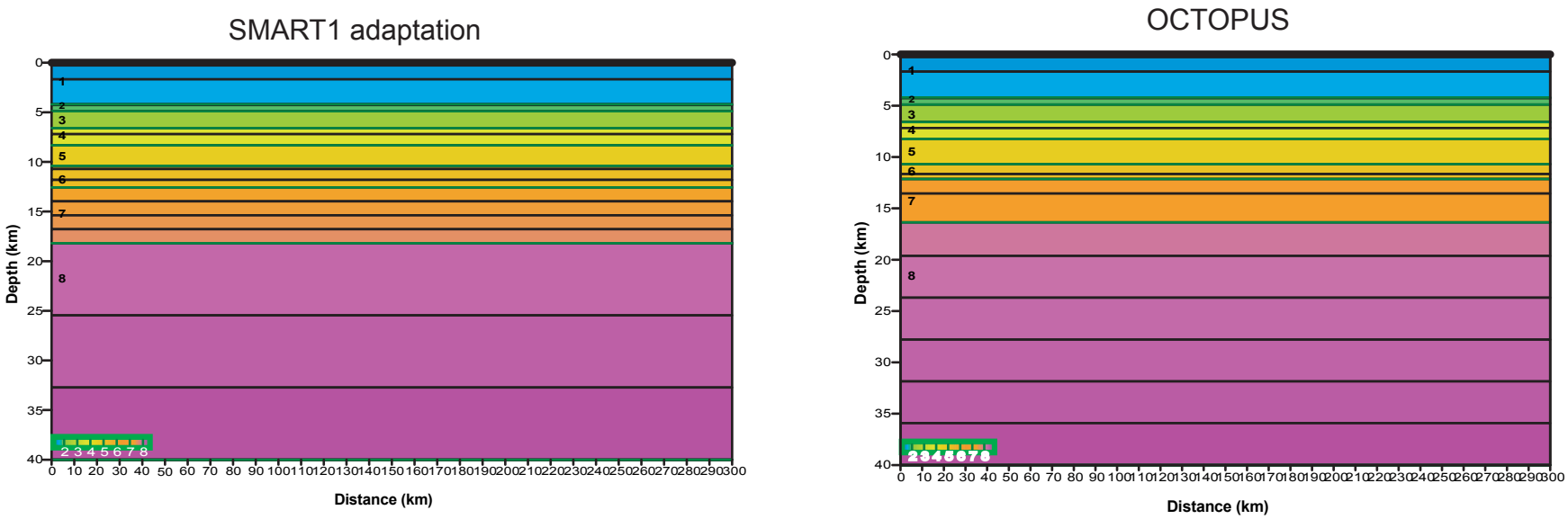

Figure 4.3.2 Comparison of 1D models. SMART1 adapation show on the left in (a) and OCTOPUS model shown on the right (b). Models share the same colour scale and layer numeration.

The difference in the velocity gradient of layer 7 between the SMART1 and OCTOPUS model show that the velocity of layer 7 does change with direction, thus allowing the conclusion that the material is anisotropic.

4.4 Comparison with West Iberia margin results

Along the west Iberia margin, Cole et al. (2002) conducted a study into the azimuthal seismic anisotropy of the upper-mantle adjacent to a rifted margin to determine if the direction of anisotropy could be used as an indicator of the stretching direction in the region. Cole et al. (2002) used a grid of wide angle seismic lines to create a 3D velocity model of the area. They determined that anisotropy of 5 – 8 % was present with a fast direction of 143° between 3.1 and 6.7km below the top of the basement. Figure 4.4.1 shows the results of Cole et al. (2002) and the variety of azimuthal velocities.

Cole et al. (2002) concluded that the fast direction was not consistent with the post-breakup mantle stretching (between Iberia and North America); however, they concluded that the motion along concave-downward faults during the exhumation of this mantle was sufficient to change the direction of anisotropy observed in these rocks.

Along the OCTOPUS line we only have two directions to determine the maximum and minimum velocities. These two directions are shown in Figure 4.4.2. When calculating the degree of anisotropy of layer 7 the assumption was made that these two directions represent the maximum and minimum velocities; however, we do not know this to be the case. With this assumption in mind, the calculated degree of anisotropy for layer 7 from the OCTOPUS and SMART1 velocities is very similar to the results from west Iberia with a result of 6 – 9 % as compared to 5 – 8 %.

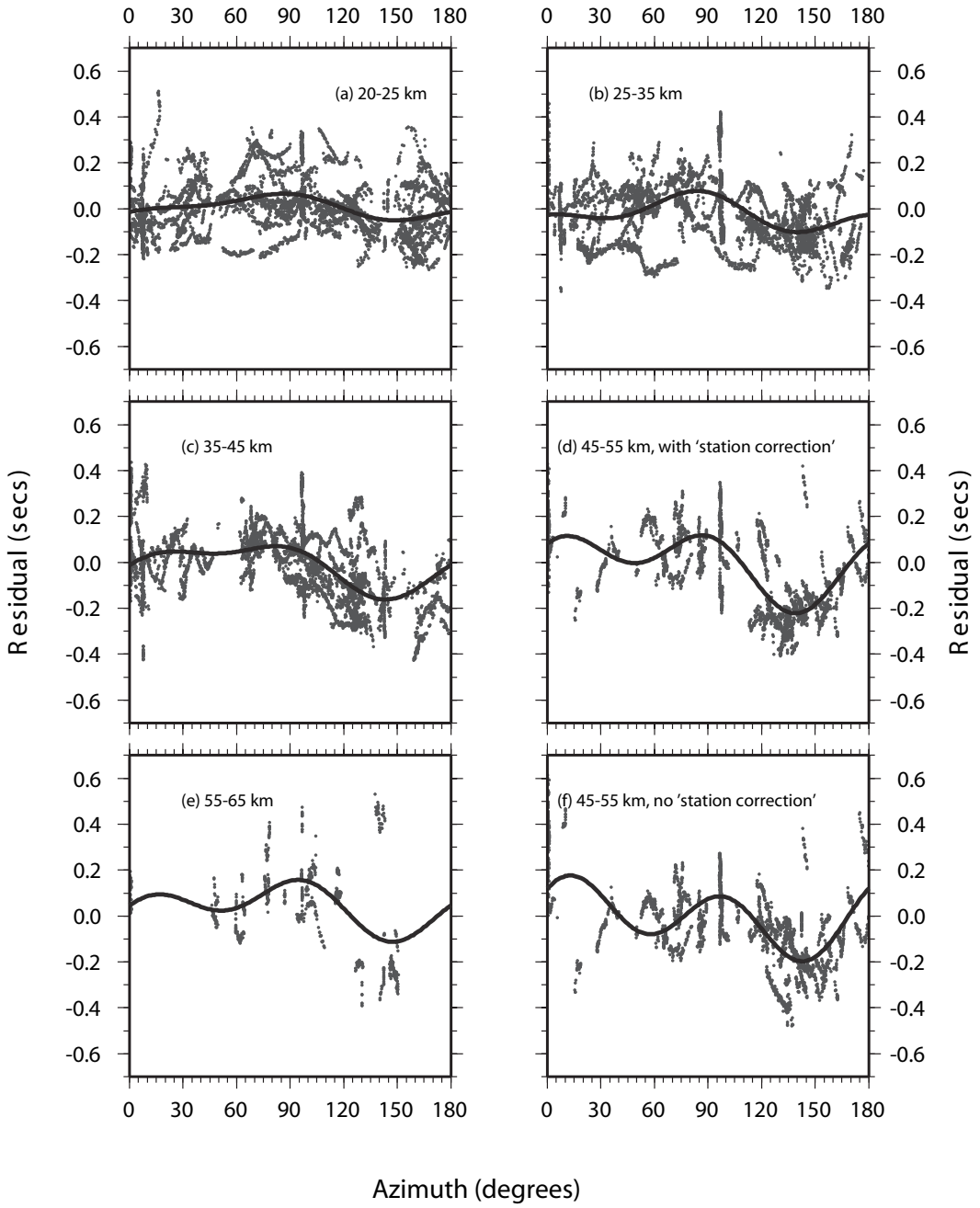

Figure 4.4.1 Results of Cole et al. (2002) of azithumal variations in travel time residuals in West Iberia. Travel time residulas are as a result of point-to-point ray tracing, and therefore can be used as a proxy to velcoity. Data is broken up into range sections (a) range bin 20–25 km; (b) range bin 25–35 km; (c) range bin 35–45 km; (d) range bin 45–55 km; (e) range bin 55–65 km. Lines representing the best fit are also plotted. (After Colet et al. 2002)

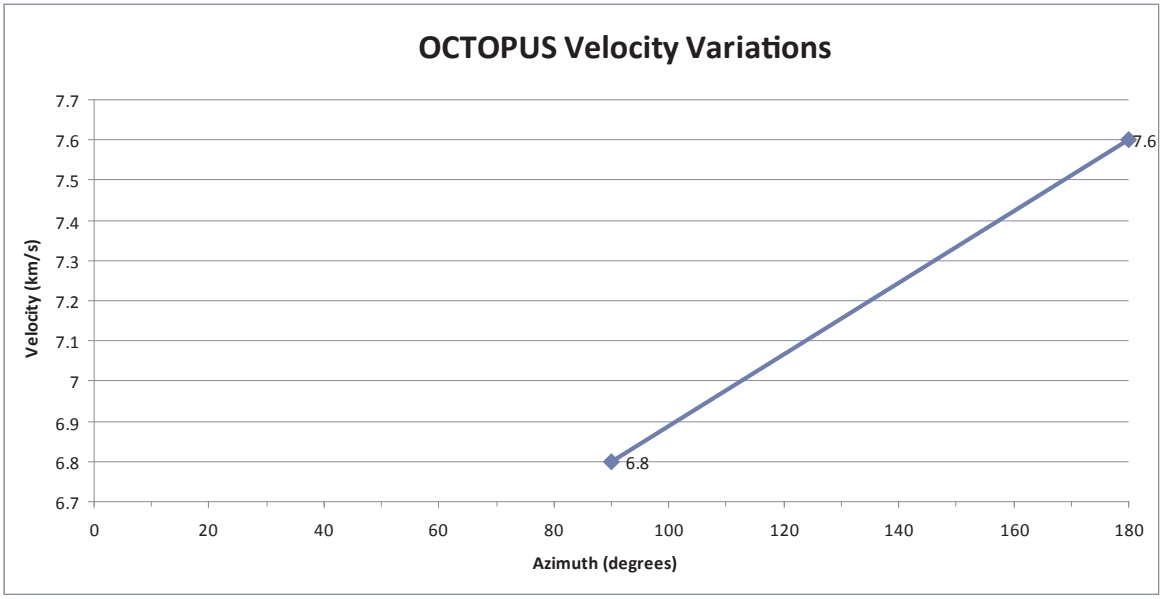

Figure 4.4.2 Velocity variation with angle between the OCTOPUS and SMART1 lines. OCTOPUS has been assumed to be at 90 azimuthal degrees and SMART1 at 180.

4.5 Comparison with MOR

Along the Nova Scotia rifted margin the fast direction is perpendicular to the margin (along the SMART1 line with velocities of 7.2 – 7.6 km/s) and the slow direction is parallel to the margin (along the OCTOPUS line with velocities of 6.8 – 6.9 km/s). Relating these directions to the direction of spreading at the MOR, the fast direction is parallel to the direction of spreading and the slow direction is perpendicular. This relationship has been seen elsewhere (in the Pacific along the East Pacific Rise, a MOR, during the MELT experiment (Jones, 1999)) and this relationship of fast and slow P-wave velocity directions has been related to upper mantle anisotropy in these cases. This kind of anisotropy is consistent with a result of an olivine rich upper mantle, as olivine has large P-wave velocities differences along its principle crystallographic axes, and it is a mineral known to develop a preferred orientation in a stress field (Jones, 1999). Olivine has been shown in lab tests to have different P-wave velocities along its three principle crystallographic axis: axis *a* shows a P-wave velocity of 9.89 km/s, *b* shows 7.73 km/s and *c* shows 8.65 km/s (Hess, 1964). The most probable glide plane of an olivine crystal to form during deformation is 010 (axis *a*) (Jones, 1999). In a stress field, such as mantle deformation, a proportion of olivine crystals in the upper mantle would be likely to develop glide planes aligned with the direction of deformation. As this is the fast direction of an olivine crystal, the direction of deformation would also be the fast direction of the olivine rich upper mantle (Jones, 1999). This was observed by Hess (1964) in the eastern Pacific along the east-west Mendocino and Molokai Fracture Zones. Hess (1964) observed fast directions parallel to the fracture zone, and slow directions on north-south trending lines. He argued that this change reflected anisotropy of the upper

mantle rather than lateral variations as the difference in observed seismic velocities was ~0.7 km/s and the difference between the *b* and *c* axes of olivine is 0.9 km/s. These results are consistent with the fast and slow directions observed along the OCTOPUS and SMART1 seismic lines; suggesting that the HVLC (layer 7) is composed of deformed mantle with a preferred orientation of olivine grains.

4.6 Along Strike Marginal Variations

The differing crustal structure towards the northeast and the southwest along the OCTOPUS line agree with the hypothesis of along strike crustal variations of the Nova Scotia margin. As visible in Figure 3.2.2.2 the structure of the lower crust is discontinuous along the Nova Scotia margin as we see differing refraction arrivals to the northeast and southwest. Figure 4.6.1 is a plot of OBS 14 channel 2 which also shows the same type of along strike variation in crustal structure as the data of OBS 13, thus showing that this difference is consistent with OBS 13 data. Both of these plots show a strong layer 7 towards the northeast and are lacking a strong layer 7 towards the southwest, thus suggesting a change in this layer along the margin.

Figure 4.6.2 is the previously collected MCS reflection profile section of the OCTOPUS line. OCTOPUS OBS station positions are indicated with yellow dots. As is indicated, there is a very strong relatively flat reflector at the top of layer 6 and the top of layer 7. The reflector at the top of layer 7 continues towards the southwest, and pinches off towards the northeast. This apparent pinching off is due to the orientation of the line along the margin, not due to pinching off of the layer itself as it has been observed further towards the northwest along the OETR line (Louden et al., 2010).

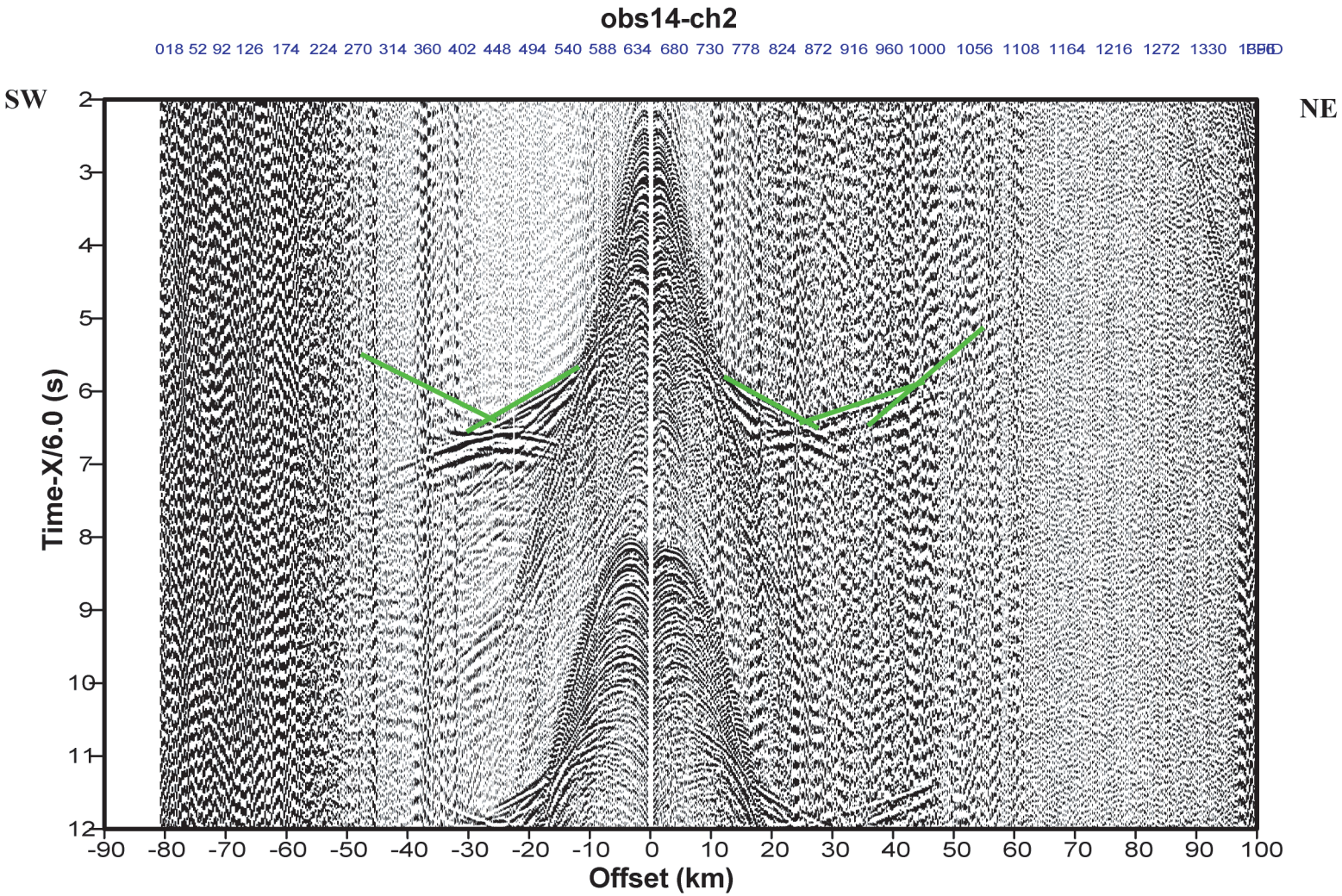

Figure 4.6.1 OBS station 14 channel 2 data showing similar lateral variations along the OCTOPUS line. Filter of 2-4-16-22 Hz applied to data. Approximate tracing of refraction arrivals highlighting the along strike marginal differences are shown in green.

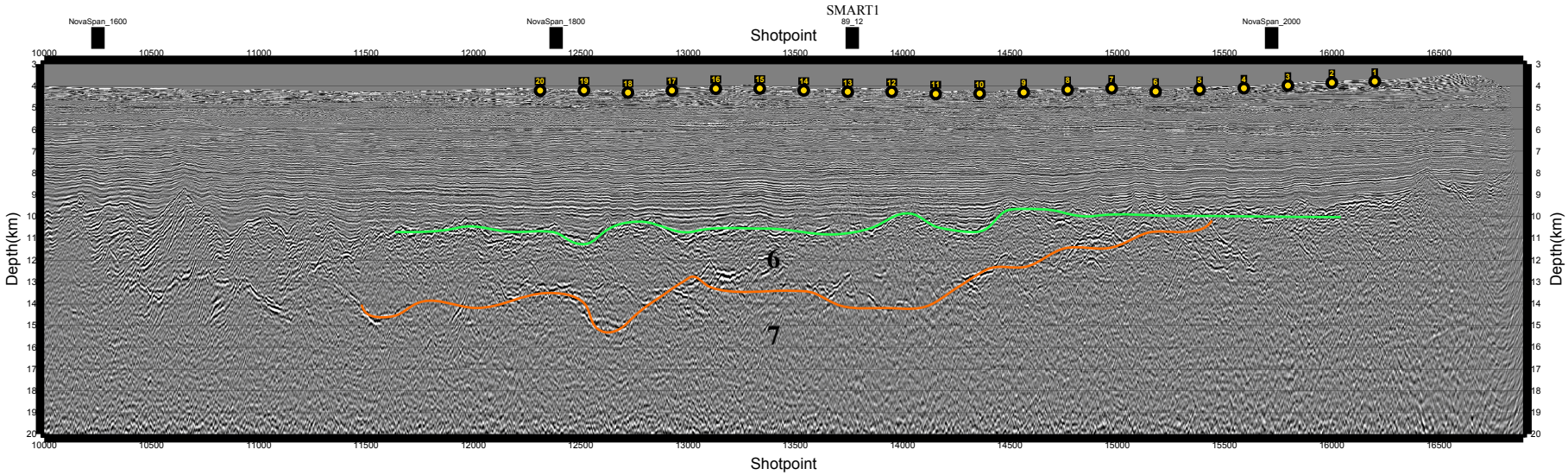

Figure 4.6.2 MCS reflection profile of the OCTOPUS line (Novaspan 5100). OBS positions and station numbers are shown in yellow. Green line shows an approximation of the strong layer 6 top boundary reflecor, and orange line show the strong reflector at the top of layer 7. Layers 6 and 7 are numbered.

Toward the south of these two lines lies the wide angle seismic line SMART2. Wu (2006) performed a comparison of SMART1 and 2 lines and saw a change in the thickness of layer 7, the HVLC. Wu (2006) saw a thinning and increasing velocity in SMART2 as compared to SMART1 (shown in Figure 2.3.6).

There are two possibilities for the along strike marginal crustal changes observed in the OCTOPUS data. First, the boundary between layer 6 and layer 7 is gradually dipping towards the southwest and eventually pinches out. This dipping boundary would account for the reduction in the presence of layer 7 towards the southwest, with the continued presence of layer 7 towards the northeast. However, this would suggest that the thickness of layer 6 would be changing along the margin. This is not observed as the thickness of layer 6 in SMART1 is very similar to the thickness in OCTOPUS (only 0.76 km difference). As well, in the MCS line in Figure 4.6.2 this boundary does not show any overprinting dip.

The second possible explanation for this SW-NE variation is that the layer 7/mantle boundary is dipping. This would create a decreasing thickness of layer 7 towards the southwest as layer 7 essentially vanishes and becomes mantle. An increasing velocity in layer 7 has been observed by Wu (2006) in his comparison of SMART1 and 2.

An interesting observation is that the change in the syn-rift salt structures along the Nova Scotia margin coincides with this change in structure of the HVLC (layer 7). This change in salt structure its relationship to the SMART1/OCTOPUS line intersection is shown clearly in Figure 2.3.1. Although the salt presently lies landwards of the OCTOPUS line in this area, it is presumable that the salt has been removed from this area

(due to the ability of salt to flow) but was present during rifting. The presence of salt in the area during rifting could have acted as an impermeable layer, preventing the hydration of the brittle mantle and impacting the degree of serpentinization. And possibly impacting the along strike variations in the upper mantle.

4.7 Sources of Error

As previously mentioned I did not perform any picking of refraction arrivals to create my model. I performed visual fitting of the OCTOPUS model to OBS 13, and thus did not get a statistical fit of my model to the data. Typical uncertainties in P-wave velocities of the HVLC are ±0.1 km/s (Funck et al., 2004); as the observed velocities of Funck et al. (2004), Wu (2006) and the OCTOPUS model vary by much greater values than this typical uncertainty it is safe to compare the velocities, even though the OCTPUS model velocities were calculated with a visual fit.

This type of modeling also produces a non-unique result, as different users will produce differing models that visually fit the data in similar ways. However, as the arrivals are clear and the crustal structures are relatively simple this should not have too great an effect. As the OCTOPUS model I created is 1D and does not show any variations in crustal structure, the resulting velocities are the apparent velocities of each layer. This is because my model is flat and therefore the velocities produced by the model are the average velocity over the horizontal range of rays traveling though a layer. This assumes it is flat with no variations. It is evident that the crustal layers in the area are not flat as there are differing refraction arrivals to the northeast and southwest along the OCTOPUS line. These differing arrivals indicate that there is crustal structure present.

While calculating the anisotropy, the assumption was made that the velocity different between the two directions was in fact the maximum difference of velocities in the layer. This is not known, and as we only had two directions, we assumed this difference was the maximum velocity change. As a result of this the values calculated for anisotropy are only average values.

CHAPTER 5: CONCLUSIONS

The eastern North American continental margin features a shift from volcanic style rifting off the eastern USA, to nonvolcanic style off Newfoundland; the Nova Scotia margin has been suggested to be a transitional style margin between the two. A P-wave velocity model of margin-perpendicular, wide-angle seismic line SMART1 (Funck et al., 2004) shows a layer of PSM above the mantle. The newly collected margin-parallel, wide-angle seismic line OCTOPUS also shows this layer; however, with slower velocities than those of the SMART1 model (6.8 to 6.9 km/s as compared to 7.2 to 7.6 km/s). The composition of this layer (HVLC or layer 7) in the OCT has been debated; the differing velocities of SMART1 and OCTOPUS show that layer 7 is anisotropic; therefore suggesting that this layer is composed of serpentinized mantle, not grabbro. This suggests that the margin has a greater nonvolcanic style. The degree of anisotropy observed was 6 – 9 %; this is within the similar range as observed along the west Iberia margin by Cole et al. (2002).

Comparison of the observed fast direction to the direction of spreading at the MOR shows that the fast direction is parallel to the direction of spreading. Given that olivine crystals are likely to align their fast axis with the direction of stress (rifting), this give further evidence towards the conclusion that the HVLC is composed of serpentinized olivine-rich mantle. Along strike marginal variations in the HLVC were also observed along the OCTOPUS line; these variations are consistent with the variations noted by Wu (2006) of the HVLC thinning towards the southwest.

Areas of future work include the production of a 2D model for the entire OCTOPUS line; this would allow for greater understand of along strike marginal changes

in the HVLC. Also, the collection of 3D data to further investigate the seismic anisotropy of this layer as was done by Cole et al. (2002) in west Iberia. Further investigation into the coincidence of the change in nature of the syn-rift salt and the change in the HVLC at the OCTOPUS/SMART1 intersection may also lead to interesting results about the formation of this PSM.

REFERENCES

Armstrong, R.L. Besancon, J. 1970. A Triassic time scale dilemma: K-Ar dating of Upper Triassic mafic igneous rocks, Easter U.S.A. and Canada and post-Upper Triassic plutons, Western Idaho, U.S.A. Ecolgae Geol. Helv., **63**: 15-28.

ARGOS, Software information can be found at: http://www.argos-system.org/html/services/tracking-monitoring_en.html

Austin, J.A., Jr., Stoffa, L., Phillips, J.D., Oh, J., Sawyer, D.S., Purdy, G.M., Reiter, E., Makris, J. 1990. Crustal structure of the southeast Georgia embayment-Carolina trough: Preliminary results of a composite seismic image of a continental suture(?) and a volcanic passive margin. Geology, **18**: 1023-1027.

Barry, K. M., Cavers, D. A. and Kneale, C. W., 1975, Report on recommended standards for digital tape formats: Geophysics, 40, no. 02, 344-352.

Benn, K., Horne, R.J.,Kontak,D.J., Pignotta, G.S., Evans,N.G., 1997. Syn-Acadian emplacement model for the South Mountain batholith, Meguma Terrane, Nova Scotia: magnetic fabric and structural analyses, Geological Society of America Bulletin, **109:** 1279–1293.

Carmichael, C.M., Palmer, H.C. 1968. Paleomagnetism of the Late Triassic North Mountain Basalt of Nova Scotia. J. Geophys. Res., **73**: 2811-2822.

Clarke, D.B., Chatterjee, A.K. 1992. Origin of peraluminous granites in the Meguma Zone of southern Nova Scotia: a synthesis. Joint Annual Meting of GAC/AGC, Wolfville, abstract, **17**, A18.

Coffin, M.F., Gahagan, L.M., Lawver, L.A., Lee, T.-Y. Rosencrantz, E. 1992. Atlas of Mesozoic/Cenozoic reconstructions (200 Ma to Present Day), Plate Progress Report No. 1-0192, University of Texas Institute for Geophysical Technical Report 122, 49 pp.

Cole, P.B., Minshull, T.A., Whitmarsh, R.B. 2002. Azimuthal seismic anisotropy in a zone of exhumed continental mantle, West Iberia margin. Geophys. J. Int. **151**: 517-533.

Eldholm, O., Thiede, J., Taylor, E. 1989. Evolution of the Voting volcanic margin. Proc. Ocean Drill. Program Sci. Res. **104**: 1033-1065.

Funck, T., Jackson, H.R., Louden, K.E., Dehler, S.A., Wu, Y. 2004. Crustal structure of the northern Nova Scoita rifted continental margin (eastern Canada). Journal of Geophsyical Research, **109** (B09102)**.**

Hess, H.H. 1964. Seismic anisotropy of the uppermost mantle under the oceans. Nature, **203**: 629-631

Hiscott, R.N., Wilson, R.C.L., Gradstein, F.M., Pujalte, V., Garcia-Mondejar, J., Boudreau, R.R., Wishart, H.A. 1990. Comparative stratigraphy and subsidence history of Mesozoic rift basin of North American. Am. Ass. Petrol. Geol. Bull., **74**: 60-76.

Jones, E.J.W. 1999. Marine Geophysics. John Wiley and Sons. Rexdale, Canada.

Keen, C.E., Beaumont, C. 1990. Geodynamics of rifted continental margins. *In* Geology of the Continental Margin of Eastern Canada, *Edited by* Keen, M.J. & Williams, G.L., Geological Survey of Canada, Geology of Canada, No. 2. pp. 393–472.

Keen, C.E., Potter, D.P. 1995a. The transition from a volcanic to a nonvolcanic rifted margin off eastern Canada. Tectonics, **14** (2): 259-371.

Keen, C.E., Potter, D.P. 1995b. Formation and evolution of the Nova Scotian rifted margin: Evidence from deep seismic reflection data. Tectonics, **14** (4): 918-932.

Keen, C.E., MacLean, B.C., Kay, W.A. 1991. A deep seismic reflection profile across the Nova Scotia continental margin, offshore eastern Canada. Can. J. Earth Sci., **28**: 1112-1120.

Keppie, J.D. 1989. North Appalachian terranes and their accreationary history. *In* Terranes in the circum-Atlantic Paleozoic Orogen. *Edited by* Dallmeyer, R.D., Geological Society of America, Special Paper, **230**:159-192 .

Keppie, J.D., Dallmeyer, R.D. 1995. Late Paleozoic collision, delamination, short-lived magmatism, and rapid denundation in the Meguma Terrane, (Nova Scotia, Canada): constraints from 40Ar/19Ar isotopic data. Can. J. Earth Sci., **32**:644-659.

Louden, K.E., Lau, H., Wu, Y., Nedimovic, M. July 2010 Refraction Crustal Models and Plate Reconstruction of the Nova Scotia and Morocco Margins, Unpublished report, Dalhousie University.

Louden, K.E. & Chian, D., 1999. The deep structure of non-volcanic rifted continental margins. Phil Trans. Roy. Soc. Lond., Ser., A., **357**: 767–804.

Minshall, T.A. 2008. Geophysical characterization of the ocean-continent transition at magma-poor rifted margins. C.R. Geoscience, **(341)**: 382-393.

Moullade, M., Brunet, M.-F., Boillot, G. 1988. Subsidence and deepening of the 160 Galicia margins: the paleoenvironmental control. *In* Proceedings of the Ocean Drilling Program, Scientific Results, *Edited by* Mazullo, E.K. Ocean Drilling Program, College Station, TX. **103**: 733-740.

Perez-Gussinye, M. & Reston, T.J. 2001. Rheological evolution during extension at nonvolcanic rifted margins: onset of serpentinization and development of detachments leading to continental breakup, Journal of Geophysical Research, **106** (B3)**:**3961–3975.

Pe-Piper, G., Jansa, L.F. 1986. Triassic olivine- normative diabase from Northumberland Strait, Eastern Canada: implications for continental rifting. Can. J. Earth Sci., **23**: 1013-1021.

Pe-Piper, G., Jansa, L.F., Lambert,R., St.J. 1992. Early Mesozoic magmatism of the eastern Canadian margin: Petrogenetic and tectonic significance. *In* Eastern North American Mesozoic Magmatism: Geological Society of America Special Paper 268: 13-36. *Edited by* Puffer, J.H. and Ragland, P.C.

Reston, T.J. 2008.The structure, evolution and symmetry of the magma-poor rifted margins of the North and Central Atlantic: A synthesis, Tectonophysics, doi:10.1016/j.tecto.2008.09.002

Schenck, P.E. 1970. Regional variation of the flysch-like Meguma Group (Lower Paleozoic) of Nova Scotia compared to recent sedimentation off the Scotia Shelf. Geological Association of Canada, **Special Paper 7**: 127-153.

Sheridan, R.E., Musser, D.L., Glover III, L., Ewing, J.I., Holbrook, W.S., Purdy, G.M., Hawman, R., Smithson, S. 1993. Deep seismic reflection data of EDGE U.S. mid-Atlantic continental-margin experiment: Implications for Appalachian sutures and Mesozoic rifting and magmatic underplating. Geology, **21**: 563-567.

Watt, W.S. 1969. The coast-parallel dike swarm of southern Greenland in relation of the opening of the Labrador Sea. Can. J. Earth Sci., **6**: 1320-1321.

Webster, T.L., Murphy, J.B., Barr, S.M. 1998. Anatomy of a terrane boundary, an integrated structural, geographic information system and remote sensing study of the Late Paleozoic Avalon-Meguma terrane boundary drift. Can. Journal Earth Science. **35**: 787-801.

Welsink, H.J., Dwyer, J.D. & Knight, R.J., 1989. Tectono-stratigraphy of the passive margin off Nova Scotia, *in* Extensional tectonics and stratigraphy of the North Atlantic margin, *Edited by* Tankard, A.J. & Balkwill, H.R., American Association of Petroleum Geologists, Memoir, **46**: 215–231.

Wheeler, J.O., Hoffman, P.F., Card, K.D., et al. 1997. Geological Map of Canada, Geological Survey of Canada, Map D1860A, Ottawa Geological Survey of Canada.

White, R.S., Westbrook, G.K., Fowle,r S.R., Spence, G.D., Barton, J., Joppen, M., Morgan, J., Bowen, A.N., Prescott, C., Bott, M.H. 1987.Hatton Bank (northwest U.K.) continental margin structure. Geophys. J. R. Astr. Soc. **89:** 265-272.

Williams, H. 1979. Appalachian Orogen in Canada. Can. J. Earth Sci., **16**: 792-807.

Withjack, M. O., P. E. Olsen, and R. W. Schlische, 1995, Tectonic evolution of the Fundy rift basin, Canada: evidence of extension and shortening during passive margin development: Tectonics, **14:** 390–405

Wu, Y., Louden, K.E., Funck, T., Jackson, H.R. & Dehler, S.A. 2006. Crustal structure of the central Nova Scotia margin off Eastern Canada. Geophysical Journal International, **166**: 878–906.

Wu, Y. 2007. Crustal structure of the central Nova Scotia margin and the transition from volcanic to non-volcanic rifting off Eastern Canada. PhD. Thesis, Department of Earth Sciences, Dalhousie University, Halifax, N.S.

Yilmaz, O. 1987. Seismic Data Processing. Society of Exploration Geophysicists. Tulsa, OK

Zelt, C.A. 1993. Documentation for RAYINVR and Related Program.

APPENDIX A

obs_loc_mod_part

OBS relocation routine run in Matlab. The "part" specifies that the five shot positions closest to the OBS are removed to produce a lower error. Files needed for this program are: 'water_vel.txt', 'dtime_part.pick', 'shot_table.txt'.

```
%This program aims at ray trace on basis of travel time.
%This Matlab program is transversed from a FORTRAN programs

clear;
global water

% open files for input data:water velocity,direct time and shottable
% open a file for water depths and velocities
%[filename, pathname] = uigetfile('*.*', 'Enter a file for water
% velocities');
[fid1,message]=fopen('water_vel.txt','r');

% open file for direct time
%[filename, pathname] = uigetfile('*.*', 'Enter a file for direct time');
% commoname='dtime_#.pick';
% OBS=input('OBS number:','s');
% filename=regexprep(commoname,'#',OBS);
[fid2,message]=fopen('dtime_part.pick','r');

% open file for shottable
%[filename, pathname] = uigetfile('*.*','Enter the shot_table');
% commoname='shot_table_#.txt';
% Shotable=input('Shot table number:','s');
% filename=regexprep(commoname,'#',Shotable);
[fid3,message]=fopen('shot_table.txt','r');

% open file for output
%[filename, pathname] = uiputfile('*.*', 'Save the relocted OBS position in');
% commoname='obs#.out';
% filename=regexprep(commoname,'#',OBS);
[fid5,message]=fopen('obs_part.out','w');
[fid4,message]=fopen('tempfile1','w');

%prompt={'Enter specified maximal range:','Enter specified least increment:'};
%def={'5000','10'}; % change this for default values <----------
% dlgTitle='Specify the range and least increment:';
% lineNo=1;
% answer=inputdlg(prompt,dlgTitle,lineNo,def);
%ymax=str2num(char(answer(1)));
ymax=2000;
xmax=ymax;
%ydely=str2num(char(answer(2)));
ydely=10;
xdely=ydely;

%read data from water.vel file
status=fseek(fid1,0,-1);
water=fscanf(fid1,'%f %f',[2 inf]);
water=water';
```

```
number_water_layer=size(water,1); % mean row index for water velocity

%Extend velocity distribution to greater depths
vel_inc=water(number_water_layer-1,2)-...
   water(number_water_layer-2,2);
dis_inc=water(number_water_layer-1,1)-...
   water(number_water_layer-2,1);
lay_inc=150-number_water_layer;  % Note: make sure that 150 is enough

for j= 1 : lay_inc
   water(number_water_layer+j-1,1)= ...
      water(number_water_layer+j-2,1)+dis_inc;
   water(number_water_layer+j-1,2)=...
      water(number_water_layer+j-2,2)+vel_inc;
end

%read location (Lat&Lon) at which OBS is launched
%status=fseek(fid3,50, -1);
status=fseek(fid3,0,-1);
inputline0=fgetl(fid3);
Latitude=fscanf(fid3,'%f',[1 1]);
Longitude=fscanf(fid3,'%f',[1 1]);
for n=0:5
   inputline=fgetl(fid3);
end

pre_position3=ftell(fid3);


%fprintf(fid4,'%12.7f %12.7f\n',Latitude,Longitude);

%read header from DirectTime.inp
headDT(1:2)=0;
status=fseek(fid2,0, -1);
headDT(1)=fscanf(fid2,'%f',[1 1]);
headDT(2)=fscanf(fid2,'%f',[1 1]);
Lat_retrieval=fscanf(fid2,'%f',[1 1]);
Lon_retrieval=fscanf(fid2,'%f\n',[1 1]);

DEPTH=true_depth(headDT(1));  %corrected depth,i.e.,true depth
pre_position2=ftell(fid2);

% using retrieval location as center of grid
% Latitude=Lat_retrieval; % uncomment this when not using latlon in shot table
% Longitude=Lon_retrieval;% uncomment this when not using latlon in shot table

fprintf(fid4,'%12.7f %12.7f\n',Latitude,Longitude); % uncomment this when not using latlon in shot table

%find the layer_number just below seabed
i=1;
while water(i,1)<DEPTH
   i=i+1;
   if i>50     % make sure 50 is not too small
      break
   end
end
```

```
water_layer_below_seabed=i;

%calculate the interface number at shot
for i=1:35
   if water(i,1) >= headDT(2)
      interface_at_detonation=i;
      break
   end
end

%calculate the interface number at seabed
for j=1:50
   if water(j,1) >= DEPTH
      interface_at_seabed=j;
      break
   end
end

%calculate which layer(at shot/seabed)is the shallower one
if headDT(2) < DEPTH
   upper_layer=interface_at_detonation;
   lower_layer=water_layer_below_seabed;
   upper_depth=headDT(2);
   lower_depth=DEPTH;
else
   upper_layer=water_layer_below_seabed;
   lower_layer=interface_at_detonation;
   upper_depth=DEPTH;
   lower_depth=headDT(2);
end

%find the maximum, minimum and mean velocity of water
Vmax=water(upper_layer,2);
Vmin=water(upper_layer,2);

if (lower_layer-1) >= upper_layer
   for k=upper_layer:(lower_layer-1)  % This loop may be simplify with Matlab function
      if water(k,2) > Vmax
         Vmax=water(k,2);
      elseif water(k,2) < Vmin
         Vmin=water(k,2);
      end
   end
end

%problem could occur at the following part
if lower_layer == upper_layer
   Vmean=water(upper_layer,2); % for very shallow seabed
else
   Dint=lower_depth-upper_depth;  % depth between gun and seabed
   Vmean=(water(upper_layer,1)-upper_depth)/Dint...
      *water(upper_layer,2);
   if lower_layer ~= (upper_layer+1)
      n=lower_layer-2;
      for i=upper_layer : n
         Vmean=(water(i+1,1)-water(i,1))/...
```

```
            Dint*water(i,2)+Vmean;
        end
    end
    Vmean=Vmean+(lower_depth-water(lower_layer-1,1))/...
        Dint*water(lower_layer-1,2);
end

velocity_check=Vmax*Vmax-Vmin*Vmin;
Depth_difference=DEPTH-headDT(2); % depth between gun and seabed

%read shot_number and direct_time from DirectTime.inp file
status=fseek(fid3,0, 1);
P_fid3=ftell(fid3);
status=fseek(fid2,0, 1);
P_fid2=ftell(fid2);

Direct_time(1:2)=0;
status=fseek(fid3,pre_position3, -1);
status=fseek(fid2,pre_position2, -1);
position_fid2=ftell(fid2);
position_fid3=ftell(fid3);


h = waitbar(0,'It is ray tracing,Please wait...');
while feof(fid2) ==0      %read data if not end of file
    Direct_time=fscanf(fid2,'%d %f',[2,1])';
    position_fid2=ftell(fid2);
    waitbar(position_fid2/P_fid2,h)
    if isempty(Direct_time)==0
        Direct_time=Direct_time';
    else
        break;
    end
    time_difference=Direct_time(2)/1000.0;

    shot_table(1:8)=0;
    while feof(fid3) ==0
        shot_table=fscanf(fid3,'%d %d %d %d %f %f %f %f',[8,1]);
        position_fid3=ftell(fid3);
        if (Direct_time(1)) == (shot_table(1))
            break
        end
    end
    shot_table(8)=abs(shot_table(8)); % range from shot table

    Depth_check=Depth_difference*Depth_difference/...
        (time_difference*time_difference);

    if (velocity_check >= Depth_check)
        Velocity_del=Vmax*Vmax-Depth_check;
        if Velocity_del <= 0
            Velocity_del=0.0001;
        end
        Vmin=sqrt(Velocity_del)+0.1;
    end
```

```
   % Calculate maximal and minimal P value for direct water (I don't understand)
   QC(1:3)=0;
   COS=Depth_difference/(time_difference*Vmax);
   if COS >= 1.0
      COS=1.0-0.1e-09;
   end
   QC(2)=sqrt(1.0 -COS*COS)/Vmin;

   COS=Depth_difference/(time_difference*Vmin);
   if COS >= 1.0
      COS=1.0-0.1e-09;
   end
   QC(1)=sqrt(1.0 - COS*COS)/Vmax;

   %Calculate the horizontal distance between shot and OBS
   Distance= get_distance(QC,Vmean,DEPTH,...
      upper_layer,headDT(2),...
      time_difference,lower_depth,upper_depth);
   Distance=Distance/1000.0;
   Distance_diferrence=Distance-shot_table(8);
   fprintf(fid4,'%d %10.5f %11.5f %7.3f %7.3f %7.3f\n',...
      Direct_time(1),shot_table(6),shot_table(7),...
      Distance,shot_table(8),Distance_diferrence);
end


close(h);
fclose(fid1);
fclose(fid2);
fclose(fid3);
fclose(fid4);




%This program aims at re_locating OBS

global A A0 A2 A4 A6 A8 B E1 E2 F RECIPF k0 degrad

%Ellipsoidal parameters from Clark 1866 ellipsoid
%format long A
%format long B

A=6378206.4;
RECIPF=294.97898;
K0=0.9996;
RADDEG=57.29577951;
FE=500000.0;
F=1.0/RECIPF;
B=A-A*F;
E1=(A*A-B*B)/(A*A);
E2=(A*A-B*B)/(B*B);
degrad=1.7453292519945e-2;
```

```
DELM=100.0;

%Arc length constants:
A0=1.-0.25*E1-0.046875*E1*E1-0.01953125*E1^3.0-175.0/16384.*E1^4.0;
A2=0.375*(E1+0.25*E1*E1+0.1171875*E1^3.0-455.0/4096.0*E1^4.0);
A4=0.05859375*(E1*E1+0.75*E1^3.0-77.0/128.0*E1^4.0);
A6=35.0/3072.0*(E1^3.0-1.28125*E1^4.0);
A8=-315.0/131072.0*E1^4.0;

[fid4,message]=fopen('tempfile1','r');
[fid6,message]=fopen('tempfile2','w');
%read location (Lat&Lon) at which OBS is launched
status=fseek(fid4, 0, -1);
North1=fscanf(fid4,'%f' ,[1 1]);
East1=fscanf(fid4,'%f' ,[1 1]);

%calculate the central meridian in each zone
CM=round(East1);
cm=-177:6:177;
n=size(cm');
for i=1:n
   if CM < cm(i)+3 & CM > cm(i)-3
      CM=cm(i);
      break
   end
end

%transfer Lat&lon of OBS position into UTM
UTM=latlon(North1,East1,CM);
UTMretrieval=latlon(Lat_retrieval,Lon_retrieval,CM);

North=UTM(1);
East=UTM(2);
Northretrival=UTMretrieval(1);
Eastretrival=UTMretrieval(2);

%input data from fid1:input file
obs_loc=fscanf(fid4,'%d %f %f %f %f %f',[6,inf]);
obs_loc=obs_loc';
[number_of_record,n]=size(obs_loc);
N=number_of_record;

%fprintf(fid5,'%s %s %s\n',c1,c2,c3);
fprintf(fid5,'Deployment: %9.5f %9.5f\n',North1,East1);

fprintf(fid5,'Retrival: %9.5f %9.5f\n',Lat_retrieval,Lon_retrieval);

fprintf(fid5,'Range: %4.1f; Increment: %4.1f; Number of record: %5d;\n',...
   ymax,ydely,number_of_record);

fprintf(fid6,'%9.5f %9.5f %4.1f %4.1f %5d\n',...
   North1,East1,ymax,ydely,number_of_record);

L=2.0*ymax/ydely+1;
M=2.0*xmax/xdely+1;
```

```
east=(East-xdely*((M+1.0)/2.0-1.0)):...
   xdely*(-1.0+M)/(M-1):...
   (East-xdely*((M+1.0)/2.0-M));

north=(North-ydely*((L+1.0)/2.0-1.0)):...
   ydely*(-1.0+L)/(L-1):...
   (North-ydely*((L+1.0)/2.0-L));

DELR(1:L,1:M)=0;
north_east(1:N,1:2)=0;

%a,b,c are the coeficients of a linear equation aX+bY+c=0%
a=0;
b=0;
c=0;
%r,s,t,w are tempery variables for calculating a,b,c%
r=0;
t=0;
s=0;
w=0;
for i=1:N
   north_east(i,:)=latlon_utm(obs_loc(i,2),obs_loc(i,3),CM);
   s=s+north_east(i,2)*north_east(i,2);
   t=t+north_east(i,2);
   w=w+north_east(i,2)*north_east(i,1);
   r=r+north_east(i,1);
end
a=N*w-t*r;
b=t*t-N*s;
c=-(b*r+a*t)/N;
h= waitbar(0,'It is re-locating, Please wait...');
for K=1:L
   for J=1:M
      for I=1:N
         DELN=(north(K)-north_east(I,1))*1.0e-3;
         DELE=(east(J)-north_east(I,2))*1.0e-3;
         RR2=sqrt(DELN*DELN+DELE*DELE);
         DDL(I)=RR2-obs_loc(I,4);
         DELR(J,K)=DELR(J,K)+DDL(I)*DDL(I);
      end
      DELR(J,K)=sqrt(DELR(J,K)/N);
      if DELR(J,K) < DELM
         DELM=DELR(J,K);
         for i=1:N
            DDLM(i)=DDL(i);
         end
         KMIN=K;
         JMIN=J;
      end
   end
   if rem(K,100)==0
      waitbar(K*J/(L*M),h)
   end
end
close(h)
```

```
%Compute the position of OBS based on the computed minimum

delty=ydely*((L+1.0)/2.0-KMIN);
deltx=xdely*((M+1.0)/2.0-JMIN);
YOBSM=North-delty;
XOBSM=East-deltx;
drift=sqrt(deltx*deltx+delty*delty);

for i=1:N   %re-consider this N
   fprintf(fid6,'%d %10.5f %10.5f %10.5f %10.5f\n',...
      obs_loc(i,1),obs_loc(i,2),obs_loc(i,3),obs_loc(i,4),DDLM(i));
end

LON_LAT=utm(YOBSM,XOBSM,CM);
YOBSM1=LON_LAT(1);
XOBSM1=LON_LAT(2);

fprintf(fid5,'the best  fit OBS location is :%11.6f %11.6f %8.5f\n',...
   YOBSM1,XOBSM1,DELM);

%biginning of the first insert

second_XOBSM=(b*b*XOBSM-a*b*YOBSM-a*c)/(a*a+b*b);
second_YOBSM=(a*a*YOBSM-a*b*XOBSM-b*c)/(a*a+b*b);
second_XOBSM=second_XOBSM+second_XOBSM-XOBSM;
second_YOBSM=second_YOBSM+second_YOBSM-YOBSM;


second_LON_LAT=utm(second_YOBSM,second_XOBSM,CM);
second_YOBSM1=second_LON_LAT(1);
second_XOBSM1=second_LON_LAT(2);
fprintf(fid5,'the conjugate OBS location is :%11.6f %11.6f\n',...
   second_YOBSM1,second_XOBSM1);
% begining the second insert


fprintf(fid5,'the best  fit OBS drifts:%10.5f\n',drift);
if drift > xmax
   fprintf(fid5,'Please increase the range for searching this OBS!\n');
end

fclose(fid4);
fclose(fid5);
fclose(fid6);

scrsz = get(0,'ScreenSize');
f=figure('name','The Relocated  OBS Position','NumberTitle','off',...
      'Position',[scrsz(3)/2 1 scrsz(3)/4 scrsz(4)]);
DELR=DELR';
level=[0 0.005 0.01 0.02 0.04 0.08 0.12 0.16 0.2 ...
   0.5 1 1.5 2.0];
label=[0 0.005 0.01 0.02 0.04 0.08 0.5 2.0];


num_xtick=(east(M)-east(1))/10;
```

```
num_ytick=(north(L)-north(1))/10;
axis off
x_tick=east(1):num_xtick:east(M);
[xx,xnum]=size(x_tick);
maxlabel=0.5*(east(M)+east(1));
for i=1:xnum
   xlabel(i)={num2str(round(x_tick(i)-maxlabel))};
end

y_tick=north(1):num_ytick:north(L);
[xx,ynum]=size(y_tick);
maxlabel=0.5*(north(M)+north(1));
for j=1:ynum
   ylabel(j)={num2str(round(y_tick(j)-maxlabel))};
end

hold on
axes('YLim',[north(1) north(L)],'Ytick',y_tick,...
   'YTickmode','manual','YTickLabel',ylabel,...
   'YTickLabelMode','manual',...
   'XLim',[east(1) east(M)],'Xtick',x_tick,...
   'XTickmode','manual','XTickLabel',xlabel,...
   'XTickLabelMode','manual')
box on
grid on
hold on

axis square;
hold on

[hh,hc]=contour(east,north,DELR,level);

hold on
plot(XOBSM,YOBSM,'r+')


hold on
plot(XOBSM,YOBSM,'rO')

if second_YOBSM > north(1) & second_YOBSM < north(L)...
      & second_XOBSM > east(1) & second_XOBSM < east(M)
   hold on
   plot(second_XOBSM,second_YOBSM,'m+')

   hold on
   plot(second_XOBSM,second_YOBSM,'gO')
end

hold on
plot(East,North,'b*')
plot(Eastretrival,Northretrival,'ro')


%label=0.01:0.04:0.2;
hold on
clabel(hh,label)
```

```
%clabel(hh,'manual');

hold on
%inputnew=[inputline0 ' OBS-' OBS];
title(inputline0)

hold on
pXOBSM=east(M)-xmax;
pYOBSM=north(M)-ymax/20;
East=num2str(East1);
North=num2str(North1);
inputline=['Deploy :',North,' ',East];
text(pXOBSM,pYOBSM,inputline)

pXOBSM=east(M)-xmax;
pYOBSM=north(M)-2.5*ymax/20;
East=num2str(Lon_retrieval);
North=num2str(Lat_retrieval);
inputline=['Recover:',North,' ',East];
text(pXOBSM,pYOBSM,inputline)

pXOBSM=east(M)-xmax;
pYOBSM=north(M)-4*ymax/20;
XOBSM1=num2str(XOBSM1);
YOBSM1=num2str(YOBSM1);
inputline=['Relocat:',YOBSM1,' ',XOBSM1];
text(pXOBSM,pYOBSM,inputline)

pXOBSM=east(M)-xmax;
pYOBSM=north(M)-5.5*ymax/20;
East=num2str(second_XOBSM1);
North=num2str(second_YOBSM1);
inputline=['Mirror :',North,' ',East];
text(pXOBSM,pYOBSM,inputline)

pXOBSM=east(M)-xmax;
pYOBSM=north(M)-7*ymax/20;
newposition=num2str(DELM);
inputline=['Err: ',newposition];
text(pXOBSM,pYOBSM,inputline)

pXOBSM=east(M)-xmax;
pYOBSM=north(M)-8.5*ymax/20;
newposition=num2str(headDT(1));
inputline=['Water depth: ',newposition,'m'];
text(pXOBSM,pYOBSM,inputline)

pXOBSM=east(M)-xmax;
pYOBSM=north(M)-10*ymax/20;
newposition=num2str(drift);
inputline=['The OBS drifts ',newposition,'m'];
text(pXOBSM,pYOBSM,inputline)

if drift > xmax
   fprintf(-east(M),0,'Please increase the range for searching this OBS!\n');
end
```

```
for i=1:N
   if north_east(i,1) > north(1) & north_east(i,1) < north(L)...
         & north_east(i,2) > east(1) & north_east(i,2)...
         < east(M)
      hold on
      plot(north_east(i,2),north_east(i,1),'g+')
      plot(north_east(i,2),north_east(i,1),'gO')
   end
end

saveas(gcf,'fig_part.pdf')
```

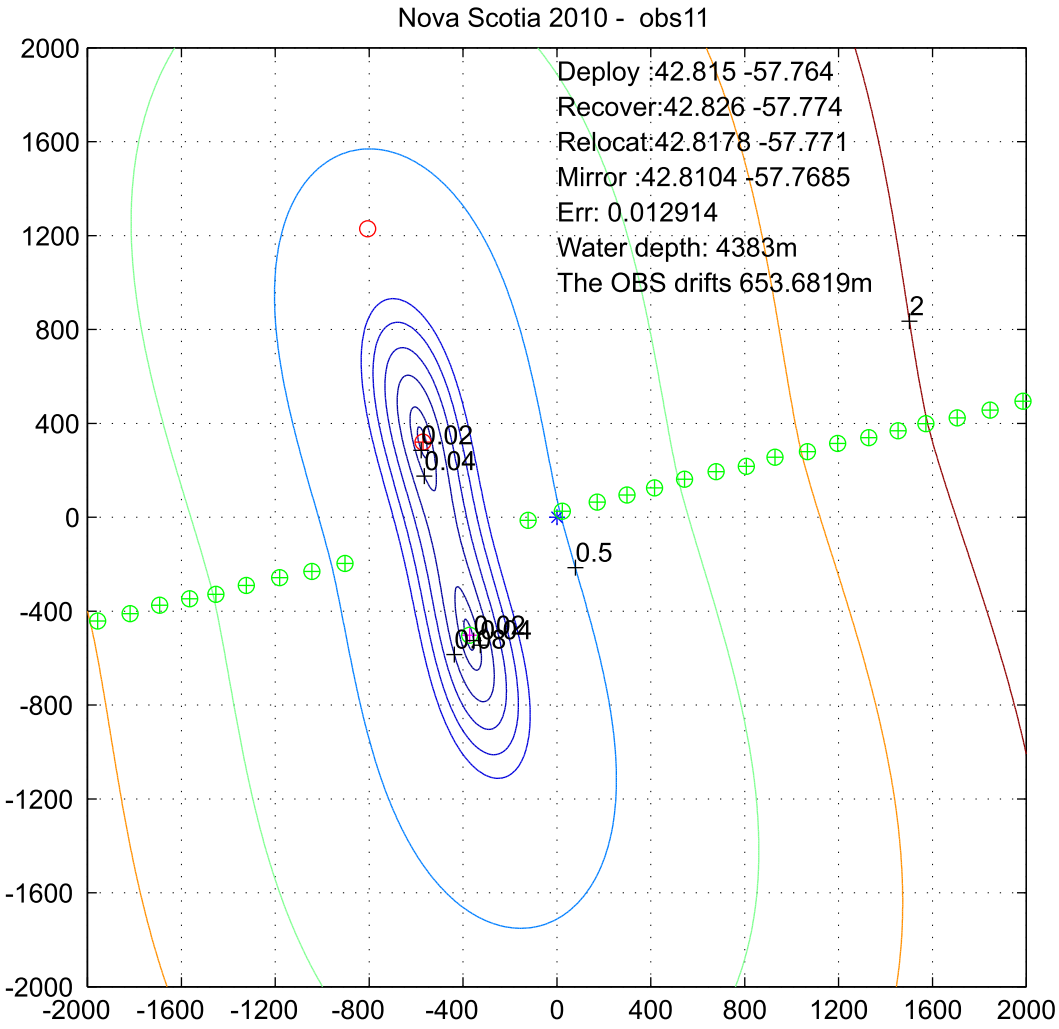

Relocation of OBS 11 in Matlab. Blue star indicates deployed position, open red circule indicates recovery position, green cricles with crosses are shot points along the OCTOPUS line, and the red cricle with cross is the relocated position.

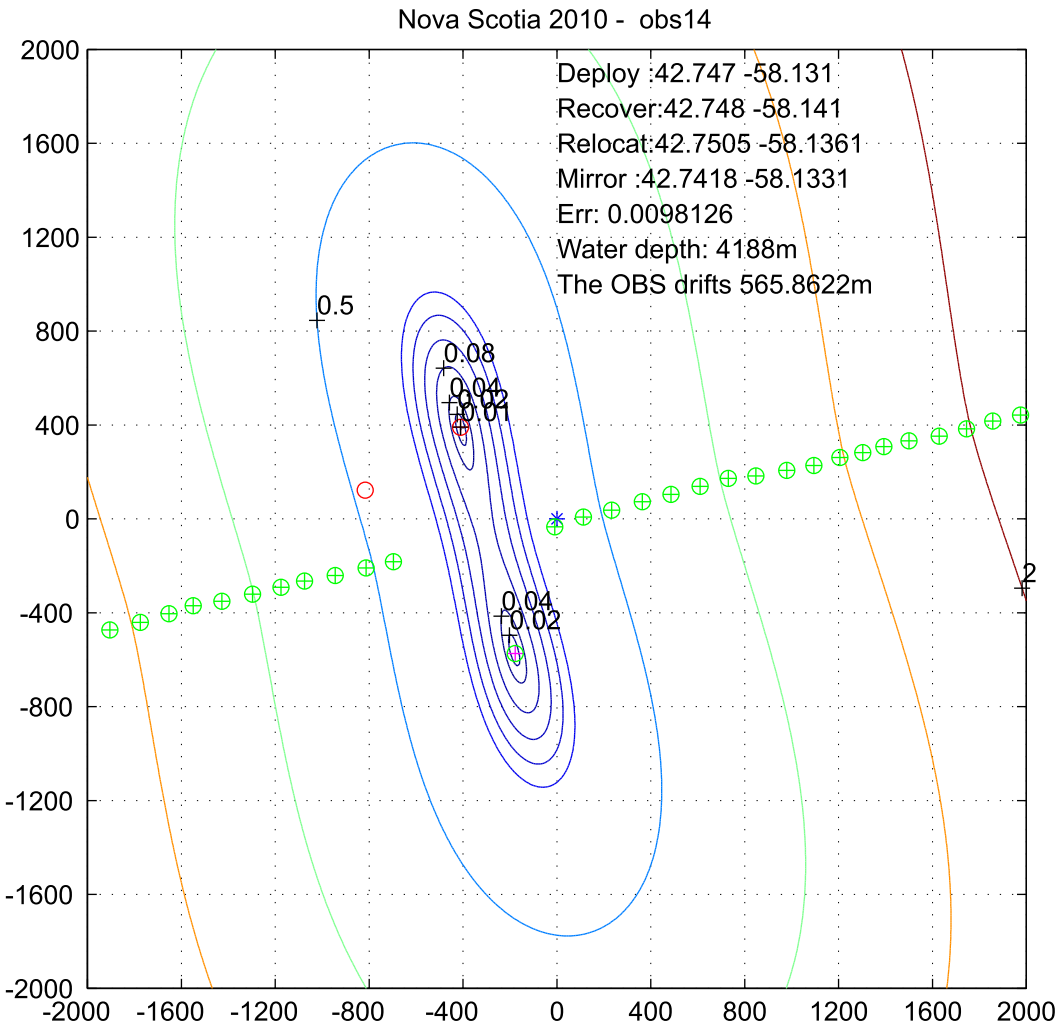

Relocation of OBS 14 in Matlab. Blue star indicates deployed position, open red circule indicates recovery position, green cricles with crosses are shot points along the OCTOPUS line, and the red cricle with cross is the relocated position.

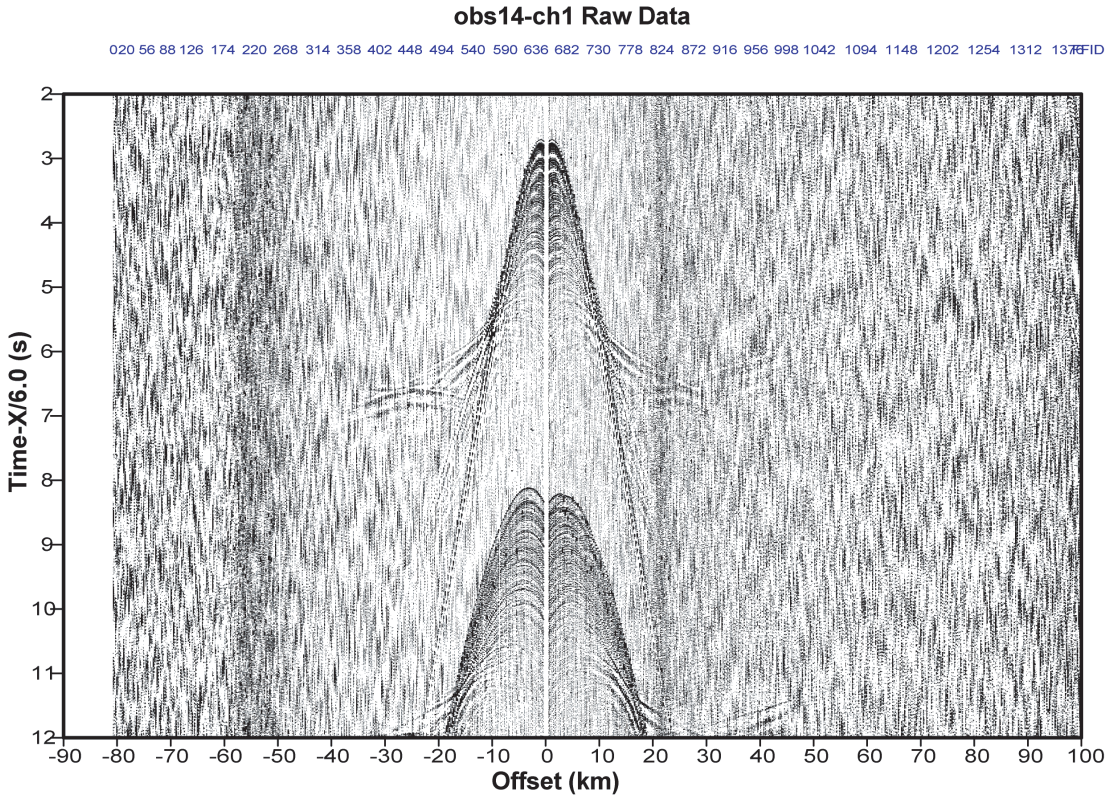
obs14-ch1 Raw Data
020 56 88 126 174 220 268 314 358 402 448 494 540 590 636 682 730 778 824 872 916 956 998 1042 1094 1148 1202 1254 1312 1374FID
Time-X/6.0 (s)
2
3
4
5
6
7
8
9
10
11
12
-90 -80 -70 -60 -50 -40 -30 -20 -10 0 10 20 30 40 50 60 70 80 90 100
Offset (km)

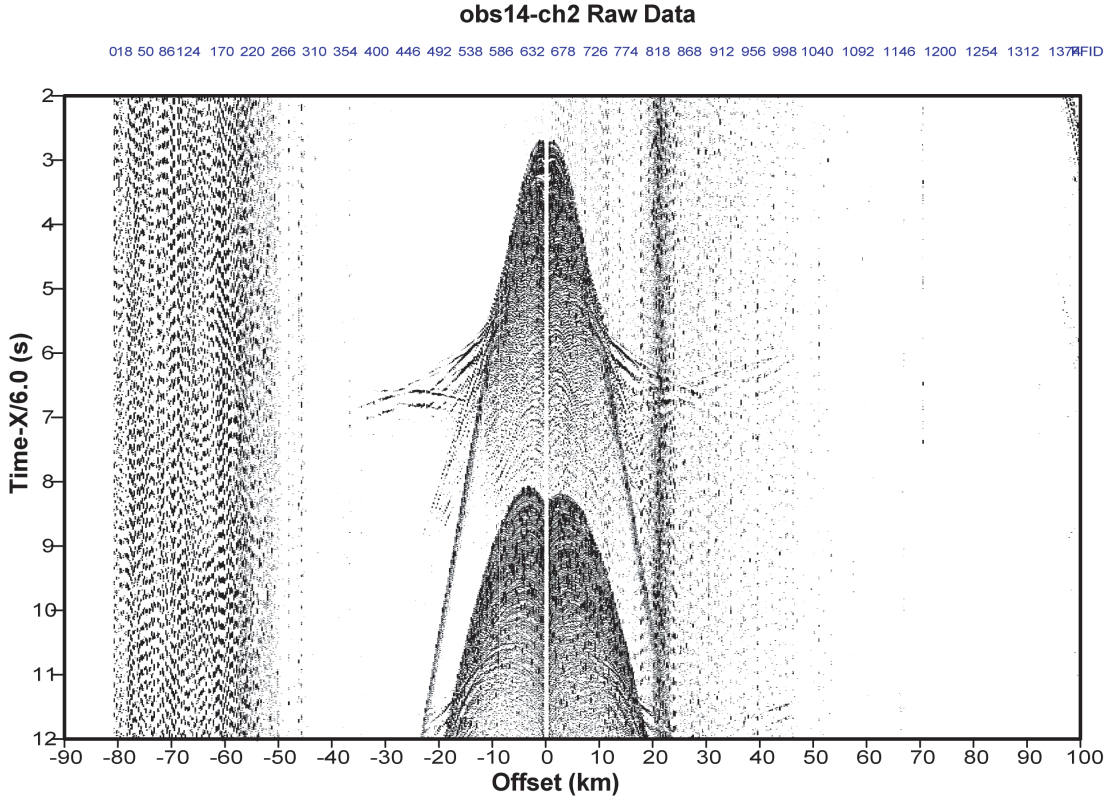
obs14-ch2 Raw Data
018 50 86 124 170 220 266 310 354 400 446 492 538 586 632 678 726 774 818 868 912 956 998 1040 1092 1146 1200 1254 1312 1374FID
Time-X/6.0 (s)
2
3
4
5
6
7
8
9
10
11
12
-90 -80 -70 -60 -50 -40 -30 -20 -10 0 10 20 30 40 50 60 70 80 90 100
Offset (km)

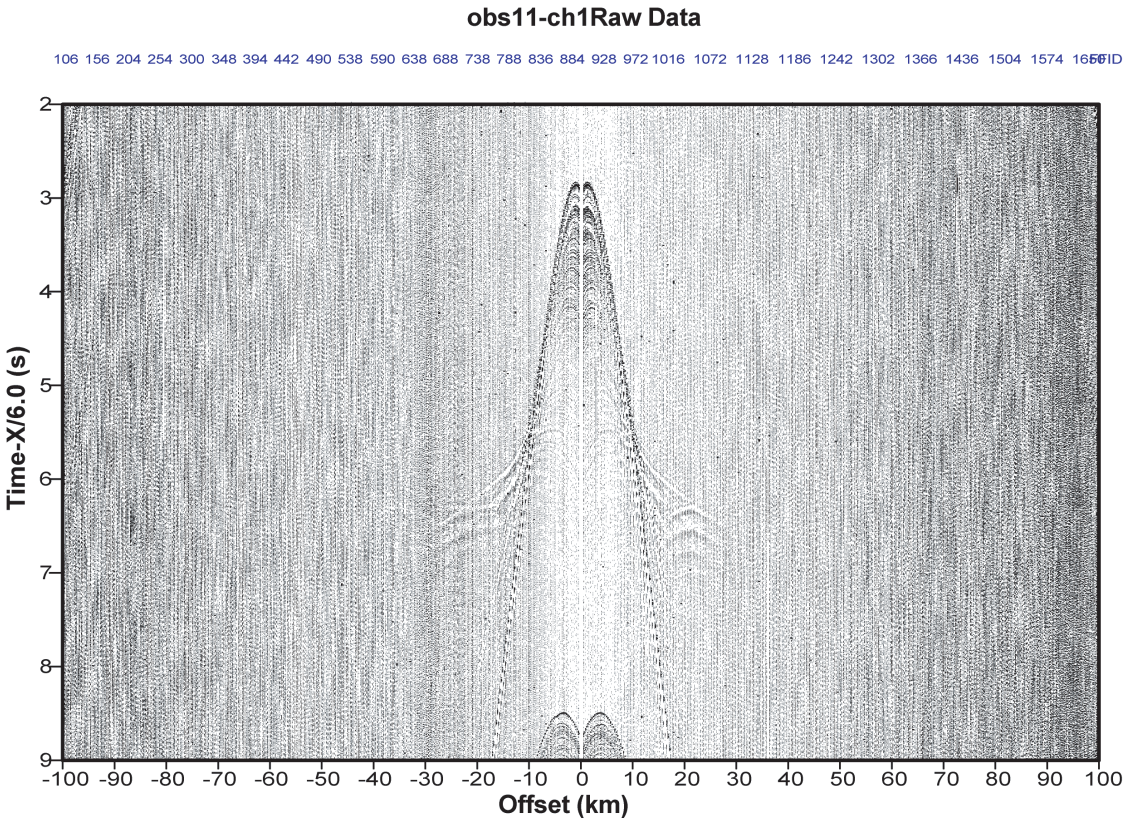
obs11-ch1Raw Data
106 156 204 254 300 348 394 442 490 538 590 638 688 738 788 836 884 928 972 1016 1072 1128 1186 1242 1302 1366 1436 1504 1574 1656 FID
Time-X/6.0 (s)
2 3 4 5 6 7 8 9
-100 -90 -80 -70 -60 -50 -40 -30 -20 -10 0 10 20 30 40 50 60 70 80 90 100
Offset (km)

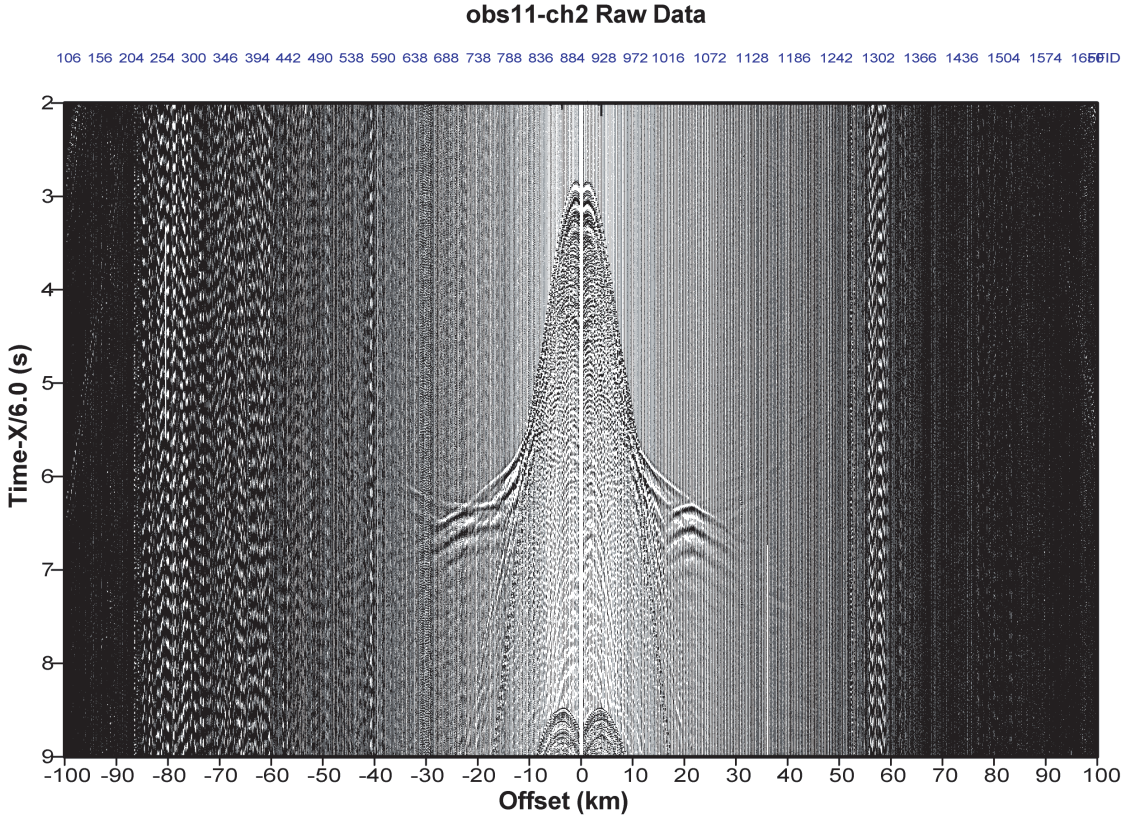
obs11-ch2 Raw Data
106 156 204 254 300 346 394 442 490 538 590 638 688 738 788 836 884 928 972 1016 1072 1128 1186 1242 1302 1366 1436 1504 1574 1656 FID
Time-X/6.0 (s)
2 3 4 5 6 7 8 9
-100 -90 -80 -70 -60 -50 -40 -30 -20 -10 0 10 20 30 40 50 60 70 80 90 100
Offset (km)

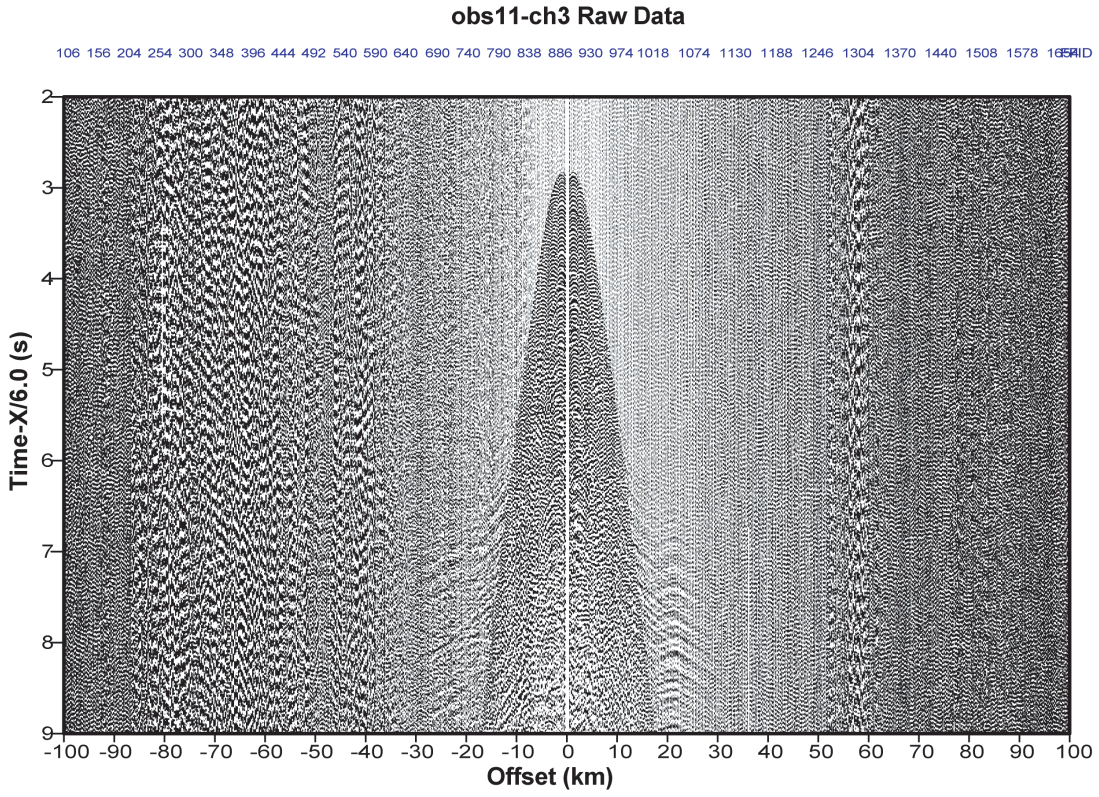
obs11-ch3 Raw Data
106 156 204 254 300 348 396 444 492 540 590 640 690 740 790 838 886 930 974 1018 1074 1130 1188 1246 1304 1370 1440 1508 1578 1654 FID
Time-X/6.0 (s)
2
3
4
5
6
7
8
9
-100 -90 -80 -70 -60 -50 -40 -30 -20 -10 0 10 20 30 40 50 60 70 80 90 100
Offset (km)

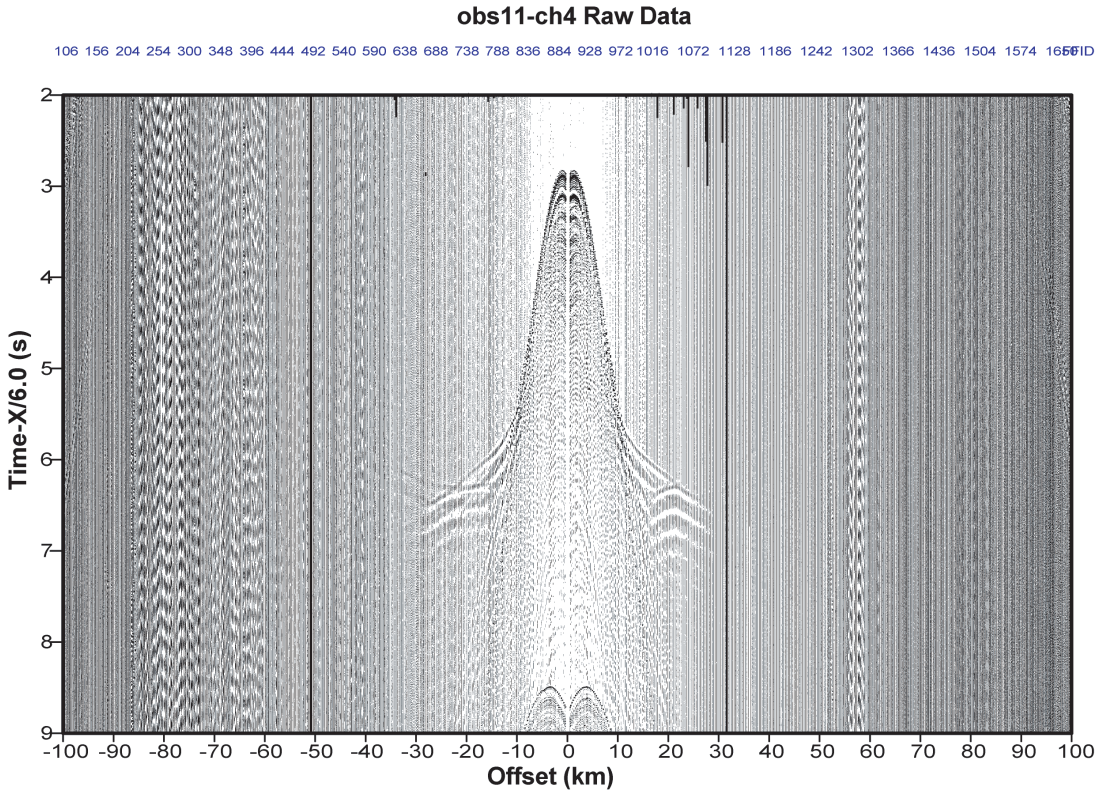
obs11-ch4 Raw Data
106 156 204 254 300 348 396 444 492 540 590 638 688 738 788 836 884 928 972 1016 1072 1128 1186 1242 1302 1366 1436 1504 1574 1656 FID
Time-X/6.0 (s)
2
3
4
5
6
7
8
9
-100 -90 -80 -70 -60 -50 -40 -30 -20 -10 0 10 20 30 40 50 60 70 80 90 100
Offset (km)

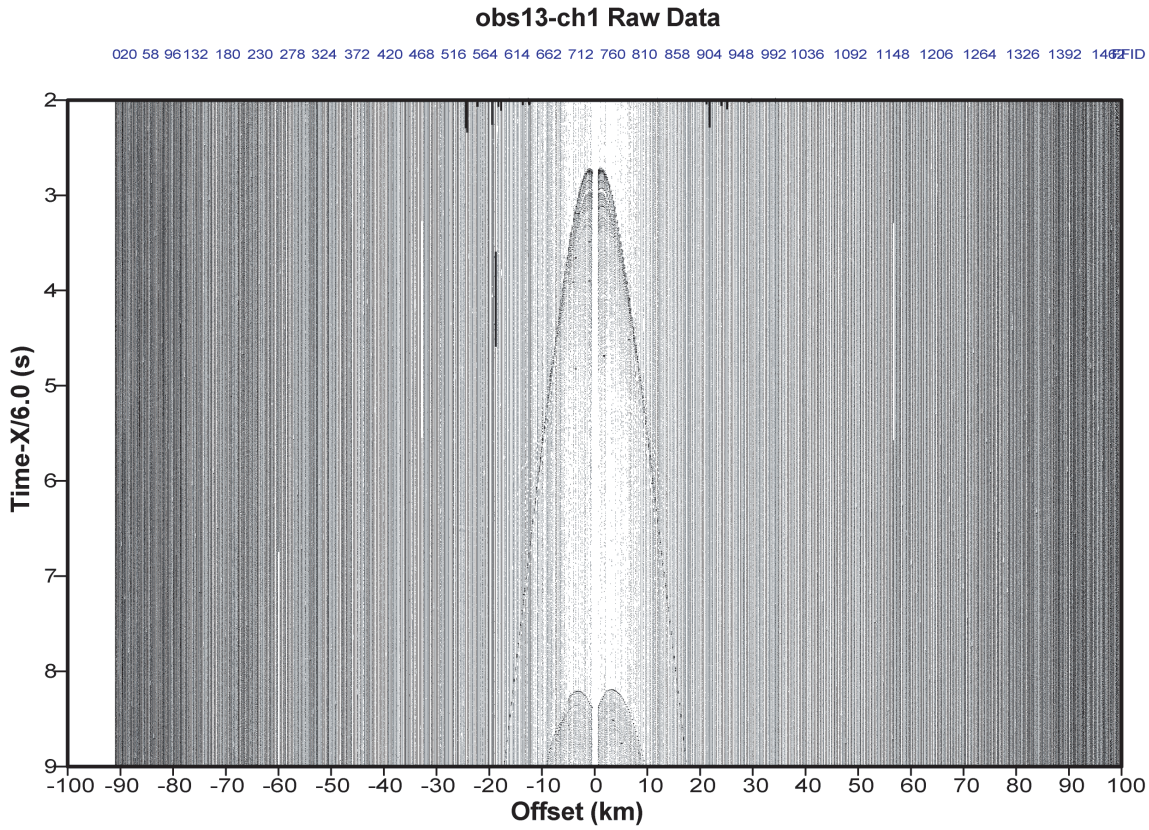
obs13-ch1 Raw Data
020 58 96 132 180 230 278 324 372 420 468 516 564 614 662 712 760 810 858 904 948 992 1036 1092 1148 1206 1264 1326 1392 1462 FID
Time-X/6.0 (s)
2
3
4
5
6
7
8
9
-100 -90 -80 -70 -60 -50 -40 -30 -20 -10 0 10 20 30 40 50 60 70 80 90 100
Offset (km)

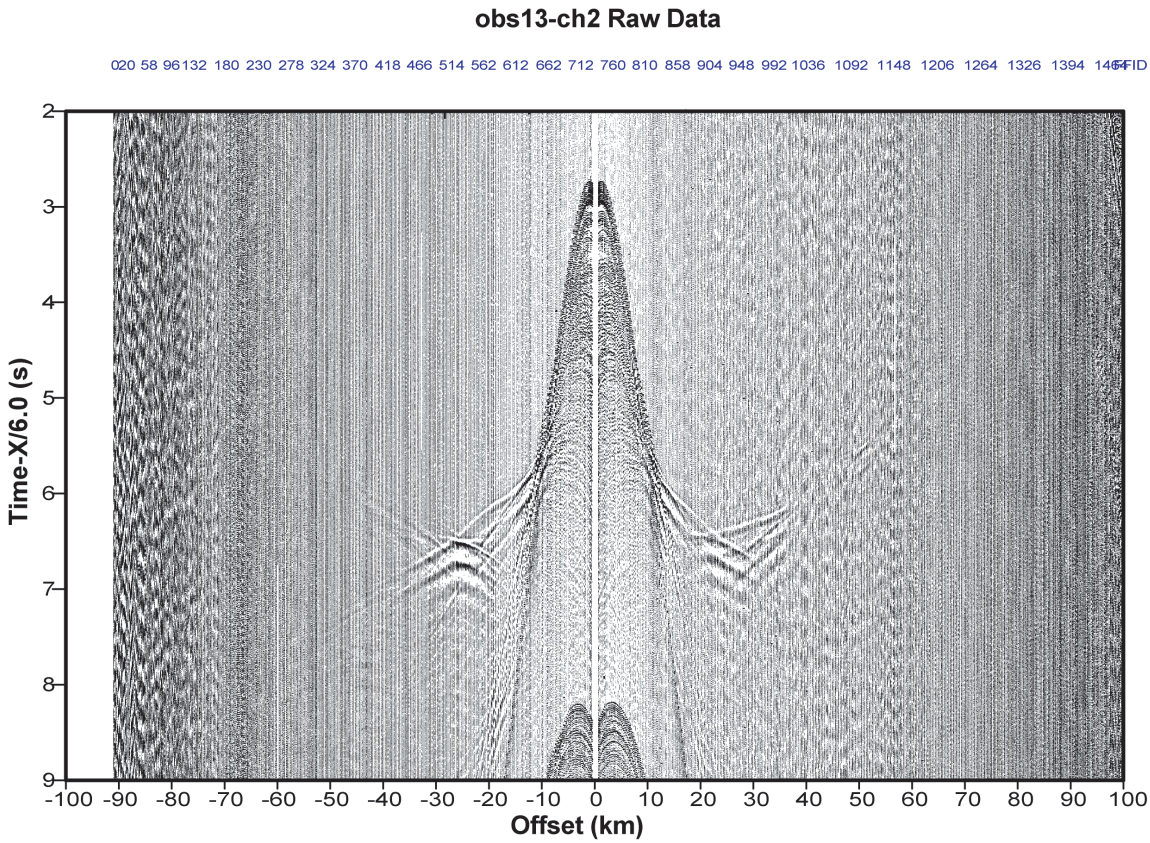
obs13-ch2 Raw Data
020 58 96 132 180 230 278 324 370 418 466 514 562 612 662 712 760 810 858 904 948 992 1036 1092 1148 1206 1264 1326 1394 1464 FID
Time-X/6.0 (s)
2
3
4
5
6
7
8
9
-100 -90 -80 -70 -60 -50 -40 -30 -20 -10 0 10 20 30 40 50 60 70 80 90 100
Offset (km)

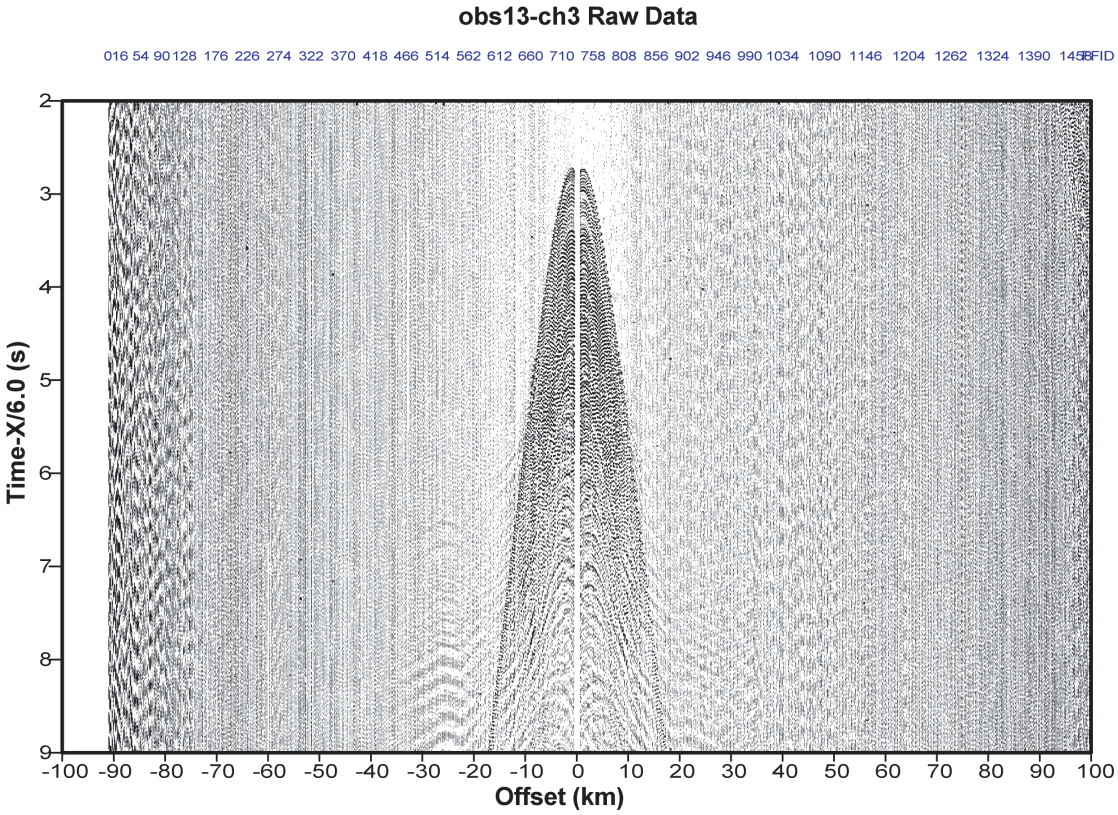
obs13-ch3 Raw Data
016 54 90 128 176 226 274 322 370 418 466 514 562 612 660 710 758 808 856 902 946 990 1034 1090 1146 1204 1262 1324 1390 1458 FID
Time-X/6.0 (s)
2
3
4
5
6
7
8
9
-100 -90 -80 -70 -60 -50 -40 -30 -20 -10 0 10 20 30 40 50 60 70 80 90 100
Offset (km)

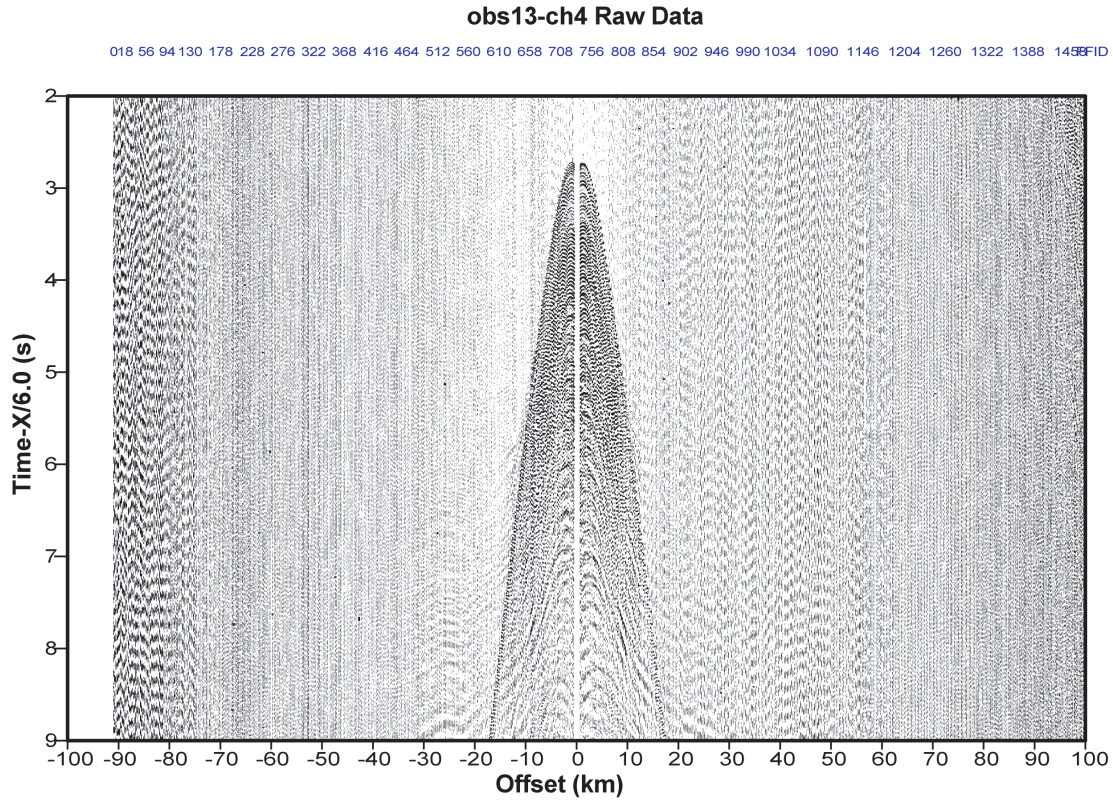
obs13-ch4 Raw Data
018 56 94 130 178 228 276 322 368 416 464 512 560 610 658 708 756 808 854 902 946 990 1034 1090 1146 1204 1260 1322 1388 1458 FID
Time-X/6.0 (s)
2
3
4
5
6
7
8
9
-100 -90 -80 -70 -60 -50 -40 -30 -20 -10 0 10 20 30 40 50 60 70 80 90 100
Offset (km)

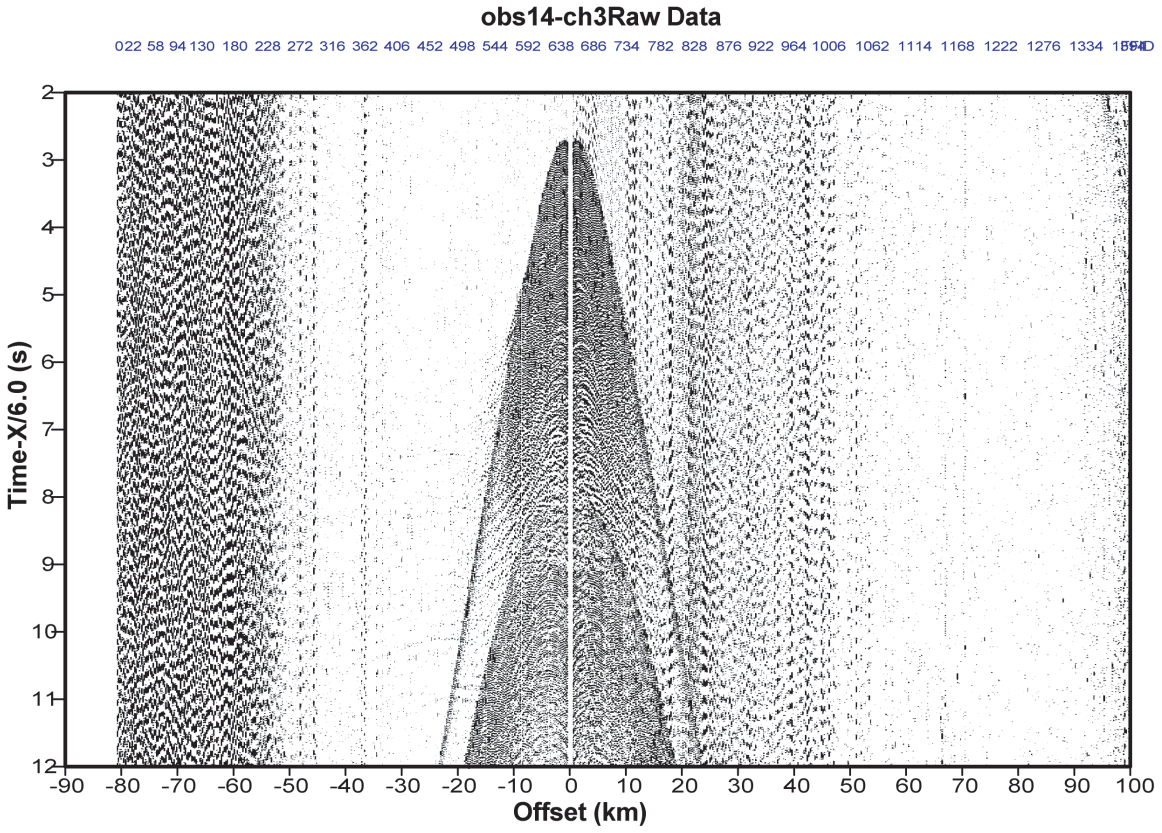
obs14-ch3Raw Data
022 58 94 130 180 228 272 316 362 406 452 498 544 592 638 686 734 782 828 876 922 964 1006 1062 1114 1168 1222 1276 1334
Time-X/6.0 (s)
2
3
4
5
6
7
8
9
10
11
12
-90 -80 -70 -60 -50 -40 -30 -20 -10 0 10 20 30 40 50 60 70 80 90 100
Offset (km)

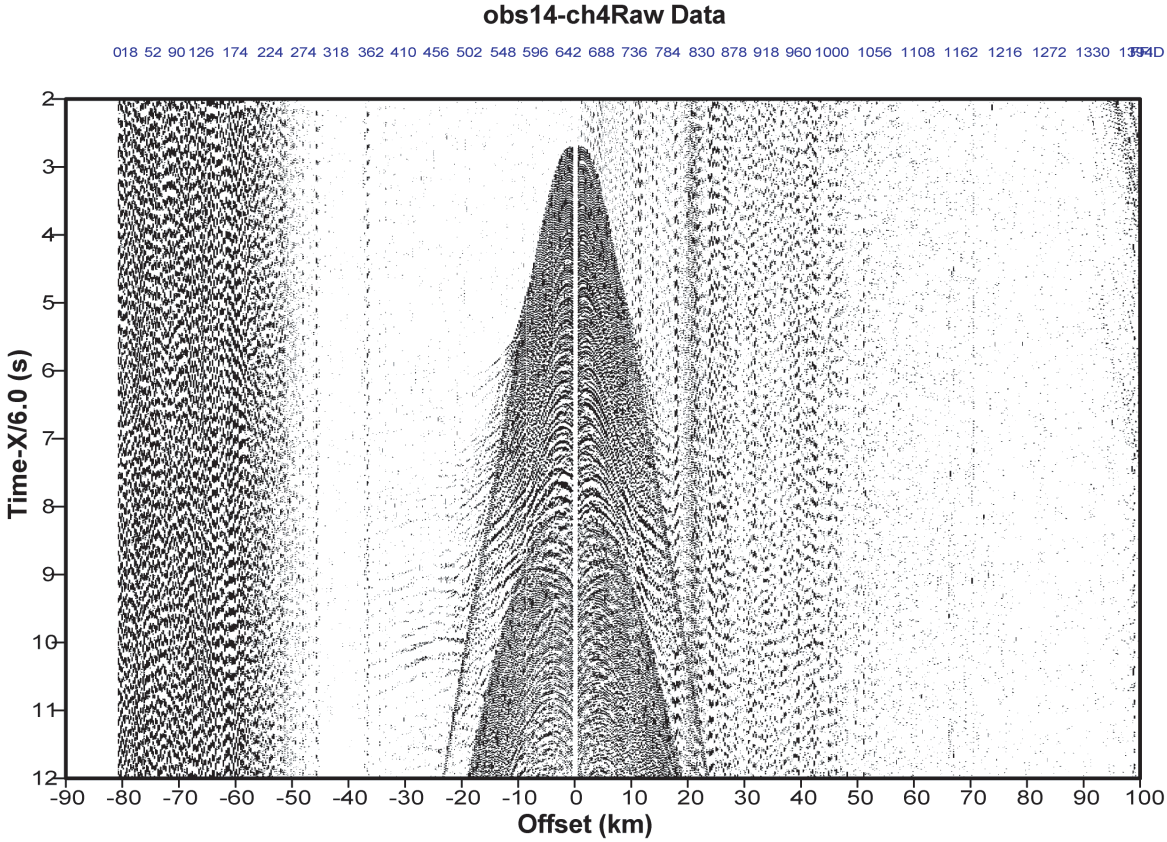
obs14-ch4Raw Data
018 52 90 126 174 224 274 318 362 410 456 502 548 596 642 688 736 784 830 878 918 960 1000 1056 1108 1162 1216 1272 1330
Time-X/6.0 (s)
2
3
4
5
6
7
8
9
10
11
12
-90 -80 -70 -60 -50 -40 -30 -20 -10 0 10 20 30 40 50 60 70 80 90 100
Offset (km)

obs 14- ch 1 Debias

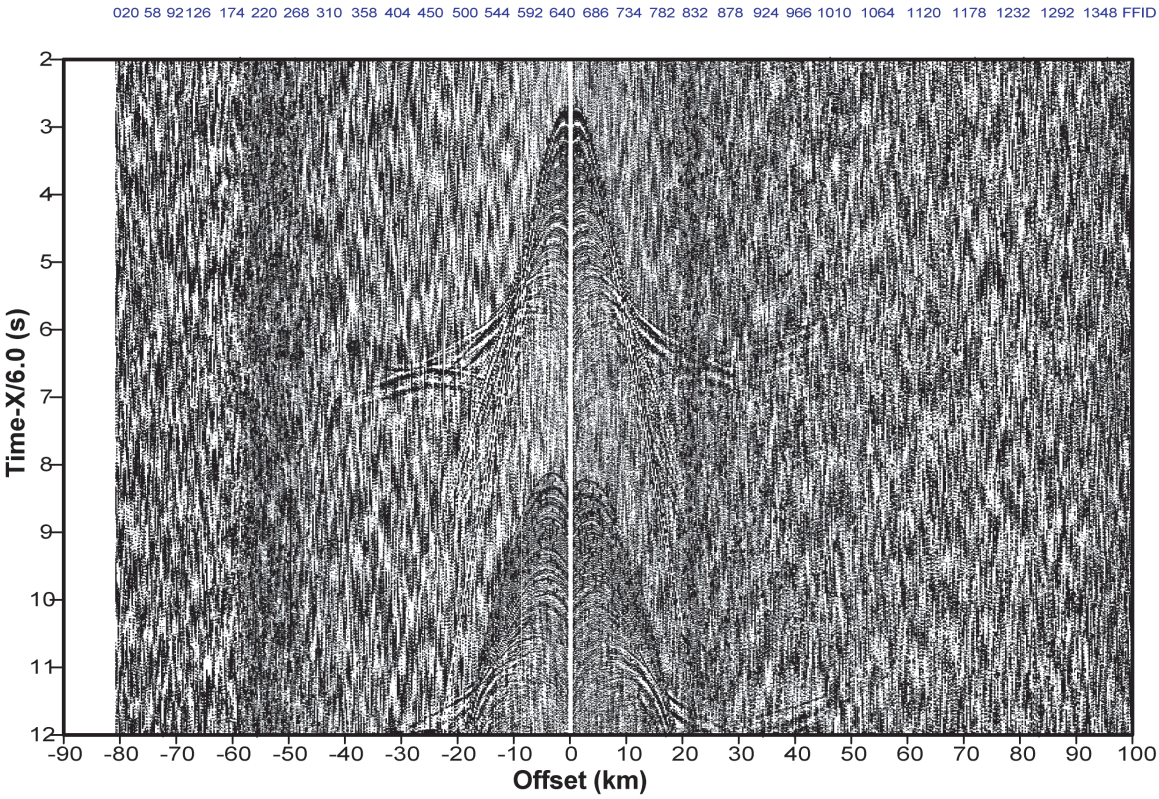

obs 14- ch 2 Debias

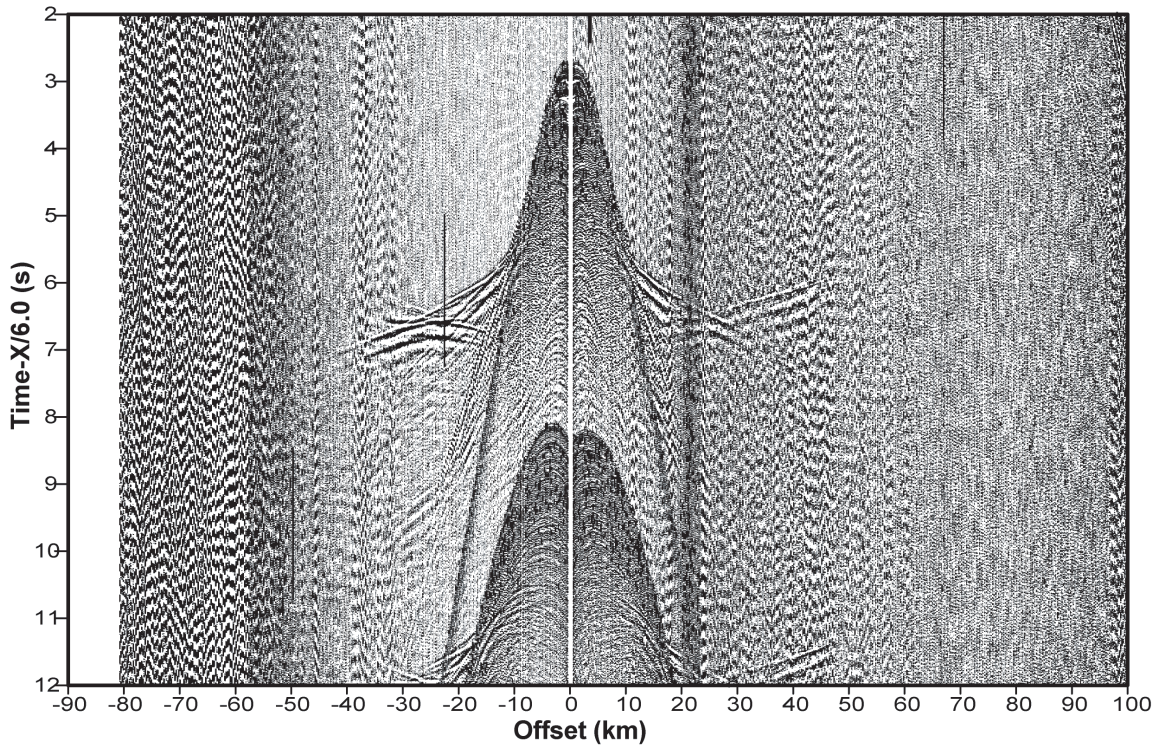

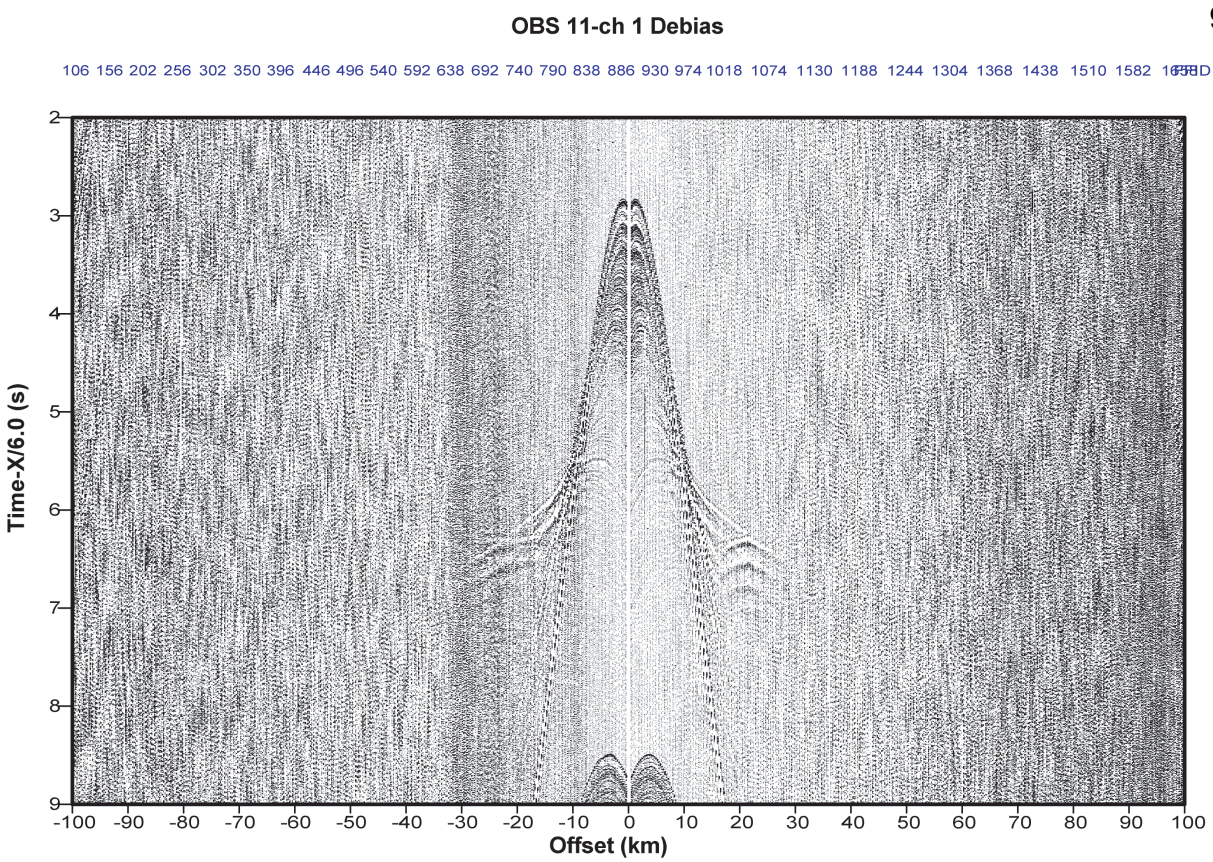
OBS 11-ch 1 Debias
106 156 202 256 302 350 396 446 496 540 592 638 692 740 790 838 886 930 974 1018 1074 1130 1188 1244 1304 1368 1438 1510 1582
Time-X/6.0 (s)
2
3
4
5
6
7
8
9
-100 -90 -80 -70 -60 -50 -40 -30 -20 -10 0 10 20 30 40 50 60 70 80 90 100
Offset (km)

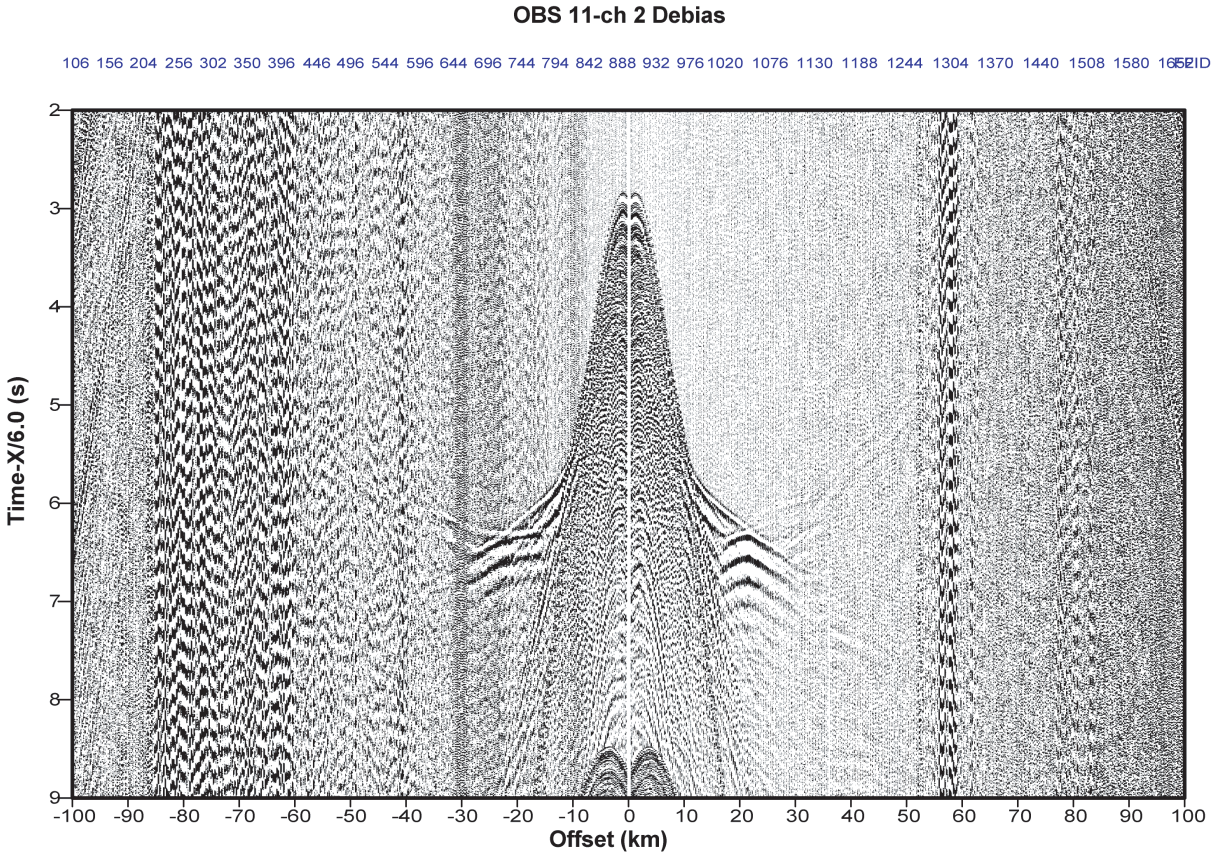
OBS 11-ch 2 Debias
106 156 204 256 302 350 396 446 496 544 596 644 696 744 794 842 888 932 976 1020 1076 1130 1188 1244 1304 1370 1440 1508 1580
Time-X/6.0 (s)
2
3
4
5
6
7
8
9
-100 -90 -80 -70 -60 -50 -40 -30 -20 -10 0 10 20 30 40 50 60 70 80 90 100
Offset (km)

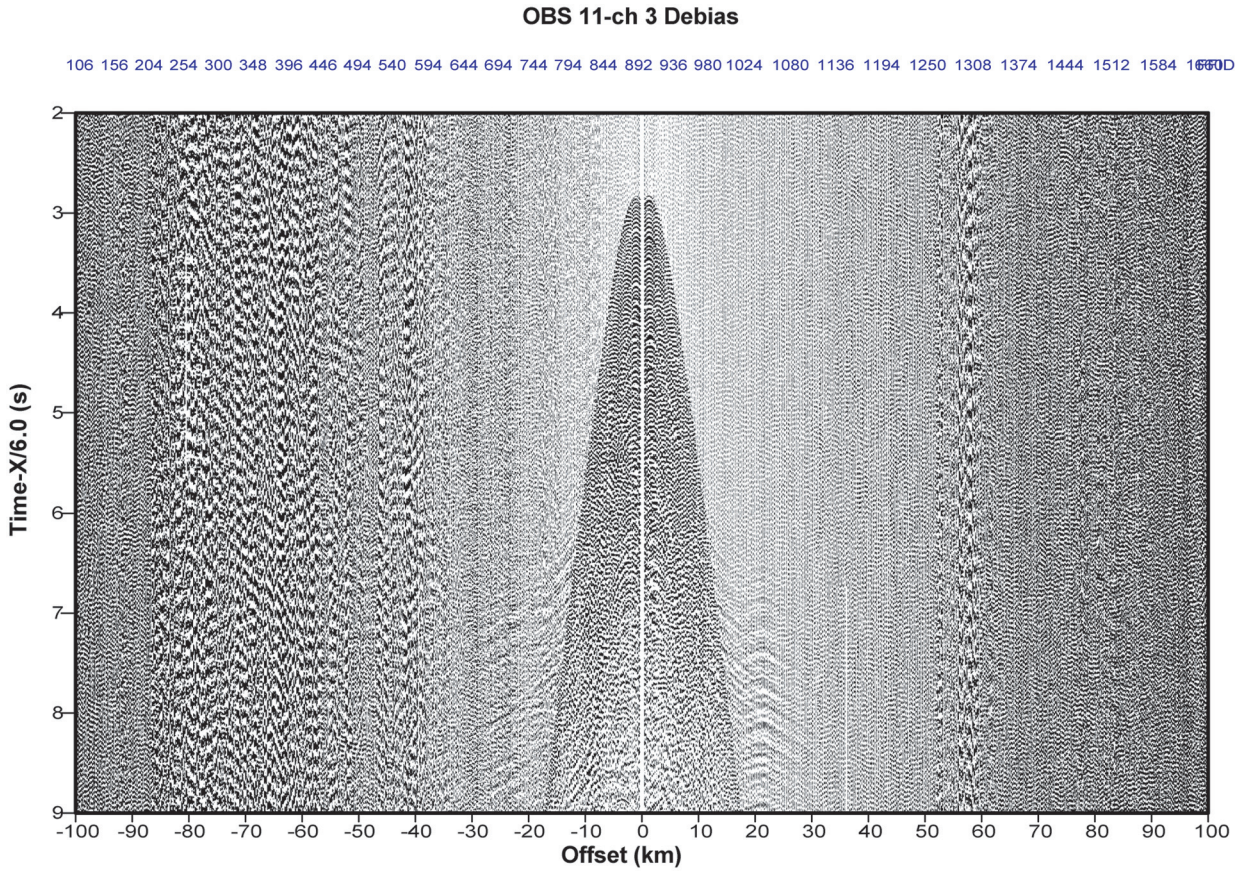
OBS 11-ch 3 Debias
106 156 204 254 300 348 396 446 494 540 594 644 694 744 794 844 892 936 980 1024 1080 1136 1194 1250 1308 1374 1444 1512 1584
Time-X/6.0 (s)
2 3 4 5 6 7 8 9
-100 -90 -80 -70 -60 -50 -40 -30 -20 -10 0 10 20 30 40 50 60 70 80 90 100
Offset (km)

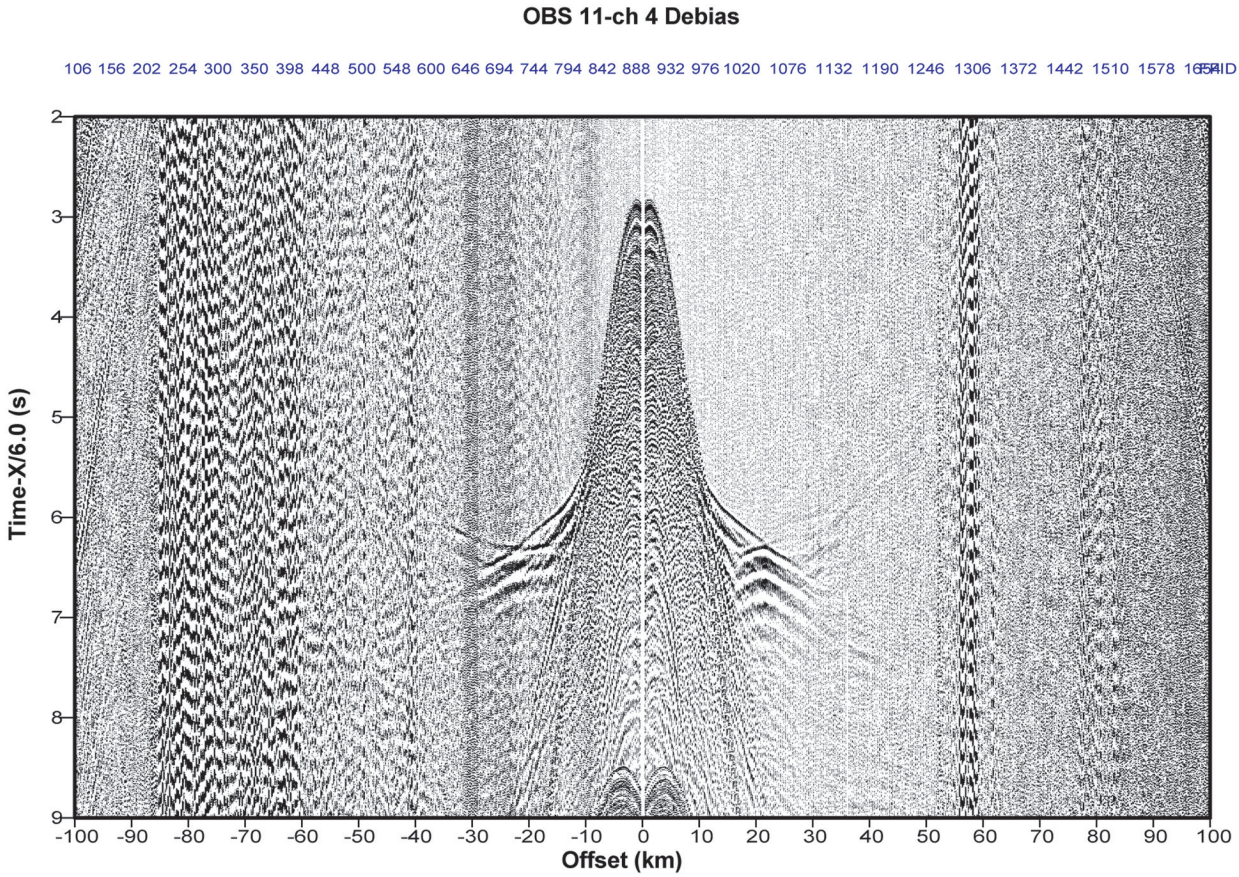
OBS 11-ch 4 Debias
106 156 202 254 300 350 398 448 500 548 600 646 694 744 794 842 888 932 976 1020 1076 1132 1190 1246 1306 1372 1442 1510 1578
Time-X/6.0 (s)
2 3 4 5 6 7 8 9
-100 -90 -80 -70 -60 -50 -40 -30 -20 -10 0 10 20 30 40 50 60 70 80 90 100
Offset (km)

obs 13- ch 1 Debias

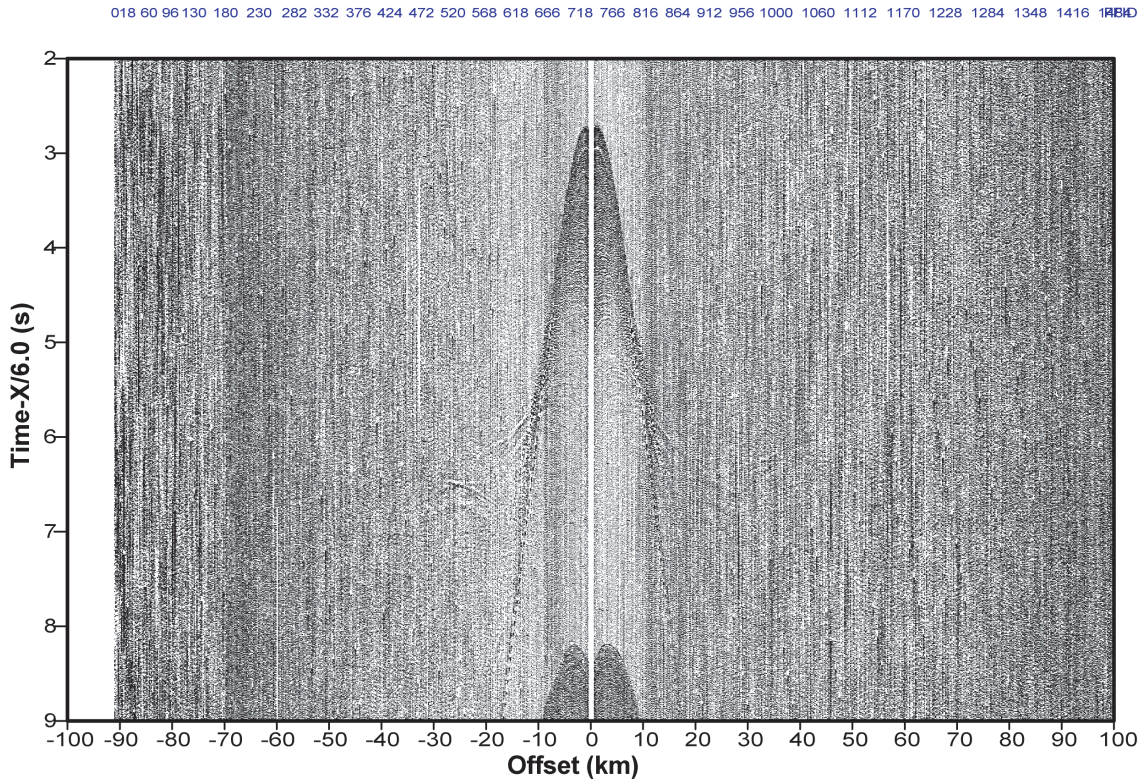

obs 13- ch 2 Debias

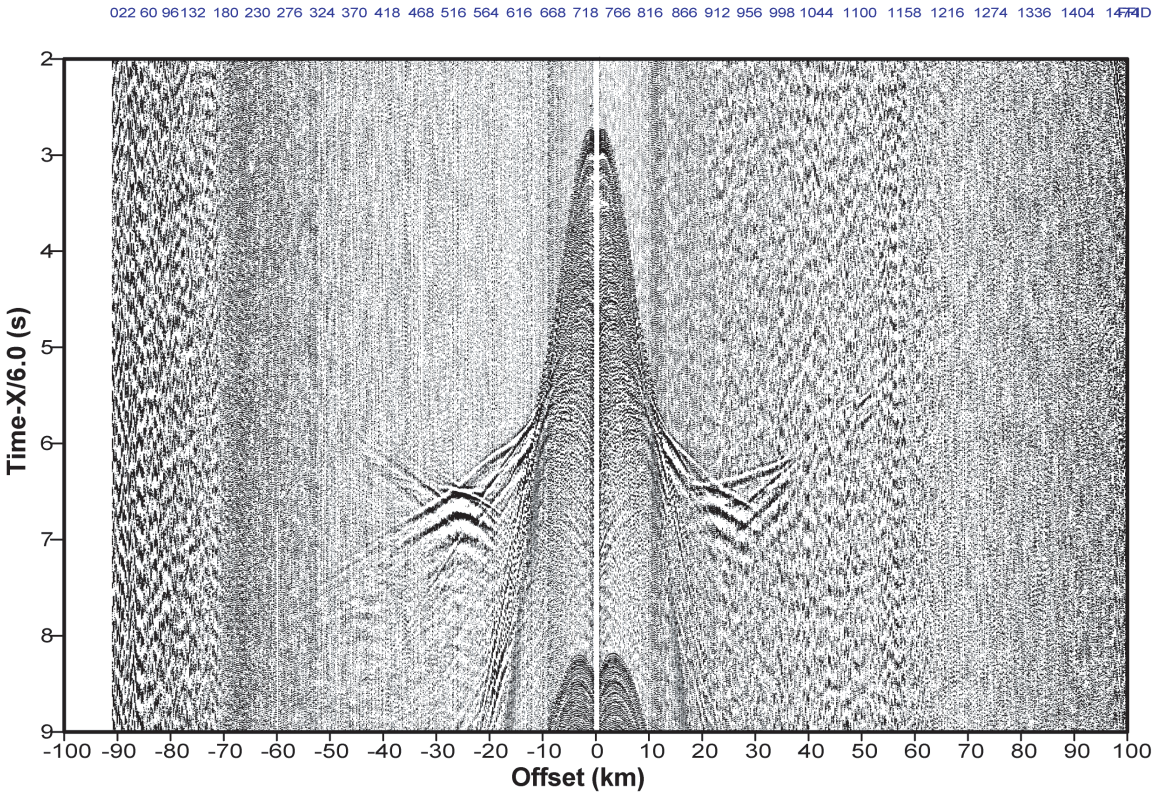

obs 13- ch 3 Debias

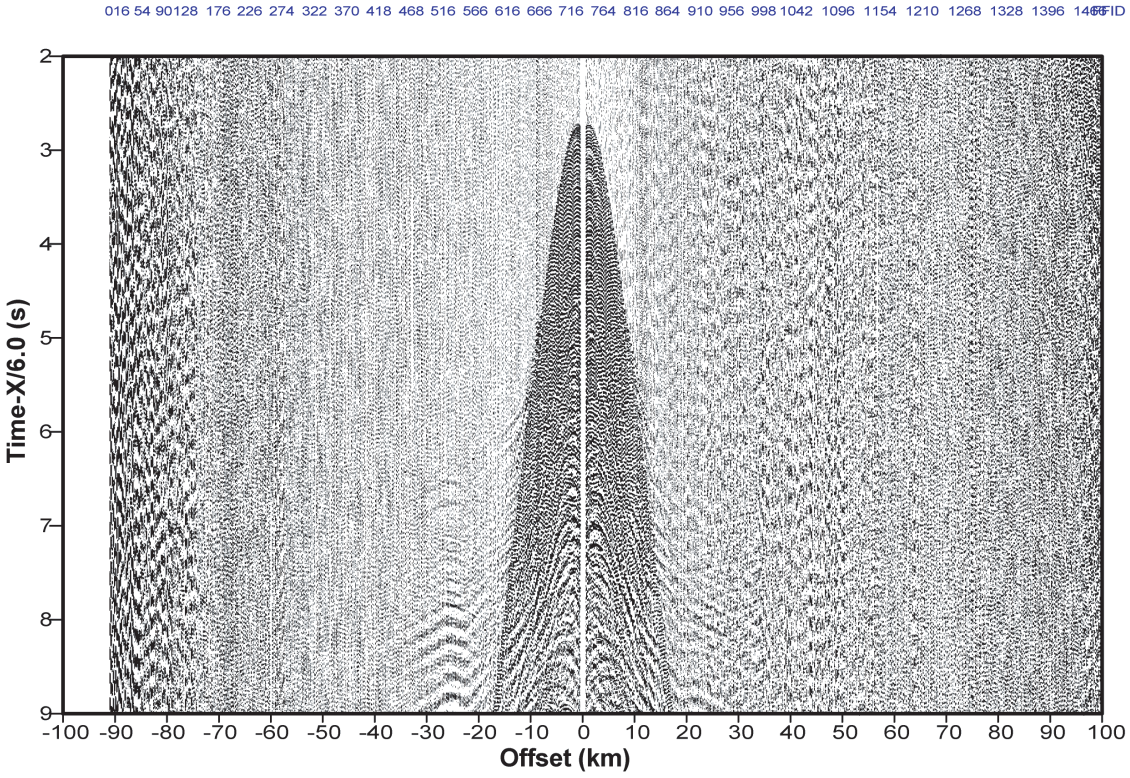

obs 13- ch 4 Debias

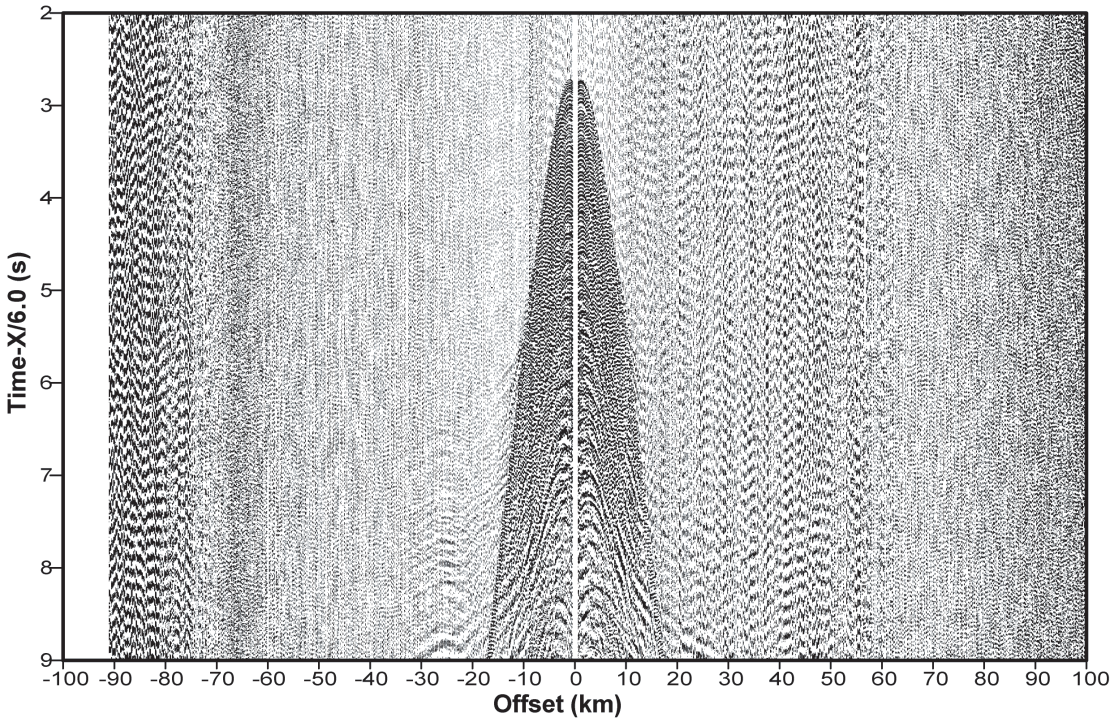

obs 14- ch 3 Debias

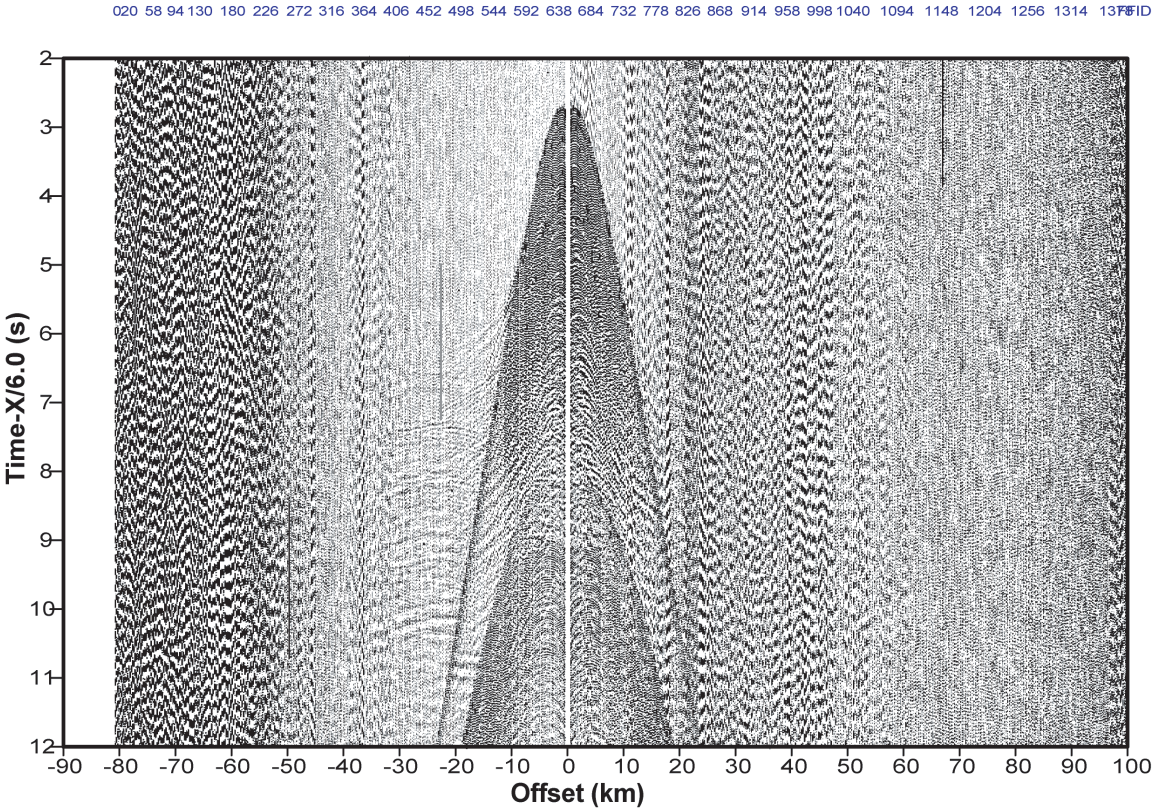

obs 14- ch 4 Debias

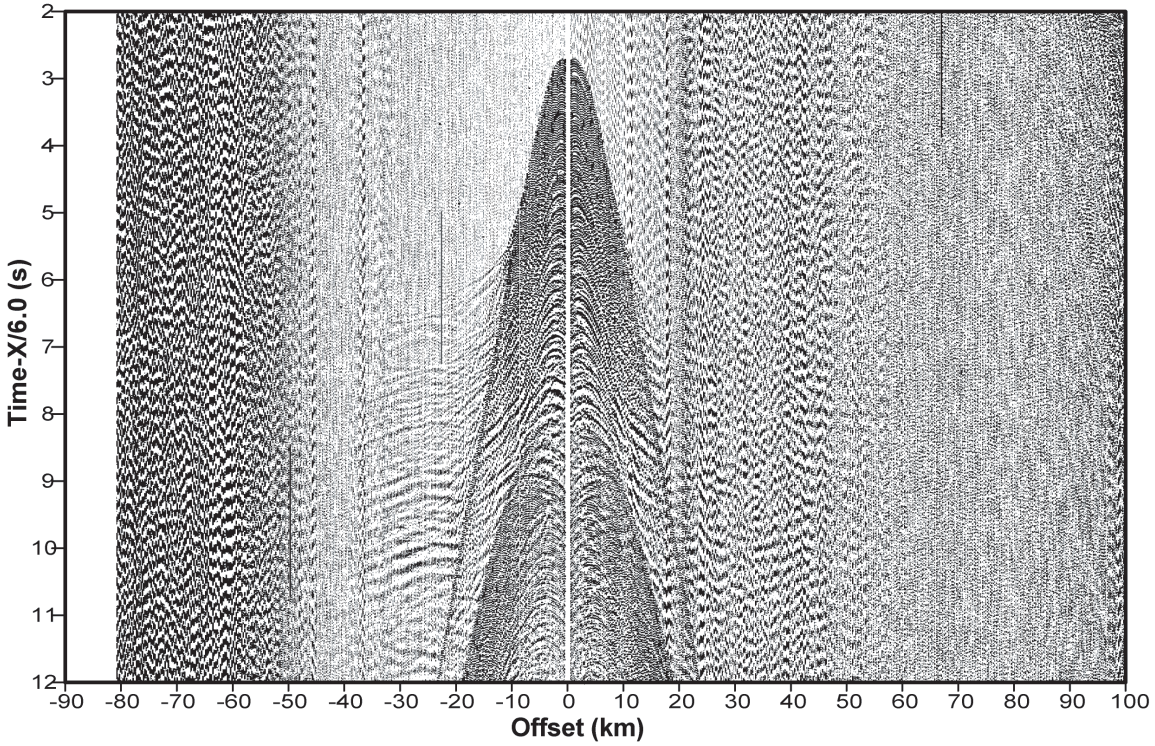

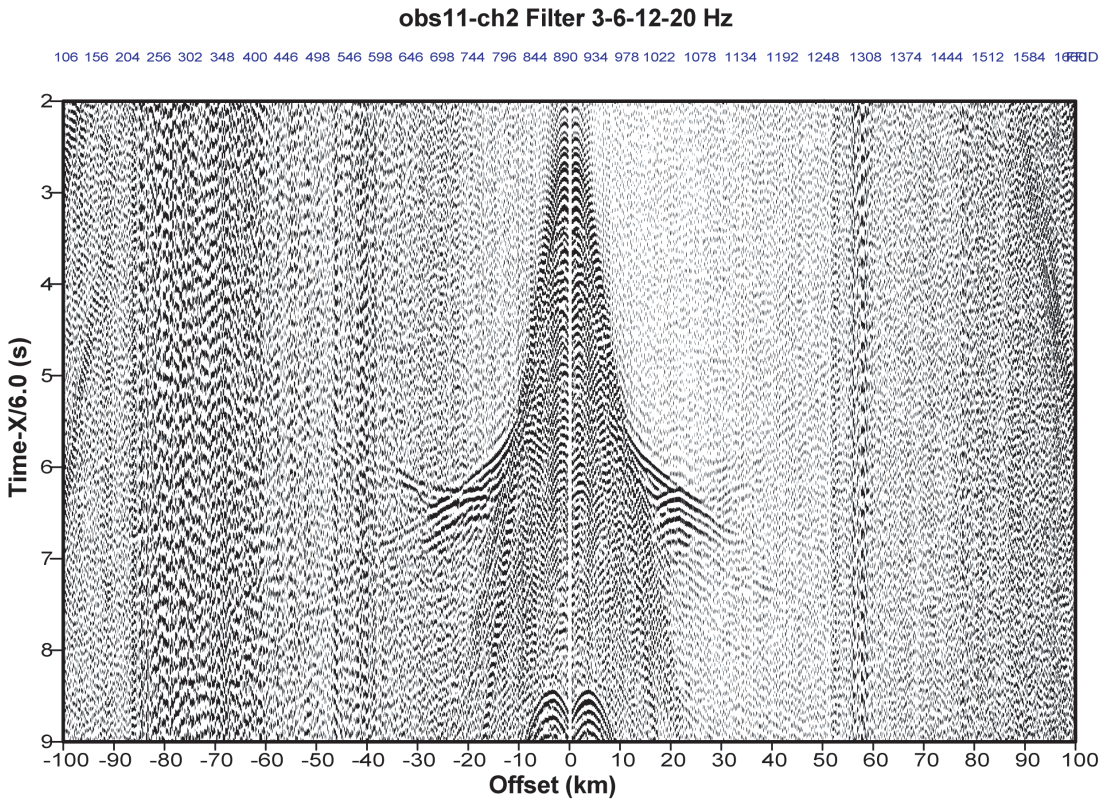
obs11-ch2 Filter 3-6-12-20 Hz
106 156 204 256 302 348 400 446 498 546 598 646 698 744 796 844 890 934 978 1022 1078 1134 1192 1248 1308 1374 1444 1512 1584
Time-X/6.0 (s)
2
3
4
5
6
7
8
9
-100 -90 -80 -70 -60 -50 -40 -30 -20 -10 0 10 20 30 40 50 60 70 80 90 100
Offset (km)

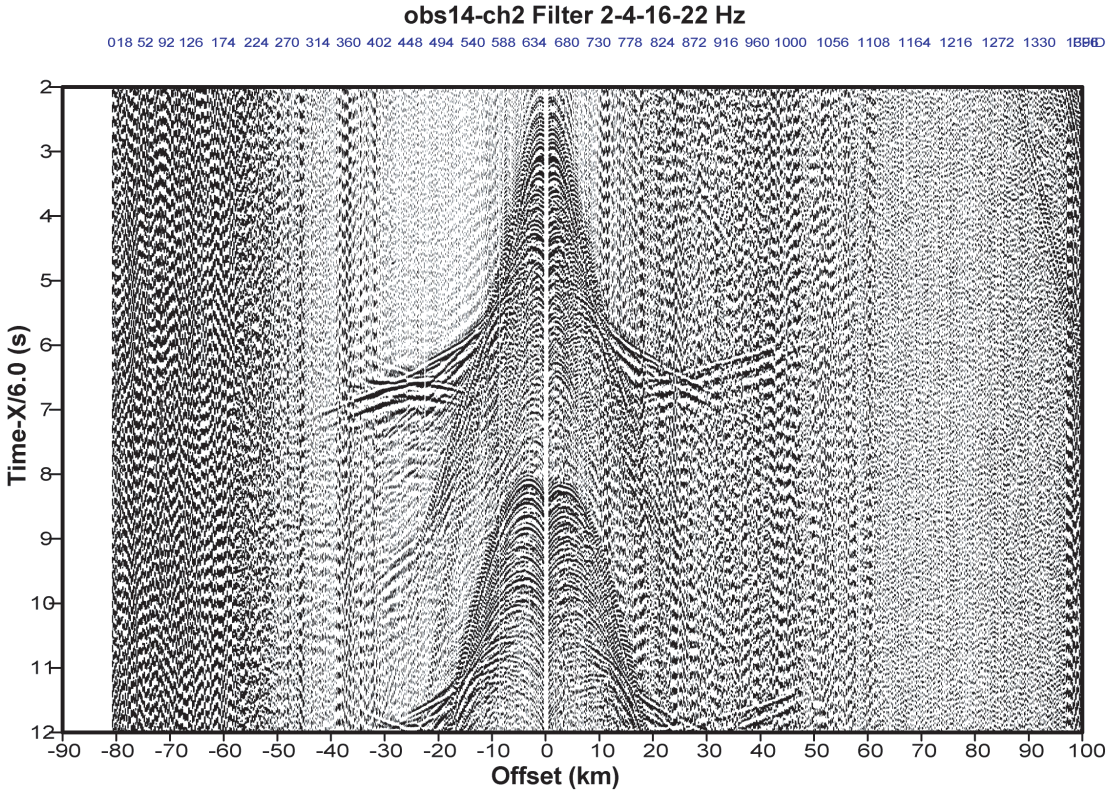
obs14-ch2 Filter 2-4-16-22 Hz
018 52 92 126 174 224 270 314 360 402 448 494 540 588 634 680 730 778 824 872 916 960 1000 1056 1108 1164 1216 1272 1330
Time-X/6.0 (s)
2
3
4
5
6
7
8
9
10
11
12
-90 -80 -70 -60 -50 -40 -30 -20 -10 0 10 20 30 40 50 60 70 80 90 100
Offset (km)

APPENDX B

Smart1_r.in

r.in file of Fucnk et al. (2004) for the SMART1 P-wave velocity model.

```
&pltpar  isep=0, itx=1, idata=1,
          imod=1, iray=2, ibnd=0, isum=2, irayps=1,
          xwndow=292., ywndow=175.,
          ircol=1, itcol=1, iplot=0, idump=1, iroute=4,
          vred=6.0, itxout=1,
 &end
 &axepar  xmin=0., xmax=490., xmm=245.,
          zmin=0., zmax=40., zmm=80.,
          ztmin=0.,ztmax=10.,ntickz=5,
          tmin=0., tmax=12.,  tmm=80.,
          albht=3.5, orig=5., sep=5.,
 &end
 &trapar  imodf=1, ibsmth=1, i2pt=0,
          ishot=0,0,0,0,0,0,0,2,0,0,
                0,0,0,0,0,0,0,0,0,0,

xshot=461.19,440.77,420.63,399.70,379.87,359.70,340.06,319.75,299.30,27
9.31,

249.48,222.52,199.15,175.70,138.85,109.18,79.55,39.63,0.00
          zshot=4.96,4.88,4.82,4.77,4.70,4.58,4.43,4.29,4.05,3.79,
                3.60,3.03,2.23,0.77,0.05,0.05,0.25,0.07,0.08,
          ray=1.2,
              2.1,2.2,3.1,3.2,4.1,4.2,5.1,5.2,6.1,6.2,
              7.1,7.2,8.1,8.2,9.1,9.2,10.1,10.2,
              11.1,11.2,12.1,12.2,13.1,13.2,14.1,14.2,15.1,
              15.2,16.1,
          nsmax=15, hws=3.,
          nray=10,
               10,10,10,10,10,10,10,10,10,10,
               10,10,10,10,10,10,10,0,
               10,10,10,10,10,10,20,10,10,
               10,10,
          space=1,
          aamin=0.05, aamax=90.,
 &end
 &invpar  invr=1,
          ivray=1,
                2,3,4,5,27,28,6,7,
                8,9,25,26,10,11,12,13,
                14,15,16,17,18,19,15,19,16,
                19,20,
 &end
 &amppar  iamp=1, isect=1,
          xmins=0.20, xmaxs=489.80, xincs=0.80,
 &end
```

OCTOPUS_r.in

The r.in file for my OCTOPUS model, modified from Funck et al. (2004).

```
&pltpar  isep=0, itx=1, idata=1,
          imod=1, iray=2, ibnd=0, isum=2, irayps=1,
          xwndow=292., ywndow=175.,
          ircol=1, itcol=1, iplot=0, idump=1, iroute=4,
          vred=6.0, itxout=1,
 &end
 &axepar  xmin=0., xmax=300., xmm=150.,
          zmin=0., zmax=40., zmm=80.,
          ztmin=0.,ztmax=10.,ntickz=5,
          tmin=0., tmax=12.,  tmm=80.,
          albht=3.5, orig=5., sep=5.,
 &end
 &trapar  imodf=1, ibsmth=1, i2pt=0,
          ishot=2,
          xshot=100.,
          zshot=4.19,
          ray=1.2,
              2.1,2.2,3.1,3.2,4.1,4.2,
              5.1,5.2,6.1,6.2,
              7.1,7.2,8.1,
          nsmax=15, hws=3.,
          nray=5,
               5,5,5,5,5,5,
               5,5,10,5,
               10,5,10,
          space=1,
          aamin=0.05, aamax=90.,
 &end
 &invpar  invr=1,
          ivray=1,
                2,3,4,5,6,7,
                10,11,12,13,
                19,15,16,
 &end
 &amppar  iamp=1, isect=1,
          xmins=0.20, xmaxs=489.80, xincs=0.80,
 &end
```

Smart1_v.in

The v.in file of Funck et al. (2004) for the SMART1 model.

```
1    0.00 100.00 150.00 200.00 300.00 315.00 400.00 490.00
 0    0.00   0.00   0.00   0.00   0.00   0.00   0.00   0.00
         0      0      0      0      0      0      0      0
 1    0.00 100.00 150.00 160.00 170.00 176.00 200.00 250.00 300.00
315.00
 1    1.51   1.51   1.51   1.51   1.51   1.50   1.48   1.48   1.48
1.48
         0      0      0      0      0      0      0      0      0
0
 1  320.00 400.00 490.00
 0    1.48   1.48   1.48
         0      0      0
 1    0.00 100.00 150.00 160.00 170.00 176.00 200.00 250.00 300.00
315.00
 1    1.51   1.51   1.51   1.51   1.51   1.50   1.50   1.52   1.53
1.53
         0      0      0      0      0      0      0      0      0
0
 1  320.00 400.00 490.00
 0    1.53   1.53   1.54
         0      0      0
 2    0.00  10.18  22.23  39.63  53.98  66.31  67.60  69.51  72.03
74.40
 1    0.09   0.11   0.10   0.08   0.09   0.19   0.29   0.30   0.09
0.09
         0      0      0      0      0      0      0      0      0
0
 2   76.43  79.55  84.79  91.62 100.00 109.18 138.85 150.00 157.47
165.09
 1    0.26   0.26   0.23   0.07   0.07   0.06   0.06   0.08   0.09
0.15
         0      0      0      0      0      0      0      0      0
0
 2  168.91 175.70 177.29 179.23 184.02 189.29 191.96 194.63 196.70
199.15
 1    0.21   0.78   1.04   1.10   1.59   1.85   2.20   2.28   2.16
2.24
         0      0      0      0      0      0      0      0      0
0
 2  200.00 200.85 202.19 203.68 222.52 224.23 225.72 234.44 236.79
240.02
 1    2.25   2.26   2.14   2.30   3.04   3.09   3.02   3.16   3.02
3.15
         0      0      0      0      0      0      0      0      0
0
 2  243.82 245.35 249.35 249.48 253.04 263.66 268.95 279.31 299.30
300.00
 1    3.43   3.43   3.61   3.61   3.61   3.75   3.68   3.80   4.06
4.07
         0      0      0      0      0      0      0      0      0
0
 2  315.00 319.75 324.35 328.88 340.06 359.70 379.87 394.75 399.70
400.00
```

```
 1    4.24   4.30   4.40   4.36   4.44   4.59   4.71   4.83   4.78
4.78
         0      0      0      0      0      0      0      0      0
0
 2  420.63 440.77 461.19 464.98 469.54 490.00
 0    4.83   4.89   4.97   4.97   4.99   5.04
         0      0      0      0      1      1
 2    0.00  40.00 100.00 150.00 160.00 165.00 184.02 200.00 300.00
315.00
 1    1.69   1.69   1.69   1.69   1.69   1.79   1.79   1.79   1.79
1.79
         0      0      0      0      0      0      0      0      0
0
 2  400.00 490.00
 0    1.79   1.79
         0      0
 2    0.00  40.00 100.00 150.00 160.00 165.00 184.02 200.00 300.00
315.00
 1    1.79   1.79   1.79   1.79   1.79   1.89   1.89   1.89   1.89
1.89
         0      0      0      0      0      0      0      0      0
0
 2  400.00 490.00
 0    1.89   1.89
         0      0
 3    0.00  30.00  35.00  72.00  80.00  85.00 100.00 110.00 120.00
130.00
 1    0.20   0.20   0.20   0.50   0.63   0.72   0.68   0.70   0.84
0.78
         0      0      0      0      0      0      0      0      0
0
 3  150.00 160.00 172.00 176.00 180.00 184.02 189.29 195.00 200.00
205.00
 1    0.86   1.00   1.45   1.67   1.90   2.00   2.75   2.80   2.80
2.80
         0      0      0      0      0      0      0      0      0
0
 3  220.00 240.00 265.00 275.00 300.00 315.00 330.00 340.00 350.00
360.00
 1    3.63   4.22   4.47   4.44   4.69   4.84   5.00   5.10   5.16
5.23
         0      0      0      0      0      0      0      0      0
0
 3  370.00 380.00 390.00 400.00 410.00 420.00 430.00 440.00 450.00
460.00
 1    5.40   5.45   5.50   5.54   5.56   5.60   5.72   5.75   5.75
5.75
         0      0      0      0      0      0      0      0      0
0
 3  470.00 490.00
 0    5.74   5.80
         0      0
 3    0.00  60.00  70.00  85.00  90.00 100.00 120.00 130.00 150.00
180.00
 1    2.21   2.21   2.66   2.66   2.30   2.30   2.30   2.45   2.45
2.48
```

```
         0      0      0      0      0      0      0      0      0
0
 3  190.00 200.00 210.00 240.00 250.00 300.00 315.00 355.00 360.00
400.00
 1    2.48   2.22   2.00   2.10   2.10   2.22   2.22   2.22   2.32
2.32
         0      0      0      0      0      0      0      0      0
0
 3  490.00
 0    2.32
         0
 3    0.00  60.00  70.00  85.00  90.00 100.00 120.00 130.00 150.00
180.00
 1    2.43   2.43   2.80   2.80   2.50   2.50   2.50   2.65   2.65
2.52
         0      0      0      0      0      0      0      0      0
0
 3  190.00 200.00 210.00 240.00 250.00 300.00 315.00 355.00 360.00
400.00
 1    2.52   2.27   2.05   2.15   2.15   2.27   2.27   2.27   2.37
2.37
         0      0      0      0      0      0      0      0      0
0
 3  490.00
 0    2.37
         0
 4    0.00   9.00  17.50  40.00  45.00  50.00  70.00  80.00 100.00
110.00
 1    1.10   1.10   1.10   1.15   1.38   1.58   1.77   1.74   1.49
1.53
         0      0      0      0      0      0      0      0      0
0
 4  125.00 135.00 145.00 150.00 155.00 160.00 167.00 174.00 190.00
195.00
 1    1.56   1.58   1.62   1.70   1.74   1.79   1.91   2.01   3.20
3.54
         0      0      0      0      0      0      0      0      0
0
 4  200.00 210.00 215.00 220.00 250.00 258.00 260.00 280.00 282.00
285.50
 1    3.87   4.00   4.30   4.41   5.21   5.31   5.90   6.07   6.10
6.41
         0      0      0      0      0      0      0      0      0
0
 4  300.00 305.00 320.00 340.00 480.00 490.00
 0    6.50   6.55   6.60   6.80   7.50   7.50
         0      0      0      0      0      0
 4    0.00 100.00 150.00 160.00 190.00 200.00 205.00 255.00 260.00
300.00
 1    3.10   3.10   3.10   3.10   3.10   3.10   3.00   3.00   3.00
3.00
         0      0      0      0      0      0      0      0      0
0
 4  315.00 400.00 490.00
 0    3.00   3.10   3.10
         0      0      0
```

```
 4    0.00 100.00 150.00 160.00 190.00 200.00 205.00 255.00 260.00
300.00
 1    3.10   3.10   3.10   3.10   3.20   3.20   3.10   3.10   3.00
3.00
         0      0      0      0      0      0      0      0      0
0
 4  315.00 400.00 490.00
 0    3.00   3.10   3.10
         0      0      0
 5    0.00   9.00  17.50  40.00  45.00  50.00  70.00  80.00 100.00
110.00
 1    1.10   1.10   1.10   1.15   1.38   1.58   1.77   1.74   1.49
1.53
         0      0      0      0      0      0      0      0      0
0
 5  125.00 135.00 145.00 150.00 155.00 160.00 167.00 174.00 177.00
190.00
 1    1.56   1.58   1.62   1.70   1.74   1.79   2.04   2.26   2.68
4.20
         0      0      0      0      0      0      0      0      0
0
 5  200.00 210.00 220.00 250.00 260.00 280.00 282.00 285.50 300.00
305.00
 1    4.68   5.17   5.18   5.81   5.90   6.07   6.10   6.41   6.50
6.55
         0      0      0      0      0      0      0      0      0
0
 5  320.00 340.00 480.00 490.00
 0    6.60   6.80   7.50   7.50
         0      0      0      0
 5    0.00   9.00  17.50  30.00  50.00 100.00 150.00 155.00 175.00
180.00
 1    3.95   3.95   3.15   3.15   3.49   3.49   3.49   3.80   3.80
3.49
         0      0      0      0      0      0      0      0      0
0
 5  200.00 205.00 250.00 300.00 305.00 315.00 345.00 350.00 370.00
400.00
 1    3.49   3.65   3.65   3.65   3.65   3.65   3.65   3.45   3.45
3.45
         0      0      0      0      0      0      0      0      0
0
 5  480.00 490.00
 0    3.45   3.45
         0      0
 5    0.00   9.00  17.50  30.00  50.00 100.00 150.00 155.00 175.00
180.00
 1    4.05   3.95   3.15   3.35   3.69   3.69   3.69   3.89   3.89
3.69
         0      0      0      0      0      0      0      0      0
0
 5  200.00 205.00 250.00 300.00 305.00 315.00 345.00 350.00 370.00
400.00
 1    3.69   3.79   3.79   3.79   3.79   3.79   3.79   3.59   3.59
3.59
         0      0      0      0      0      0      0      0      0
0
```

```
 5  480.00 490.00
 0    3.59   3.59
         0      0
 6    0.00   9.00  17.50  40.00  70.00  80.00  83.00  90.00 100.00
120.00
 1    2.00   1.10   1.10   2.21   2.80   2.80   2.75   2.75   2.85
2.95
         0      0      0      0      0      0      0      0      0
0
 6  125.00 140.00 150.00 160.00 170.00 180.00 190.00 200.00 210.00
220.00
 1    2.97   3.05   3.00   3.15   3.70   4.45   5.80   6.52   6.62
6.65
         0      0      0      0      0      0      0      0      0
0
 6  230.00 240.00 250.00 260.00 270.00 280.00 287.00 310.00 315.00
320.00
 1    6.75   6.82   6.80   7.20   7.60   7.64   8.17   8.23   8.30
8.29
         0      0      0      0      0      0      0      0      0
0
 6  360.00 380.00 400.00 420.00 440.00 450.00 457.00 470.00 480.00
490.00
 0    8.20   8.30   8.25   8.10   8.00   8.00   7.83   8.03   8.03
8.03
         0      0      0      0      0      0      0      0      0
0
 6    0.00 100.00 125.00 150.00 170.00 180.00 200.00 265.00 270.00
300.00
 1    4.20   4.23   4.23   4.23   4.23   4.23   4.23   4.23   4.23
4.23
         0      0      0      0      0      0      0      0      0
0
 6  315.00 400.00 490.00
 0    4.20   4.20   4.20
         0      0      0
 6    0.00 100.00 125.00 150.00 170.00 180.00 200.00 265.00 270.00
300.00
 1    4.20   4.23   4.23   4.30   4.30   4.30   4.30   4.30   4.23
4.23
         0      0      0      0      0      0      0      0      0
0
 6  315.00 400.00 490.00
 0    4.20   4.20   4.20
         0      0      0
 7    0.00   9.00  17.50  40.00  70.00  80.00  83.00  90.00 100.00
120.00
 1    2.00   1.10   1.10   2.21   2.80   2.80   2.75   2.75   2.85
2.95
         0      0      0      0      0      0      0      0      0
0
 7  125.00 150.00 160.00 175.00 180.00 190.00 200.00 210.00 233.50
256.50
 1    2.97   3.79   4.14   5.14   6.35   7.50   7.73   7.96   8.29
7.91
         0      0      0      0      0      0      0      0      0
0
```

```
 7  260.00 270.00 280.00 287.00 310.00 315.00 320.00 360.00 380.00
400.00
 1    7.80   7.60   7.64   8.17   8.23   8.30   8.29   8.20   8.30
8.25
         0      0      0      0      0      0      0      0      0
0
 7  420.00 440.00 450.00 457.00 470.00 480.00 490.00
 0    8.10   8.00   8.00   7.83   8.03   8.03   8.03
         0      0      0      0      0      0      0
 7    0.00  40.00 100.00 150.00 160.00 190.00 200.00 270.00 280.00
287.00
 1    4.40   4.40   4.40   4.40   4.45   4.45   4.40   4.40   4.40
4.42
         0      0      0      0      0      0      0      0      0
0
 7  400.00 490.00
 0    4.40   4.40
         0      0
 7    0.00  40.00 100.00 150.00 160.00 190.00 200.00 270.00 280.00
287.00
 1    4.40   4.40   4.60   4.60   4.55   4.55   4.50   4.49   4.46
4.42
         0      0      0      0      0      0      0      0      0
0
 7  400.00 490.00
 0    4.40   4.40
         0      0
 8    0.00   9.00  17.50  40.00  60.00  62.00  71.00  80.00 100.00
125.00
 1    2.00   1.10   1.10   2.21   3.41   3.79   4.12   4.12   4.21
4.26
         0      0      0      0      0      0      0      0      0
0
 8  135.00 159.00 172.00 174.00 180.50 184.50 187.00 193.00 200.00
208.00
 1    4.58   5.35   6.91   7.37   9.62  11.00  12.11  11.72  11.71
11.69
         0      0      0      0      0      0      0      0      0
0
 8  221.00 230.00 235.00 245.00 250.00 258.00 267.50 273.00 276.00
282.00
 1   11.15  11.06  10.53  10.37  10.49  10.19   9.63   9.24   9.52
9.34
         0      0      0      0      0      0      0      0      0
0
 8  284.00 287.00 310.00 315.00 320.00 360.00 380.00 400.00 420.00
440.00
 1    8.88   8.17   8.23   8.30   8.29   8.20   8.30   8.25   8.10
8.00
         0      0      0      0      0      0      0      0      0
0
 8  450.00 457.00 470.00 480.00 490.00
 0    8.00   7.83   8.03   8.03   8.03
         0      0      0      0      0
 8    0.00 100.00 150.00 187.00 200.00 205.00 250.00 275.00 280.00
300.00
```

```
 1    4.65   4.65   4.65   4.62   4.62   4.62   4.62   4.62   4.62
4.62
         0      0      0      0      0      0      0      0      0
0
 8  320.00 325.00 330.00 335.00 340.00 360.00 380.00 385.00 400.00
490.00
 0    4.62   4.43   4.23   4.23   4.33   4.33   4.23   4.23   4.23
4.23
         0      0      0      0      0      0      0      0      0
0
 8    0.00 100.00 150.00 187.00 200.00 205.00 250.00 275.00 280.00
300.00
 1    4.65   4.65   4.65   4.62   4.64   4.67   4.67   4.67   4.67
4.67
         0      0      0      0      0      0      0      0      0
0
 8  320.00 325.00 330.00 335.00 340.00 360.00 380.00 385.00 400.00
490.00
 0    4.67   4.47   4.27   4.27   4.37   4.37   4.27   4.27   4.27
4.27
         0      0      0      0      0      0      0      0      0
0
 9    0.00   9.00  17.50  40.00  60.00  62.00  71.00  80.00 100.00
125.00
 1    2.00   1.10   1.10   2.21   3.41   3.79   4.12   4.12   4.21
4.26
         0      0      0      0      0      0      0      0      0
0
 9  135.00 150.00 159.00 180.50 184.50 187.00 193.00 197.00 200.00
205.00
 1    4.58   5.86   7.11   9.62  11.00  12.11  12.25  12.62  12.50
12.40
         0      0      0      0      0      0      0      0      0
0
 9  208.70 214.00 218.00 220.00 229.00 237.50 243.00 255.00 257.50
278.50
 1   13.27  12.86  13.26  12.89  13.09  11.92  12.48  12.14  11.70
11.76
         0      0      0      0      0      0      0      0      0
0
 9  284.00 288.00 292.00 315.50 318.00 324.50 325.50 328.00 335.00
340.00
 1   11.10  11.80  11.16  10.91  10.40  10.17  10.10  10.46  10.30
9.68
         0      0      0      0      0      0      0      0      0
0
 9  356.00 360.00 366.00 368.00 372.50 374.00 377.00 382.00 383.50
388.00
 1    9.58  10.53   8.92   9.82   9.47   8.86  10.26   9.93   9.34
9.23
         0      0      0      0      0      0      0      0      0
0
 9  389.50 391.50 393.00 394.00 396.50 400.00 403.00 407.00 409.50
413.00
 1    8.63   8.82   9.81   9.81   8.88   8.80   9.64   9.66   8.91
8.76
```

```
         0      0      0      0      0      0      0      0      0
0
 9  419.50 420.50 423.00 427.00 430.00 432.50 433.50 435.00 438.00
440.00
 1    9.29   9.55   9.51   8.19   9.41   8.80   9.41   9.21   8.41
9.07
         0      0      0      0      0      0      0      0      0
0
 9  443.00 444.50 449.00 451.00 454.50 456.00 458.00 459.00 460.20
462.00
 1    9.25   9.67   9.62   8.80   8.66   8.03   8.05   8.39   8.60
9.28
         0      0      0      0      0      0      0      0      0
0
 9  465.00 468.00 471.50 476.00 482.00 486.50 490.00
 0    9.73   8.47   8.49   9.62   9.14   8.16   8.12
         0      0      0      0      0      0      0
 9    0.00  70.00 100.00 150.00 184.00 187.00 200.00 490.00
 0    5.20   5.20   5.20   5.20   5.27   5.40   5.40   5.40
         0      0      0      0      0      0      0      0
 9    0.00  70.00 100.00 150.00 184.00 187.00 200.00 490.00
 0    5.20   5.20   5.40   5.40   5.40   5.40   5.40   5.40
         0      0      0      0      0      0      0      0
10    0.00   9.00  17.50  40.00  60.00  62.00  71.00  77.50  89.50
96.00
 1    2.00   1.10   1.10   2.21   3.41   3.79   4.12   7.45   8.58
10.26
         0      0      0      0      0      0      0      0      0
0
10   98.00 100.00 107.50 111.50 116.00 128.00 132.50 141.00 146.00
150.00
 1   10.26   9.65   7.34   7.34   9.64  15.06  12.61  12.47  11.34
11.55
         0      0      0      0      0      0      0      0      0
0
10  156.00 165.00 175.00 182.50 187.00 193.00 197.00 200.00 205.00
208.70
 1   12.87  13.00  12.50  12.50  12.11  12.25  12.62  12.50  12.40
13.27
         0      0      0      0      0      0      0      0      0
0
10  214.00 218.00 220.00 229.00 237.50 243.00 255.00 257.50 278.50
284.00
 1   12.86  13.26  12.89  13.09  11.92  12.48  12.14  11.70  11.76
11.10
         0      0      0      0      0      0      0      0      0
0
10  288.00 292.00 315.50 318.00 324.50 325.50 328.00 335.00 340.00
356.00
 1   11.80  11.16  10.91  10.40  10.17  10.10  10.46  10.30   9.68
9.58
         0      0      0      0      0      0      0      0      0
0
10  360.00 366.00 368.00 372.50 374.00 377.00 382.00 383.50 388.00
389.50
 1   10.53   8.92   9.82   9.47   8.86  10.26   9.93   9.34   9.23
8.63
```

```
         0      0      0      0      0      0      0      0      0
0
10  391.50 393.00 394.00 396.50 400.00 403.00 407.00 409.50 413.00
419.50
 1    8.82   9.81   9.81   8.88   8.80   9.64   9.66   8.91   8.76
9.29
         0      0      0      0      0      0      0      0      0
0
10  420.50 423.00 427.00 430.00 432.50 433.50 435.00 438.00 440.00
443.00
 1    9.55   9.51   8.19   9.41   8.80   9.41   9.21   8.41   9.07
9.25
         0      0      0      0      0      0      0      0      0
0
10  444.50 449.00 451.00 454.50 456.00 458.00 459.00 460.20 462.00
465.00
 1    9.67   9.62   8.80   8.66   8.03   8.05   8.39   8.60   9.28
9.73
         0      0      0      0      0      0      0      0      0
0
10  468.00 471.50 476.00 482.00 486.50 490.00
 0    8.47   8.49   9.62   9.14   8.16   8.12
         0      0      0      0      0      0
10    0.00  89.50  93.50 100.00 112.00 116.00 128.00 132.00 150.00
152.00
 1    4.40   4.40   4.40   4.40   4.40   4.40   4.40   4.40   4.40
4.40
         0      0      0      0      0      0      0      0      0
0
10  156.00 200.00 490.00
 0    4.50   4.50   4.50
         0      0      0
10    0.00  89.50  93.50 100.00 112.00 116.00 128.00 132.00 150.00
152.00
 1    4.40   4.40   4.50   4.50   4.50   4.40   4.40   4.50   4.50
4.50
         0      0      0      0      0      0      0      0      0
0
10  156.00 200.00 490.00
 0    4.50   4.50   4.50
         0      0      0
11    0.00   9.00  17.50  40.00  60.00  62.00  71.00  77.50  89.50
100.00
 1    2.00   1.10   1.10   2.21   3.41   3.79   4.12   7.45   8.58
12.39
         0      0      0      0      0      0      0      0      0
0
11  116.00 128.00 150.00 156.00 165.00 175.00 182.50 187.00 193.00
197.00
 1    9.64  15.06  12.25  12.87  13.00  12.50  12.50  12.11  12.25
12.62
         0      0      0      0      0      0      0      0      0
0
11  200.00 205.00 208.70 214.00 218.00 220.00 229.00 237.50 243.00
255.00
 1   12.50  12.40  13.27  12.86  13.26  12.89  13.09  11.92  12.48
12.14
```

```
         0      0      0      0      0      0      0      0      0
0
11  257.50 278.50 284.00 288.00 292.00 315.50 318.00 324.50 325.50
328.00
 1   11.70  11.76  11.10  11.80  11.16  10.91  10.40  10.17  10.10
10.46
         0      0      0      0      0      0      0      0      0
0
11  335.00 340.00 356.00 360.00 366.00 368.00 372.50 374.00 377.00
382.00
 1   10.30   9.68   9.58  10.53   8.92   9.82   9.47   8.86  10.26
9.93
         0      0      0      0      0      0      0      0      0
0
11  383.50 388.00 389.50 391.50 393.00 394.00 396.50 400.00 403.00
407.00
 1    9.34   9.23   8.63   8.82   9.81   9.81   8.88   8.80   9.64
9.66
         0      0      0      0      0      0      0      0      0
0
11  409.50 413.00 419.50 420.50 423.00 427.00 430.00 432.50 433.50
435.00
 1    8.91   8.76   9.29   9.55   9.51   8.19   9.41   8.80   9.41
9.21
         0      0      0      0      0      0      0      0      0
0
11  438.00 440.00 443.00 444.50 449.00 451.00 454.50 456.00 458.00
459.00
 1    8.41   9.07   9.25   9.67   9.62   8.80   8.66   8.03   8.05
8.39
         0      0      0      0      0      0      0      0      0
0
11  460.20 462.00 465.00 468.00 471.50 476.00 482.00 486.50 490.00
 0    8.60   9.28   9.73   8.47   8.49   9.62   9.14   8.16   8.12
         0      0      0      0      0      0      0      0      0
11    0.00  75.00 100.00 116.00 128.00 150.00 190.00 200.00 230.00
235.00
 1    5.70   5.65   5.65   5.65   5.80   5.75   5.75   5.76   5.76
5.37
         0      0      0      0      0      0      0      0      0
0
11  243.00 250.00 270.00 280.00 288.00 300.00 315.00 360.00 365.00
400.00
 1    5.37   5.37   5.37   5.37   5.37   5.37   5.00   5.00   4.61
4.61
         0      0      0      0      0      0      0      0      0
0
11  490.00
 0    4.61
         0
11    0.00  75.00 100.00 116.00 128.00 150.00 190.00 200.00 230.00
235.00
 1    6.00   5.90   5.90   5.90   5.90   5.90   5.90   5.89   5.89
5.45
         0      0      0      0      0      0      0      0      0
0
```

```
11  243.00 250.00 270.00 280.00 288.00 300.00 315.00 360.00 365.00
400.00
 1    5.45   5.45   5.45   5.45   5.37   5.37   5.00   5.00   5.00
5.00
         0      0      0      0      0      0      0      0      0
0
11  490.00
 0    5.00
         0
12    0.00  55.00  71.00  76.00  80.00 100.00 129.00 169.00 195.00
200.00
 1   11.02  10.54  12.21  15.09  16.85  16.53  17.02  16.50  16.34
16.06
         0      0      0      0      0      1      1      1      1
0
12  220.00 230.00 232.00 240.00 244.00 250.00 260.00 273.00 280.00
288.00
 1   15.25  14.68  14.71  14.82  14.88  14.98  14.59  14.60  13.64
11.80
         0      0      0      0      0      1      1      1      1
0
12  292.00 315.50 318.00 324.50 325.50 328.00 335.00 340.00 356.00
360.00
 1   11.16  10.91  10.40  10.17  10.10  10.46  10.30   9.68   9.58
10.53
         0      0      0      0      0      0      0      0      0
0
12  364.00 375.00 380.00 392.00 395.00 398.00 405.00 410.00 420.00
425.00
 1   10.44  10.55  10.70  10.93  10.70  10.40  10.45  10.70  10.73
10.00
         0      0      0      0      0      0      0      0      0
0
12  430.00 435.00 440.00 447.00 450.00 458.00 460.00 470.00 490.00
 0   10.00  10.80  10.85  10.40   9.80   9.60  10.30  10.40  10.40
         0      0      0      0      0      0      0      0      0
12    0.00  55.00  59.00  71.00  80.00 100.00 200.00 280.00 288.00
310.00
 1    6.25   6.25   6.26   6.28   6.40   6.40   5.20   5.27   5.07
5.07
         0      0      0      0      0      0      0      0      0
0
12  330.00 350.00 360.00 490.00
 0    5.07   5.07   5.17   5.25
         0      0      0      0
12    0.00  55.00  59.00  71.00  80.00 100.00 200.00 280.00 288.00
310.00
 1    6.40   6.40   6.40   6.40   6.40   6.40   5.20   5.27   5.27
5.27
         0      0      0      0      0      0      0      0      0
0
12  330.00 350.00 360.00 490.00
 0    5.27   5.27   5.17   5.25
         0      0      0      0
13    0.00  20.00  59.00  80.00 100.00 129.00 169.00 195.00 200.00
220.00
```

```
 1   17.00  17.10  16.88  16.85  16.53  17.02  16.50  16.34  16.06
15.25
         0      0      0      0      0      0      0      0      0
0
13  230.00 232.00 240.00 244.00 250.00 260.00 273.00 280.00 290.00
300.00
 1   14.68  14.71  14.82  14.88  14.98  14.59  14.60  13.64  13.48
13.22
         0      0      0      0      1      1      1      1      1
1
13  313.00 320.00 330.00 340.00 350.00 357.50 358.50 360.00 364.00
375.00
 1   13.24  12.55  11.98  11.27  11.70  11.64  11.63  10.53  10.44
10.55
         1      1      1      1      1      1      0      0      0
0
13  380.00 392.00 395.00 398.00 405.00 410.00 420.00 425.00 430.00
435.00
 1   10.70  10.93  10.70  10.40  10.45  10.70  10.73  10.00  10.00
10.80
         0      0      0      0      0      0      0      0      0
0
13  440.00 447.00 450.00 458.00 460.00 470.00 490.00
 0   10.85  10.40   9.80   9.60  10.30  10.40  10.40
         0      0      0      0      0      0      0
13    0.00  50.00 100.00 150.00 200.00 212.00 218.00 230.00 300.00
315.00
 1    6.70   6.70   6.70   6.70   6.70   6.70   6.70   6.70   6.60
6.60
         0      0      0      0      0      0      0      0      0
0
13  400.00 490.00
 0    6.65   6.65
         0      0
13    0.00  50.00 100.00 150.00 200.00 212.00 218.00 230.00 300.00
315.00
 1    6.90   6.90   6.80   6.80   6.75   6.75   6.73   6.70   6.60
6.60
         0      0      0      0      0      0      0      0      0
0
13  400.00 490.00
 0    6.65   6.65
         0      0
14    0.00  25.00  45.00  50.00  75.00  87.50 100.00 115.00 150.00
200.00
 1   36.69  37.30  37.18  36.51  32.11  28.28  27.00  26.50  24.58
20.45
         0      0      0      0      0      0      0      0      0
0
14  210.00 214.50 218.00 222.00 230.00 232.00 240.00 244.00 250.00
260.00
 1   19.63  19.00  18.27  17.49  14.68  14.71  14.82  14.88  14.98
14.59
         0      0      0      0      0      0      0      0      0
0
14  273.00 280.00 290.00 300.00 313.00 320.00 330.00 340.00 350.00
357.50
```

```
 1   14.60  13.64  13.48  13.22  13.24  12.55  11.98  11.27  11.70
11.64
         0      0      0      0      0      0      0      0      0
0
14  358.50 360.00 364.00 375.00 380.00 392.00 395.00 398.00 405.00
410.00
 1   11.63  10.53  10.44  10.55  10.70  10.93  10.70  10.40  10.45
10.70
         0      0      0      0      0      0      0      0      0
0
14  420.00 425.00 430.00 435.00 440.00 447.00 450.00 458.00 460.00
470.00
 1   10.73  10.00  10.00  10.80  10.85  10.40   9.80   9.60  10.30
10.40
         0      0      0      0      0      0      0      0      0
0
14  490.00
 0   10.40
         0
14    0.00 100.00 150.00 200.00 210.00 230.00 240.00 300.00 315.00
348.00
 1    7.50   7.40   7.40   7.60   7.60   7.20   7.20   7.20   7.20
7.20
         0      0      0      0      0      0      0      0      0
0
14  357.50 395.75 400.00 490.00
 0    7.20   7.20   7.20   7.20
         0      0      0      0
14    0.00 100.00 150.00 200.00 210.00 230.00 240.00 300.00 315.00
348.00
 1    7.50   7.40   7.40   7.60   7.60   7.60   7.60   7.60   7.60
7.45
         0      0      0      0      0      0      0      0      0
0
14  357.50 395.75 400.00 490.00
 0    7.20   7.20   7.20   7.20
         0      0      0      0
15    0.00  25.00  45.00  50.00  75.00  87.50 100.00 115.00 150.00
200.00
 1   36.69  37.30  37.18  36.51  32.11  28.28  27.00  26.50  24.58
20.45
         0      0      0      0      0      0      0      0      0
0
15  210.00 225.00 275.00 300.00 315.00 325.00 330.00 342.50 348.00
357.50
 1   19.63  19.40  19.40  19.30  18.80  17.28  16.92  14.65  14.21
11.64
         0      0      0      0      0      0      0      0      0
0
15  358.50 360.00 364.00 375.00 380.00 392.00 395.00 398.00 405.00
410.00
 1   11.63  10.53  10.44  10.55  10.70  10.93  10.70  10.40  10.45
10.70
         0      0      0      0      0      0      0      0      0
0
15  420.00 425.00 430.00 435.00 440.00 447.00 450.00 458.00 460.00
470.00
```

```
 1   10.73  10.00  10.00  10.80  10.85  10.40   9.80   9.60  10.30
10.40
         0      0      0      0      0      0      0      0      0
0
15  490.00
 0   10.40
         0
15    0.00 100.00 150.00 200.00 210.00 224.00 227.00 300.00 348.00
357.50
 1    6.30   6.30   6.30   6.30   6.30   6.30   6.30   6.30   6.55
6.46
         0      0      0      0      0      0      0      0      0
0
15  358.50 360.00 400.00 490.00
 0    6.46   6.40   6.40   6.40
         0      0      0      0
15    0.00 100.00 150.00 200.00 210.00 224.00 227.00 300.00 348.00
357.50
 1    6.30   6.30   6.30   6.30   6.30   6.30   6.30   6.30   6.55
6.55
         0      0      0      0      0      0      0      0      0
0
15  358.50 360.00 400.00 490.00
 0    6.55   6.55   6.55   6.55
         0      0      0      0
16    0.00  25.00  45.00  50.00  75.00  87.50 100.00 115.00 150.00
200.00
 1   36.69  37.30  37.18  36.51  32.11  28.28  27.00  26.50  24.58
20.45
         0      0      0      0      0      0      0      0      0
0
16  210.00 225.00 275.00 300.00 315.00 325.00 330.00 342.50 348.00
380.00
 1   19.63  19.40  19.40  19.30  18.80  17.28  16.92  14.65  14.21
13.00
         0      0      0      0      0      0      0      0      0
0
16  395.75 410.00 422.50 445.00 460.00 465.00 490.00
 0   13.69  13.23  13.00  13.00  13.20  12.90  12.90
         0      0      0      0      0      0      0
16    0.00  50.00 100.00 150.00 200.00 300.00 315.00 400.00 490.00
 0    8.00   8.00   8.00   8.00   8.00   8.00   8.00   8.00   8.00
         0      0      0      0      0      0      0      0      0
16    0.00  50.00 100.00 150.00 200.00 300.00 315.00 400.00 490.00
 0    8.10   8.10   8.20   8.30   8.30   8.30   8.30   8.30   8.30
         0      0      0      0      0      0      0      0      0
17    0.00 100.00 150.00 200.00 300.00 315.00 400.00 490.00
 0   40.00  40.00  40.00  40.00  40.00  40.00  40.00  40.00
```

OCTOPUS.bin.in

Final velocity model parameters of my OCTOPUS model.

```
1    0.00 300.00
 0    0.00   0.00
         0      0
 1    0.00 300.00
 0    1.48   1.48
         0      0
 1    0.00 300.00
 0    1.53   1.53
         0      0
 2    0.00 300.00
 0    4.20   4.20
         0      0
 2    0.00 300.00
 0    1.79   1.79
         0      0
 2    0.00 300.00
 0    1.89   1.89
         0      0
 3    0.00 300.00
 0    4.89   4.89
         0      0
 3    0.00 300.00
 0    2.22   2.22
         0      0
 3    0.00 300.00
 0    2.27   2.27
         0      0
 4    0.00 300.00
 0    6.59   6.59
         0      0
 4    0.00 300.00
 0    3.65   3.65
         0      0
 4    0.00 300.00
 0    3.79   3.79
         0      0
 5    0.00 300.00
 0    8.24   8.24
         0      0
 5    0.00 300.00
 0    4.62   4.62
         0      0
 5    0.00 300.00
 0    4.67   4.67
         0      0
 6    0.00 300.00
 0   10.69  10.69
         0      0
 6    0.00 300.00
 0    5.00   5.00
         0      0
 6    0.00 300.00
 0    5.15   5.15
```

```
        0      0
7    0.00 300.00
0   12.15  12.15
        0      0
7    0.00 300.00
0    6.75   6.75
        0      0
7    0.00 300.00
0    6.90   6.90
        0      0
8    0.00 300.00
0   16.37  16.37
        0      0
8    0.00 300.00
0    8.02   8.02
        0      0
8    0.00 300.00
0    8.60   8.60
        0      0
9  300.00
0   40.00
        0
```

APPENDIX C

SMART1 V-Z curve

V-Z Curve at Distance 320.000 of Model: C:\Documents and Settings\mwhitehead\My Documents\Thesis\SeisWide\Smart_1.bin

0.000	1.480
4.305	1.530
4.305	1.790
4.893	1.890
4.893	2.220
6.600	2.270
6.600	3.006
6.600	3.006
6.600	3.650
8.290	3.790
8.290	4.200
8.290	4.200
8.290	4.414
8.290	4.414
8.290	4.620
10.329	4.670
10.329	5.400
10.329	5.400
10.329	5.000
10.329	5.000
10.329	5.000
10.329	5.000
10.329	5.070
12.550	5.270
12.550	6.603
12.550	6.603
12.550	7.200
18.040	7.577
18.040	6.404
18.040	6.404
18.040	8.000
40.000	8.300

OCTOPUS V-Z curve

V-Z Curve at Distance 100.000 of Model: C:\Documents and Settings\mwhitehead\My Documents\Thesis\SeisWide\octop_obs13_march16_9bin.bin

0.000	1.480
4.198	1.530
4.198	1.790
4.890	1.890
4.890	2.220
6.590	2.270
6.590	3.650
8.240	3.790
8.240	4.620
10.690	4.670
10.690	5.000
12.150	5.150
12.150	6.750
16.370	6.900
16.370	8.020
40.000	8.600

OCOTPUS V-Z compared with SMART1 V-Z

OCTOPUS			SMART1		
layer no	v	z	layer no	v	z
1	1.48	0	1	1.48	0
1	1.53	4.198	1	1.53	4.305
2	1.79	4.198	2	1.79	4.305
2	1.89	4.89	2	1.89	4.893
3	2.22	4.89	3	2.22	4.893
3	2.27	6.59	3	2.27	6.6
4	3.65	6.59	5	3.65	6.6
4	3.79	8.24	5	3.79	8.29
5	4.62	8.24	8	4.62	8.29
5	4.67	10.69	8	4.67	10.329
6	5	10.69	12	5.07	10.329
6	5.15	12.15	12	5.27	12.55
7	6.75	12.15	14	7.2	12.55
7	6.9	16.37	14	7.577	18.04
8	8.02	16.37	16	8	18.04
8	8.6	40	16	8.3	40

Base model parameter

Adaptation of Funck et al. (2004) SMART1 P-wave velocity model at 320 km model distance.

```
1    0.00 300.00
 0   0.00   0.00
       0      0
 1   0.00 300.00
 0   1.48   1.48
       0      0
 1   0.00 300.00
 0   1.53   1.53
       0      0
 2   0.00 300.00
 0   4.20   4.20
       0      0
 2   0.00 300.00
 0   1.79   1.79
       0      0
 2   0.00 300.00
 0   1.89   1.89
       0      0
 3   0.00 300.00
 0   4.89   4.89
       0      0
 3   0.00 300.00
 0   2.22   2.22
       0      0
 3   0.00 300.00
 0   2.27   2.27
       0      0
 4   0.00 300.00
 0   6.59   6.59
       0      0
 4   0.00 300.00
 0   3.65   3.65
       0      0
 4   0.00 300.00
 0   3.79   3.79
       0      0
 5   0.00 300.00
 0   8.32   8.32
       0      0
 5   0.00 300.00
 0   4.62   4.62
       0      0
```

```
5    0.00 300.00
0    4.67   4.67
       0      0
6    0.00 300.00
0   10.40  10.40
       0      0
6    0.00 300.00
0    5.07   5.07
       0      0
6    0.00 300.00
0    5.27   5.27
       0      0
7    0.00 300.00
0   12.57  12.57
       0      0
7    0.00 300.00
0    7.20   7.20
       0      0
7    0.00 300.00
0    7.60   7.60
       0      0
8    0.00 300.00
0   18.19  18.19
       0      0
8    0.00 300.00
0    8.00   8.00
       0      0
8    0.00 300.00
0    8.30   8.30
       0      0
9  300.00
0   40.00
       0
```